


Spring 5-8-2021

Role and Regulation of Staphylococcal Cell Death

Abdulelah Ahmed Alqarzaee S
University of Nebraska Medical Center

Tell us how you used this information in this [short survey](#).

Follow this and additional works at: <https://digitalcommons.unmc.edu/etd>

 Part of the [Bacteriology Commons](#), [Microbial Physiology Commons](#), [Organismal Biological Physiology Commons](#), and the [Pathogenic Microbiology Commons](#)

Recommended Citation

Alqarzaee, Abdulelah Ahmed S, "Role and Regulation of Staphylococcal Cell Death" (2021). *Theses & Dissertations*. 528.

<https://digitalcommons.unmc.edu/etd/528>

This Dissertation is brought to you for free and open access by the Graduate Studies at DigitalCommons@UNMC. It has been accepted for inclusion in Theses & Dissertations by an authorized administrator of DigitalCommons@UNMC. For more information, please contact digitalcommons@unmc.edu.

Role and Regulation of Staphylococcal Cell Death

By

Abdulelah Ahmed Alqarzaee

A Dissertation

Presented to the Faculty of the University of Nebraska Graduate college in Partial Fulfillment of
the Requirements for the Degree of Doctor of Philosophy

Pathology & Microbiology Graduate Program

Under the Supervision of Vinai C. Thomas, Ph.D.

University of Nebraska Medical Center

Omaha, Nebraska

April, 2021

Supervisory Committee:

Kenneth W. Bayles, Ph.D.

Dorte Frees, Ph.D.

Paul D. Fey, Ph.D.

Steven D. Carson, Ph.D.

Role and Regulation of Staphylococcal Cell Death

Abdulelah Ahmed Alqarzaee, Ph.D

University of Nebraska Medical Center, 2021

Supervisor: Vinai C. Thomas, Ph.D.

The transition from growth to stationary phase is a natural response of bacteria to starvation and stress. When stress is alleviated and more favorable growth conditions return, bacteria resume proliferation without a significant loss in fitness. Although specific adaptations that enhance persistence and survival of bacteria in stationary phase have been identified, mechanisms that help maintain the competitive fitness potential of non-dividing bacterial populations have remained obscure. This dissertation demonstrates that staphylococci entering stationary phase following growth in excess glucose undergo regulated cell death to maintain the competitive fitness potential of the population. Upon a decrease in extracellular pH, the acetate generated as a byproduct of excess glucose metabolism induces cytoplasmic acidification and extensive protein damage in non-dividing cells. Although cell death ensues, it does not occur as a passive consequence of protein damage. Instead, we demonstrate that the expression and activity of the ClpXP protease is induced, resulting in the degeneration of cellular antioxidant capacity and, ultimately, cell death. Under these conditions, inactivation of either *clpX* or *clpP* resulted in the extended survival of unfit cells in stationary phase, but at the cost of maintaining population fitness. We show that cell death from antibiotics that interfere with bacterial protein synthesis can also be partly ascribed to the corresponding increase in *clpP* expression and activity. The functional conservation of ClpP in eukaryotes and bacteria suggests that ClpP-dependent cell death and fitness maintenance may be a widespread phenomenon in these domains of life.

Acknowledgments

There are people in my life who contributed to shaping me as a person and as scientist, and they deserve to be acknowledged. First, I would love to thank my advisor Dr. Vinai Thomas for mentoring me through graduate school and ensuring I get the best training. I have gained tremendous skills and knowledge that would not be possible to be transferred to me without having him around all time. I also want to thank my committee members, Dr. Kenneth Bayles, Dr. Paul Fey, Dr. Steven Carson, and Dr. Dorte Frees, who have been great asset during graduate school. They always encourage, support, and guide me to be good researcher. My thanks also extend to our collaborators, especially, Dr. Tammy Kielian, for giving me an opportunity to be involved in their projects.

I would love to thank Dr. Sujata Chaudhari for her time and effort in helping me on all levels, without her, struggles in the lab would have been endless. I want to thank Vinai lab members, Elizabeth, Ryan, Sasmita, and Amanda, who are amazing, professional, and fun lab mates. Lastly, I want to acknowledge all members of the Fey and Bayles labs for their valuable help, especially Jennifer who is great asset for everyone.

Outside the lab, there are beautiful and supportive sisters and a great brother, who created the best environment for a kid to grow up. A big thank you to my big family including, uncles, cousins, nephews, and nieces, and all my friends, you are the best.

My mother, Munirah, and my uncle, Yousef, are the reason I am achieving all of this, and any future success is going to be because of you. I owe you a lot.

Lastly, I want to thank my lovely wife, Bashayr, who always supports me and takes care of me 24/7 and the little kiddo, Yousef.

Table of Contents

Acknowledgments.....	ii
Table of Contents	iii
List of Figures	v
List of Tables	vi
List of Abbreviations	vii
Chapter 1: Literature review	1
1. Programmed cell death in prokaryotes	1
1.1. Mechanisms of bacterial cell death.....	2
1.1.1. Toxin–antitoxin systems	2
1.1.2. RecA protein	3
1.1.3. Holin–antiholin proteins	4
1.1.4. Fratricide	5
1.1.5 ObgE*	6
1.1.6. Proteases	6
1.2. Benefits of cell death to bacteria.....	8
1.2.1. Biofilm development	8
1.2.2. Protection against bacteriophage infection	9
1.2.3. Pathogenesis.....	10
1.2.4. Survival and environmental stressors	12
1.2.5. Genetic exchange	13
1.2.6. Sporulation.....	14
2. Cell death in <i>Staphylococcus aureus</i>	15
2.1 Cell death of <i>S. aureus</i> during biofilm development	16
2.2 Cell death of <i>S. aureus</i> during the stationary phase.....	19
Chapter 2: Materials and methods	22
2.1. Genetic manipulation	22
2.2. Strains and growth conditions.....	24
2.3. Protein aggregation	26
2.4. Protein carbonylation	27
2.5. Quantitative real-time PCR.....	27
2.6. Measurement of competitive fitness	28
2.7. Electron paramagnetic resonance (EPR) spectroscopy.....	28
2.8. SOD activity.....	29
2.9. Western blot analysis	29
2.10. LC-MS/MS analysis.....	30
2.11. Flow cytometry	31
2.12. Flow-cell biofilm assay and confocal laser scanning microscopy (CLSM)	32
2.13. Determination of acetate in the culture supernatant	33
2.14. RNA-seq analysis.....	33

Chapter 3: Staphylococcal ClpXP protease targets the cellular antioxidant system	
to eliminate fitness-compromised cells in stationary phase.....	42
3.1 Introduction.....	42
3.2 Results.....	44
Acetate increases protein oxidation and aggregation under acidic conditions.....	44
ClpXP catalyzed proteolysis is essential for acetate-mediated cell death.....	48
ClpP enhances cell death by diminishing the cellular antioxidant capacity	53
ClpP-dependent cell death enhances the competitive fitness potential of staphylococci	62
3.3 Discussion.....	63
Chapter 4: The role of Spx in the survival of <i>Staphylococcus aureus</i> in stationary	
phase	72
4.1 Introduction.....	72
4.2 Results.....	74
Spx is necessary for stationary phase survival under oxidative stress.....	74
The redox-sensing switch of Spx is not essential for <i>S. aureus</i> viability	78
The redox-sensing switch of Spx enhances stationary phase survival.....	84
YjbH is a partial contributor to ClpP-mediated cell death.....	86
Spx increases stationary phase survival independent of superoxide dismutase.....	89
4.3 Discussion	94
Chapter 5: Concluding remarks	98
5.1. Main findings	98
5.2. Is ClpXP-mediated death an active process?	100
5.3. Does ClpXP-mediated cell death contribute to biofilm development?	103
5.4. Is ClpXP protease a pro-survival or pro-death protein?	105
Appendix.....	106
Reference	110

List of Figures

Figure 3.1. Acetate production and pH profile of <i>S. aureus</i>	46
Figure 3.2. Acetic acid induces protein damage and cell death.....	47
Figure 3.3. The ClpXP proteolytic activity enhances cell death.....	51
Figure 3.4. Extracellular factors do not contribute to the survival if the <i>clpP</i> mutant in stationary phase.	52
Figure 3.5. Altered proteome of stationary phase cells undergoing acetate stress.....	55
Figure 3.6. Proteomic profiling of stationary phase cells undergoing acetate stress.....	56
Figure 3.7. Altered proteome of stationary phase cells grown in MOPS buffered TSB-G media, pH 7.4.....	57
Figure 3.8. Proteomic profile of stationary phase cells grown in MOPS buffered TSB-G media, pH 7.4.....	58
Figure 3.9. ClpXP targets SodA to subvert the antioxidant capacity of cells.....	61
Figure 3.11. Model of the ClpXP mediated cell death pathway in <i>S. aureus</i>	65
Figure 4.1. Spx enhances stationary phase survival under stress and non-stress conditions.....	77
Figure 4.2. Spx is required for <i>S. aureus</i> growth independent of its redox-sensing switch	81
Figure 4.3 Transcriptomic analysis of after thiol stress.....	82
Figure 4.4. Redox-sensing switch of Spx enhances survival of <i>clpP</i> mutant.....	85
Figure 4.5. YjbH contributes to cell death by enhancing Spx degradation	88
Figure 4.6. Spx does not enhance survival by increasing activity of SOD.....	91
Figure 4.7. Expression of thioredoxin reductase independent of Spx enhances survival.....	92
Figure 5.1. Proposed cell death model.....	99

Figure 5.2. ClpXP-mediated cell death is an active cell death process	102
Figure 5.3. ClpP is required for biofilm maturation and development	104

List of Tables

Table 2-1. List of strains used in this study.	35
Table 2-2. List of plasmids used in this study	37
Table 2-3. List of primers used in this study	38
Table 3-1. Stationary phase death rates (k_{\max}^{\dagger}).....	69
Table 3-2. Stationary phase death rates (k_{\max}^{\dagger}) following antibiotic treatment.	71
Table 4-1. Stationary phase death rates (k_{\max}^{\dagger}).....	93

List of Abbreviations

AhpC	Alkyl hydroperoxide reductase
AIP	autoinducing peptide
Ala	Alanine
ALD	Apoptosis-like death
Amp	Ampicillin
Asn	Asparagine
Asp	Aspartic acid
ATP	Adenosine triphosphate
BH	Benjamini–Hochberg
BSH	Bacillithiol
ACN	Acetonitrile
CBASS	Cyclic oligonucleotide-based antiphage signaling system
CdCl	Cadmium Chloride
CFU	Colony forming units
CHAPS	3-[(3-cholamidopropyl)-dimethylammonio]-1-propanesulfonate
CLMS	Confocal laser scanning microscopy
Clp	Caseinolytic protease
Cm	Chloramphenicol
CoASH	Coenzyme A
CRISPR-Cas	Clustered regularly interspaced short palindromic repeats
CSP	Competence-stimulating peptide
CTC	5-cyano-2,3-ditolyl tetrazolium chloride
Cys	Cysteine
DMSO	Dimethyl sulfoxide
DNA	Deoxyribonucleic acid

DNPH	2,4-dinitrophenylhydrazine
DTT	Dithiothreitol
<i>E. coli</i>	<i>Escherichia coli</i>
ECM	Extracellular matrix
EDF	Extracellular death factor
Edin	Extensive-damage-induced
eDNA	Extracellular DNA
EDTA	Ethylenediamine tetraacetic acid
EPR	Electron paramagnetic resonance
FA	Formic acid
H ₂ O ₂	Hydrogen peroxide
HOCL	Hypochlorous acid
HPF	3-(p-hydroxyphenyl) fluorescein
KatA	Catalase
LB	Luria Bertani
MIC	Minimal inhibitory concentration
MOPS	3-(N-morpholino) propanesulfonic acid, 4-morpholinepropanesulfonic acid
mRNA	Messenger RNA
MSCRAMMs	microbial surface components recognize the adhesive matrix molecules
NBT	Nitro blue tetrazolium chloride
NO–	Nitric oxide
O ₂ •–	Superoxide
OH•	hydroxyl radical
PBS	phosphate-buffered saline
PCD	Programmed cell death
PCR	Polymerase chain reaction

PIA	Polysaccharide intercellular adhesin
psm	phenol soluble modulins
PVL	Panton–Valentine leukocidin
RNA	Ribonucleic acid
RNAP	RNA polymerase
ROS	Reactive oxygen species
RPM	Round per minute
<i>S. aureus</i>	<i>Staphylococcus aureus</i>
SapI	Staphylococcus Pathogenicity island
SD	Standard deviation
SDF	Sporulation delaying factor
SDS-PAGE	Sodium dodecyl sulphate–polyacrylamide gel electrophoresis
SKF	Sporulation killing factor
SOD	Superoxide dismutase
Spx	Suppressor of <i>clpP</i> and <i>clpX</i>
SSC	side-scattered light
TCA	Trichloroacetic acid
tRNA	Transfer RNA
TrxA	Thioredoxin
TrxB	Thioredoxin reductase
TSA	Tryptic soy agar
TSB	Tryptic soy broth

Chapter 1: Literature review

1. Programmed cell death in prokaryotes

Cell death was initially characterized in developing eukaryotic cells in the 1800s. The regulation of this process was proposed by Karl Vogt in 1842 (1, 2). In 1972, Kerr et al. described a specific morphological feature of programmed cell deletion called *apoptosis* to distinguish it from the accidental cell death process called *necrosis* (3). This study set the stage for identifying more of the physiological and morphological hallmarks of apoptosis that would differentiate active and passive cell death processes. The multiple forms and mechanisms are now known as programmed cell death (PCD) (2). In general, active cell death has to be genetically encoded, is a reversible process, and usually requires energy, whereas necrosis is a passive and irreversible process resulting from extreme damage (1, 4). The “altruistic” cell death mechanisms benefit multicellular organisms during organ development, cell maintenance, and homeostasis, and other events, so that a few cells are sacrificed for the benefit of the organism (5–7).

After discovering apoptosis in eukaryotes, it took 14 years to report the first gene that regulated cell death in bacteria (8). It used to be disputable that a unicellular organism underwent cell death. However, prokaryotic cells live as a community in nature, where they function as a multicellular organism, communicate, and coordinate their behavior (9). Cell death is an important aspect of multicellularity; the sacrifice of a subpopulation may benefit the whole organism (10). Multiple studies of various microorganisms indicate that regulated cell death processes and forms are widely present in bacteria and contribute to multiple stages of development and survival (11–18). This chapter explores the reported mechanisms and determinants of regulated cell death and how they benefit the bacterial community.

1.1. Mechanisms of bacterial cell death

1.1.1. Toxin–antitoxin systems

In the 1980s, toxin-antitoxin systems were described as mediators of cell death in bacteria. Ogura et al. described plasmid-encoded genes that couple cell division with plasmid replication (19). These genes were initially called coupled cell division genes *ccdA* and *ccdB* (20, 21). The researchers concluded that the *ccdB* gene inhibited cell replication and the *ccdA* gene suppressed the actions of the *ccdB* gene; the *ccd* locus was later identified as the controller of cell death (21, 22). Subsequent studies have determined that the product (toxin) of the *ccdB* gene is a stable killer and the product (antitoxin, or antidote) of the *ccdA* gene is an unstable protein that is prone to degradation by the Lon protease (20). This model was named the addiction model because the cell needs to keep its plasmid to maintain adequate levels of the unstable antitoxin to neutralize the stable toxin. If the plasmid is lost, the toxin is free to kill the cell (23, 24). In the 1990s, studies focused on unicellular organisms with programmed cell death mechanisms mediated by the toxin-antitoxin system (24).

The most studied type II toxin–antitoxin system involved in bacterial cell death is the chromosomally encoded *mazEF* module, in which *mazF* encodes the toxin and *mazE* the antitoxin (23, 25). When the system is activated, the ClpAP protease (in the case of *Escherichia coli* [*E. coli*]) degrades the MazE antitoxin (23). This results in the enrichment of the long-lived endoribonuclease toxin MazF, which kills the cell by cleaving its mRNA (26, 27). MazF preferentially cleaves single-stranded mRNA at the ACA sequence, causing massive blockage of protein synthesis (26, 27). Although multiple studies have suggested that MazF does not kill the cell but rather causes reversible growth inhibition (bacteriostasis) (28, 29), there is also evidence to suggest that *mazF* overproduction has a bactericidal effect (25). The latter finding led to the question of whether MazF acts as an executioner of the cell or an element downstream is involved in killing (17). This question was addressed by Shahar et al. through proteomic analysis of *E. coli*

cells. They showed that although MazF blocks protein synthesis, a subset of proteins synthesized after *mazF* induction, such as ClpP, SlyD, YfiD, and ElaC, may be responsible for cell death downstream of MazF (27).

Another type II toxin–antitoxin system regulating cell death with a different target is the epsilon/Zeta system (30, 31). It is encoded either in chromosomes or plasmids and consists of the Zeta toxin and Epsilon antitoxin (30, 31). As in the MazEF system, the toxin, zeta, is more stable than the antitoxin, epsilon, because it is not continuously degraded (32, 33). An example of the regulation of cell death by the epsilon/zeta system is the chromosomally encoded pneumococcal *pezAT* operon (31). Interestingly, this system does not inhibit transcription or translation, as do most of the reported toxin-antitoxin systems (31). If the PezA antitoxin does neutralize the PezT toxin in any situation, the latter exerts its toxicity on cell wall synthesis, causing cell lysis (31).

1.1.2. RecA protein

When a bacterial cell is exposed to a DNA-damaging chemical agent, it upregulates its production of proteins to stop DNA replication and repair the damage, and to modulate metabolism to ensure minimal damage (34). These processes are encoded by a set of genes, named SOS response genes (34) that are under the regulatory control of the LexA repressor (34). Thus, LexA has to be released from the DNA to induce the SOS response, a process that depends on RecA protein (34, 35). The RecA protein is an essential component of the bacterial SOS response, and it is critical for triggering the response and upregulating many of the SOS genes (34, 36). RecA recombinase is usually inactive, but when there is DNA damage–induced single-stranded DNA present, RecA detects it and turns into the active (RecA*) protease (34). Subsequently, the RecA* protease initiates LexA autocleavage, releasing it from DNA (34). It is well known that DNA damage triggers PCD in prokaryotes and eukaryotes (37–41). Thus, it is counterintuitive to think that RecA mediates cell death because its primary function is to repair DNA damage resulting from reactive oxygen species (ROS), which is a process that should promote survival.

Studies of *E. coli* indicate that extensive DNA damage can increase the RecA* to a toxic level, eventually causing cell death (38, 39). Increased RecA* activity derepresses extensive-damage-induced (*Edin*) genes (38, 39). The upregulation of *edin* genes results in increased superoxide (O_2^-) production and subsequently, hydroxyl radical OH^\bullet in the presence of free Fe^{2+} , through the Fenton chemistry (38). The increased ROS levels cause more DNA damage and continues the process of RecA* activation and induction of *edin* genes, causing even more DNA damage so that the cell dies (38). It was proposed that if the DNA damage is extensive and beyond repair, the RecA* triggers further DNA damage to kill the cell (38). Interestingly, RecA-mediated PCD was described as apoptosis-like death (ALD) because it had some of the hallmarks associated with eukaryotic apoptosis, including increased DNA damage, increased ROS levels, and membrane depolarization (38).

1.1.3. Holin–antiholin proteins

Holins are a diverse group of small proteins. When they accumulate in the cytoplasm, they may oligomerize in the cytoplasmic membrane, forming holes and facilitating endolysin activation and delivery to the cell wall (42, 43). In their natural context, endolysins (e.g., murein hydrolase) and holins help bacteriophages to release virions into the extracellular milieu by destroying the bacterial cell (42, 43). Holins and holin-like proteins are found widely in bacteria, archaea, plants, and eukaryotes, where they serve different functions (44).

Staphylococcus aureus encodes the holin-like protein CidA and the antiholin-like protein LrgA. The CidA protein promotes cell death and lysis, and the LrgA protein counters the actions of CidA (18, 45–47). The CidA protein oligomerizes into the membrane in ways similar to the bacteriophage holins and increases the activity of murein hydrolase, thus inactivation of *cidA* decreases penicillin-induced lysis (48). It is worth noting that the eukaryotic Bax and Bcl-2 families of proteins function like bacterial holin and antiholin proteins, respectively. Bax can induce lysis in bacteria in a manner similar to that of bacterial holins (17, 49, 50). Bax causes oligomerization

of the mitochondrial membrane, leading to permeabilization of the membrane and triggering apoptosis (47, 49).

1.1.4. Fratricide

A common altruistic behavior across living organisms is fratricide (51). The common goal of this behavior is to benefit the population as a whole at the expense of a subpopulation of cells (51). In the bacterial world, altruistic behavior was documented to be necessary for various processes, and the death of a subpopulation of cells occurs at specific times, under specific conditions, and via a specific mediator (15, 52). *Streptococcus pneumoniae* (53), *E. coli* (39), *Enterococcus faecalis* (54), and *Bacillus subtilis* (55) are organisms that can regulate fratricidal processes through the secretion of a molecule into the extracellular milieu that activates an intrinsic cell death mechanism, resulting mainly in cell lysis (54, 56–59). The two death signals, extracellular death factor (EDF) and competence-stimulating peptide (CSP), will be briefly discussed.

EDF is a linear small peptide secreted into a supernatant when exponentially growing *E. coli* cells reach a density of $\sim 10^7$ to 10^8 (58). The peptide accumulates during the growth phase until it reaches a threshold at which a subpopulation of cells senses it as a death signal (58). Interestingly, EDF triggers death by activating the MazEF toxin–antitoxin system and enhancing the endoribonuclease activity of MazF (57, 58).

CSP has been well studied in *Streptococcus* species as the key factor inducing cell lysis in a liquid medium (60). CSP is part of the competence operon *comABCDE*. As cell density increases, the *comABCDE* gene cluster is activated and the CSP is synthesized from *comC*. ComA and ComB process and export the peptide to the outer membrane (61, 62). The membrane-bound histidine kinase ComD senses the CSP and phosphorylates the response regulator ComE to activate the competence genes. Activation generates more CSP, and creates a positive feedback loop (63–65). ComE activates the ComX sigma factor, which also activates competence and competence-related

genes, as well as lysis-related genes (53, 65). The cell wall hydrolases LytA, LytC, and CbpD and the bacteriocin CipB participate in a complex overlapping function that drives the lysis of a subpopulation of cells (65, 66).

1.1.5 ObgE*

ObgE is a GTPase conserved in bacteria that plays a role in multiple cellular processes, including progression through the cell cycle checkpoints, response to stress, replication of DNA, and tolerance to antibiotics (67). ObgE is essential for *E. coli* cell viability, and hence, an error-prone PCR was used to generate multiple isoforms for the study of ObgE (67). Interestingly, the ObgE_{K268I} isoform, which is denoted as ObgE*, mediated PCD in *E. coli*. Upon expression of ObgE*, dying cells exhibit hallmarks of apoptosis, including membrane blebbing, DNA fragmentation, and chromosome condensation (40, 68). Although it was reported that ObgE* induces the formation of ROS, scavenging ROS do not rescue ObgE*-mediated PCD, suggesting that another mechanism contributes to the loss of viability (40, 68). A later study found that ObgE* mediates PCD by an irreversible inhibition of cell division and induction of lysis (69, 70). It is worth mentioning that the ObgE homologues in humans, ObgH1 and ObgH2, can complement some of the bacterial ObgE functions when expressed in *E. coli* upon the loss of *obgE* expression (71).

1.1.6. Proteases

Intracellular proteases are conserved across all animal kingdoms. They are diverse in functions, components, and substrates, yet they share the same goal, which is protein degradation or cleavage irrespective of whether the protein is a native, misfolded, or aggregated (72–74). Thus, the proteolysis process is tightly regulated to orchestrate cellular processes and maintain protein quality control (75–77). The energy-dependent proteases (AAA+ proteases) have a catalytic core and an energy-dependent unfoldase; this group of proteases includes ClpCP, ClpXP, ClpAP, FtsH, and Lon (78). Their physiological roles have been extensively studied, and the findings suggest that

these proteases regulate metabolism, virulence, cell division, and responses to extracellular environmental stresses, including but not exclusive to oxidative stress, heat stress, and iron limitation (79–84). Recently, a few reports indicated that proteolysis can play a big part in the process of PCD.

B. subtilis and other spore-forming microorganisms undergo morphological and physiological changes to start the sporulation process when they are challenged with various environmental stressors (85). Not all cells that enter the sporulation pathway finally form a healthy spore (86). Checkpoints maintain the quality of the spores (86). These processes are checked at the end by the ClpXP protease to ensure the accuracy of the process, prevent errors, and ensure that high-quality spores are made (86). Simply put, spore morphogenesis starts with a mother cell engulfing a newly formed progeny and preparing the forespore for the next steps of morphogenesis (87). Subsequently, two cell envelopes are formed around the daughter cell, and multiple layers of more than 70 proteins and a specialized peptidoglycan form a coat and a cortex (87). When these layers are properly formed, the mother cell lyses and the newly formed spore is released into the environment (87). Coat morphogenesis is critical step in sporulation, and the process has to be flawless because any defect in coat formation will subsequently cause a defect in spore resistance to external environmental stresses (88). Coat morphogenesis starts with localization of SpoVM to the forespore membrane surface (daughter spore) of the structural protein SpoIVA, which acts as an essential scaffold (88). The structural protein SpoIVA is a substrate for ClpXP degradation with the help of the adaptor protein CmpA, which is produced by the mother cell during morphogenesis (88). Degradation of CmpA by ClpXP is triggered to abort the sporulation process if there is a defect in the forespore coat formation, and lysis is the fate of any defective sporulating cells (89). Thus, the mother *B. subtilis* cell ensures the quality of sporulating daughter cell through ClpXP-mediated cell death mechanism, which eliminates defective cells by destabilizing the forespore as a result of SpoIVA degradation (88).

Other PCD mechanisms also suggest different roles for the ATP-dependent ClpP protease in mediating or regulating bacterial cell death. As described in section 1.1, MazF-induced cell death occurs when the MazE antitoxin level drops inside the cell. The degradation of the MazE antitoxin is dependent on the ATP-dependent protease ClpAP in *E. coli*. It was suggested that MazF triggers the synthesis of death-specific genes, and one of those identified death proteins was ClpP (27). A very elegant study by Daniel et al (2012) described how bactericidal antibiotics induced apoptosis-like cell death in *E. coli*. Dying cells that had been exposed to antibiotics exhibited hallmarks of eukaryotic PCD, including DNA condensation and fragmentation, ROS, and membrane depolarization (90). These apoptotic phenotypes were triggered by RecA, which the researcher described as having caspase activity, a process that involves regulation by the ClpXP protease (90). In *Streptomyces* species, multiple forms of PCD were described during developmental cycles (91), and proteomic analysis indicated that the regulation of macromolecules by AAA+ ATPase and the 20S bacterial proteasome was involved in the PCD process (92). Collectively, these studies have demonstrated a strong correlation between bacterial cell death and the ATP-dependent intracellular proteases in an energy-dependent process similar to apoptosis in eukaryotes (93, 94).

1.2. Benefits of cell death to bacteria

1.2.1. Biofilm development

Bacteria can stick together to form an aggregate of bacterial cells that can enclose a complex bacterial system (95, 96). The process of biofilm development requires multiple stages before a fully mature biofilm is generated (95–97). When a planktonic cell attaches to a surface and starts multiplying, crosstalk begins between individual cells so they can work as a community (95–98). The crosstalk enables cells to form multiple networks and regulatory mechanisms to regulate biofilm development (95–98). Biofilms are composed of proteins, extracellular DNA (eDNA), and polysaccharide, which form an extracellular matrix (ECM) by which cells stick together and are

protected from multiple environmental insults, including extreme pH, antimicrobial compounds, toxic chemicals, and host immune effectors (95–98). Thus, this type of bacterial lifestyle is commonly present in environments where conditions are mostly harsh and stressful (95–98).

In general, biofilm development starts with a phase of attachment and multiplication, followed by a maturation phase, and finally a detachment or dispersal phase, which initiates attachment at a new site and starts the cycle again (97). Cell death has been reported to be an essential process during the attachment and maturation stages of biofilm development, where a subpopulation of cells dies and releases DNA and proteins that function as a biofilm scaffold and nutrient supply for siblings (49, 99–101). Thus, treating biofilms with DNase or proteases (e.g., proteinase K) can either destabilize a mature biofilm or inhibit its establishment and formation (47, 102, 103). Additionally, inactivation or modulation of cell death mechanisms during biofilm development perturbs biofilm formation, affecting one or more of the developmental stages (98, 104–106).

Multiple cell death mechanisms discussed earlier in this chapter play significant roles in shaping biofilms. The proper biofilm development process of *S. aureus* requires holin antiholin-mediated cell death to release eDNA (47). Additionally, CSP-mediated cell lysis in *Streptococcus mutans* was shown to contribute to biofilm development, as well (104), and the most studied toxin-antitoxin system, MazEF, also has multiple roles in biofilm development in multiple organisms (107, 108).

1.2.2. Protection against bacteriophage infection

Viruses are known causative agents of diseases in human, animals, and plants. All of these living organisms have innate or adaptive immune systems, or both, that can fight viral infections (109). Bacteria have developed multiple strategies to combat bacteriophage infection, including restriction modification, the CRISPR-Cas system, and abortive infection systems in addition to mechanisms that block phage attachment or injection of the phage genome (110–112). An abortive

infection system is considered a suicide mechanism that an infected cell undergoes to prevent the phage replication cycle, and it is likely to be activated only when other defense systems collapse (113). Thus, this immune strategy prevents the spread of bacteriophage infection to the population, protecting the community from predators when a single cell cannot fight a phage infection.

Although some abortive infection systems cause stasis, the prolonged inhibition of protein synthesis or degradation of the host RNA can lead to cell death (111, 113, 114). Bacteriophage-infected bacterial cells can commit suicide through multiple mechanisms that primarily disrupt the cells' inner membrane, cause abortive lysis, or degrade the genomic DNA (113). Membrane depolarization is mediated by the RexA/RexB system, in which RexA senses that the replication of the phage genome is occurring. It forms a protein–DNA complex that localizes to the membrane to activate RexB and form holes in the inner membrane (115). These events disrupt the membrane potential and Lysis is triggered after induction of the *abiz* gene (115). Abiz cooperates with the phage in creating holes and causes premature lysis and the release of noninfectious viral particles (115). Degradation of the host DNA occurs in a complex system mediated by the Nuc DNA nuclease, which is activated by several components from the CBASS system (cyclic oligonucleotide-based antiphage signaling system) as it detects phage infection (110, 116). The type II and type III toxin–antitoxin systems, MazEF and ToxIN, respectively, have been shown to mediate abortive infection through the degradation of the host mRNA that is blocking protein synthesis (114, 117). Another mechanism that inhibits protein synthesis is mediated by the anticodon nuclease, PrrC, which cleaves lysine transfer RNA (t-RNA), causing the depletion of the lysine t-RNA and eventually its dormancy and death (118).

1.2.3. Pathogenesis

The release of virulence factors is essential for microorganisms to invade a host and win the battle against the host's immune system. Toxins are well-characterized virulence factors that are usually secreted into the surrounding environment during infection to help during disease

progression (42, 119–121). *S. pneumoniae* is gram-positive bacteria that releases pneumolysin, a pore-forming toxin that causes DNA damage and the lysis of host cells (122). Interestingly, *S. pneumoniae* does not have a mechanism for releasing the toxin into the external environment because no signal peptide has been identified in the toxin (123, 124). Thus, one mechanism by which *S. pneumoniae* releases pneumolysin is by a self-lysis mechanism that is mediated by the LytA autolysin (125). LytA degrades the cell wall by cleaving the amide bond connecting the stem peptides and N-acetylmuramic acid residues causing hydrolysis of the peptidoglycan (126). LytA is an enzyme that is usually inactive in the cytoplasm when cells are not present at a high density. When the cells do reach a high density during the stationary phase, LytA localizes to the cell wall to hydrolyze peptidoglycan (126). Clearly, the lysis-dependent release of pneumolysin is important during infection because the inactivation of the pneumolysin-encoded gene, *ply*, generates a less virulent *S. pneumoniae* strain in vivo (125). It is unclear how only a subpopulation of cells undergoes lysis, but the pneumococcal PezAT toxin–antitoxin system has been proposed as playing a role in regulating the selective lysis of a subset of cells (31). Another pneumococcal suicidal gene called SpxB, which encodes pyruvate oxidase, kills stationary-phase cells by generating hydrogen peroxide (H_2O_2) independent of LytA (127). The SpxB-mediated cell death exhibits apoptotic hallmarks and is advantageous for in vivo colonization (127).

Other virulence factors that must be released by lysis are the *Clostridium difficile* toxins TcdA and TcdB, because both lack a signal peptide similar to pneumolysin (121, 128). TcdA and TcdB are potent toxins that inactivate multiple signaling pathways by glycosylating the Rho GTPases, which are important for the regulation of the actin cytoskeleton (129). Consequently, affected cells undergo apoptosis as a result of membrane blebbing (129). These toxins are released when the TcdE holin-like protein localizes to the membrane to induce lysis (121, 128). In a model of *Pseudomonas aeruginosa* infection in the lung, a PCD-like mechanism is necessary for successful host colonization (130). Lysis of a subset of cells was induced because of DNA damage

that is sensed by an AlpR repressor. Subsequently, AlpR undergoes autocleavage to activate (derepress) the expression of a holin-like lysis mechanism (130).

1.2.4. Survival and environmental stressors

Bacterial communities rely on the actions of individual cells to survive and thrive in various harsh environments (30). Thus, a division of labor is an important strategy for successful collaboration in a bacterial community; every designated subpopulation of cells performs a specific task to achieve the complex conditions of multicellularity (131, 132). During amino acid starvation or antibiotic stress, the death of a subpopulation of cells is critical for the public good of the bacterial community (siblings); it alleviates stress or kills extremely damaged cells when repairing them would be too costly for the broad population (16, 133, 134). Antibiotics, DNA-damaging chemicals, an immune response, oxidative stress, and acidic stress trigger cell death in bacteria by activating various cell death mechanisms described earlier, such as the MazEF toxin–antitoxin, RecA, and CidA–LrgA holin–antiholin systems (16, 38, 56, 63, 90, 105).

Antibiotics used at bactericidal concentrations usually kill more than 99% of the population. However, a small fraction of cells that are genetically identical to the dead cells survive even though they are just as sensitive as the dead cells when they are regrown in the presence of the same antibiotic (135). These surviving cells are called persisters, and it has been suggested that PCD mechanisms and the formation of persisters are connected (136). Thus, this is an important clinically relevant mechanism that may be used as a therapeutic target where a PCD mechanism can be activated to kill persisters (5, 8, 30, 137). Although it is counterintuitive or counterproductive to propose such altruistic traits during environmental stressors, understanding the positive outcomes of and advantages for the surviving population should help us appreciate the complexity of bacterial multicellularity.

1.2.5. Genetic exchange

Exchanging genetic material is extremely common in bacteria (138). Horizontal gene transfer enhances the acquisition of new traits, such as antibiotic resistance or virulence factors (139). Thoroughly studied mechanisms that mediate gene transfer include conjugation, transformation, and transduction (139). Genetic transformation is very common within the same bacterial species, where “naked DNA” is taken from the environment and is incorporated into the genome of the recipient strain (140).

Naked free DNA fragments are primarily released into the environment when cells undergo lysis, and thus, efficient genetic transformation requires the death of a subpopulation of cells within the bacterial community to serve as donor cells (140). This phenomenon is well characterized in *Streptococcus* species. Achieving a state of competence requires multiple factors, which are primarily triggered by the CSP (see section 1.1.4). As explained before, the competence and exchange of genetic material in *Streptococcus* depend on the lysis of a subpopulation of cells that is achieved by activation of the autolysin LytA through ComABCDE quorum sensing and the competence system (8, 63, 141). Interestingly, a sub-MIC concentration of some antibiotics, including the protein synthesis inhibitors kanamycin and streptomycin and the fluoroquinolones norfloxacin and moxifloxacin, induces the competence system of *S. pneumoniae* (142). This observation indicates a strategy by which *Streptococcus* species developed to share antibiotic resistance markers and virulence factors when treated with antibiotics, a process that occurs frequently in vivo during infections when the right conditions are met (143). Recently, competence inhibitor compounds (COM-blockers) were developed to combat the spread of antibiotic resistance that is mediated through genetic transformation (144). Mechanistically, COM-blockers inhibit the release of the CSP, blocking the competence signal that activates the system; an in vivo model of murine infection treated with COM-blockers had a decreased efficiency of horizontal gene transfer (144). Thus, it is not surprising to see multiple reports indicating an exchange of antibiotic markers within biofilms, where regulated cell death processes are widely reported (145–147). The exchange

of genetic material strengthens the advantage of having PCD to release genomic DNA into the biofilm to facilitate horizontal gene transfer (145–147).

1.2.6. Sporulation

Multiple regulated cell death mechanisms have been identified in *B. subtilis* to be part of the sporulation process (86). All of these processes contribute to the survival of the bacterial community and the quality of the surviving population (30, 86, 89, 148–150). As *B. subtilis* experiences famine because of the lack of an essential nutrient, including carbon, nitrogen, and phosphorous, the spore morphogenesis process starts (85, 151). At early stages of the process, cannibalism has been shown to play a significant role in the death of a subpopulation of cells (148). Toxins named sporulation delaying factor (SDF) and sporulation killing factor (SKF) are released into the environment by a subset of cells to trigger lysis in siblings and release nutrients that sporulating cells will utilize during starvation (148). The master regulator of sporulation, Spo0A, activates the transcription of SDF, SKF, and the necessary immunity factors that can protect a sporulating cell from the toxins (148).

The second cell death process occurs during the last steps of morphogenesis, where cells are committed to sporulation and become mature spores (86). One cell death process occurs during morphogenesis, as described in section 1.1.6. It has a checkpoint step that ensures the proper formation and assembly of the spore cell envelope, where ClpXP-mediated cell death is activated to eliminate unfit or defective spores from the population (89). After passing the quality checkpoint, the last death process involves the lysis of the mother cell to release the mature endospore to the environment; this is a self-lysis process mediated by two peptidoglycan hydrolases, LytC and CwlC (89). Clearly, spore morphogenesis is controlled by multiple cell death mechanisms at different stages serving different purposes, and the death of a subpopulation of cells is meant to enhance the survival of the fit sporulating bacterial community.

2. Cell death in *Staphylococcus aureus*

S. aureus is a gram-positive facultative pathogen that colonizes 28% to 32% of healthy individuals. It occurs primarily in the nares in 60% to 80% of humans who test positive for it (152–154). It is also isolated from the skin, intestine, and groin (155, 156). A growing number of studies indicate that *S. aureus* is spreading to animals (157). Fifty percent to 80% of infections are caused by the same strains colonizing the host asymptomatically, suggesting an increasing risk of infection carriers and the opportunistic behavior of the pathogen (155). *S. aureus* is one of the most successful human pathogens, and it causes a wide range of infections, including bacteremia, skin and soft tissue infections, infective endocarditis, and osteomyelitis (154). The numbers of *S. aureus* infections have increased dramatically since the pathogen's identification in 1880 by Alexander Ogston (158). It was estimated that more than one million cases occurred in the United States in 2005 (153). Thus, it is not surprising that it has an arsenal of virulence factors and multiple strategies to survive harsh conditions and combat the immune response (159).

S. aureus secretes multiple virulence factors that help to attack host cells, acquire nutrients, and evade immune responses (160–163). Panton–Valentine leukocidin (PVL), alpha-hemolysin, and delta-hemolysin are pore-forming secreted toxins that target host cells, such as neutrophils, macrophages, and erythrocytes. They cause lysis as a result of a compromised membrane (160, 164). Additionally, *S. aureus* secretes multiple proteases that contribute to nutrient degradation and acquisition, biofilm formation, and dissemination (165–167). These proteases include the cysteine proteases ScpA and SspB, the serine proteases SplA to SplF and SspA, and the metalloprotease Aur (168–170). Essential metals, such as iron and zinc, are also scavenged from the environment with siderophores and metallophores, and they play a significant role in battling nutritional immunity (171–173). Toxins and proteases are not the only major factors that make *S. aureus* a successful pathogen. It also has 16 two-component regulatory systems that help it sense sudden changes in the external environment so it can orchestrate virulence production and metabolism

(162, 174–176). ROS detoxifying enzymes, surface proteins, and clumping factors and antibiotic resistance are critical factors that enhance *S. aureus* pathogenesis (177, 178).

S. aureus is very well known to form biofilms on indwelling medical devices, such as catheters, implanted heart valves, and prosthetic joints (98). These biofilm infections are extremely hard to treat. They are known to be resistant to antibiotics primarily because they contain heterogeneous populations of growing and nongrowing cells; the latter population is known to be more resistant (179). One factor contributing to the increased resistance to antibiotics is a decreased flow or penetration of antibiotics within a biofilm (180–182). Thus, *S. aureus* infections associated with biofilms are usually chronic, threatening the health of individuals undergoing implantation surgery and increasing the costs of treatment; implant replacement may be the only option (183, 184). Multiple studies have indicated heterogeneity, stochasticity, and multicellularity in these biofilms, suggesting a high degree of complexity within the bacterial community; part of the complexity includes the death of subpopulations of cells at specific sites during biofilm development (98, 101, 185). As described in sections 1.1.3 and 1.2.1, the discovery of the cell death operon, *cidABC* and *lrgAB*, have increased our understanding of the cell death process in *S. aureus* within biofilms and planktonic cultures (18, 46, 47, 49, 103, 186).

2.1 Cell death of *S. aureus* during biofilm development

Multiple studies indicate that *S. aureus* biofilm undergoes multiple phases or stages during development (185). Using the BioFlux system, which is a microfluidic system attached to a microscope with a high-resolution camera, it was possible to study the development of the *S. aureus* biofilm in real time; interesting behavior was revealed showing that the *S. aureus* biofilm undergoes distinct developmental phases (101). We know that the *S. aureus* biofilm [1] starts with the attachment of free-floating cells to biotic or abiotic surfaces and then goes through stages of [2] multiplication, [3] exodus [4] maturation, and [5] dispersion (103).

The attachment of *S. aureus* in vivo to surfaces covered with host matrix proteins depends on whether the microbial surface components recognize the adhesive matrix molecules (MSCRAMMs); more than 20 proteins have been identified as having an LPXTG motif that is known to be anchored to cell wall peptidoglycan (187). Additionally, autolysin, teichoic acid, and lipase play significant roles in the adhesion of *S. aureus* to implants in vivo (96, 184, 185). However, in vitro biofilm studies showed that *S. aureus* can attach to plastic surfaces very well by relying on hydrophobic and electrostatic interactions (98). Therefore, the MCRAMMs and other factors may have negligible roles in in vitro settings lacking host proteins (98, 103).

After establishing a biofilm through attachment, the ECM starts to accumulate, causing cells to form aggregates. It has been suggested that the ECM at this stage is composed primarily of secreted proteins (188). The contributions of polysaccharide intercellular adhesin (PIA) at this initial stage may vary; the regulation of the *ica* locus differs among strains and growth conditions (189, 190). As cells multiply and the biomass increases, the lysis of subpopulations of cells releases eDNA and cytoplasmic proteins to help in forming the biofilm scaffold (99, 100, 191). Cell death and lysis are crucial at this step for releasing these macromolecules because blocking the cell death pathway mediated by CidA dramatically decreases the eDNA in the biofilm and disrupts the formation of a tower, which is seen during normal biofilm development (99). A study using *S. aureus* cells expressing the *cid::gfp* reporter in the BioFlux system showed that during biofilm development, cells that expressed *cid* were correlated or co-localized with dead cells; this indicated that the *cid* locus contributed to cell death and lysis of the *S. aureus* biofilm (103). At the end of the attachment and multiplication stages, aggregated cells in the biofilm matrix are composed of proteins and genomic eDNA, and the matrix is then disrupted by nuclease to start the exodus phase (98).

The exodus phase occurs when a dedicated subpopulation of cells expresses and secretes nuclease into the biofilm environment to degrade the eDNA (103), a process that is tightly regulated by the Sae two-component system through controlling *nuc* (nuclease) expression stochastically

(192). This event results in partial disruption of the biofilm and a decrease in the biofilm biomass and sets the stage for maturation (98, 103). During maturation, the cells continue to multiply and the ECM grows, leading to the formation of mature towers in which channels form to facilitate nutrient exchange within the biofilm (98, 103, 185). Lastly, dispersion or detachment occurs when the shear stress increases or the Agr two-component system is activated (185). The Agr two-component regulatory system is a typical quorum-sensing system that senses the extracellular autoinducing peptide (AIP) (193). As the cell density increases during maturation, the AIP reaches a threshold at which the expression of *agr*-dependent genes can take place (193). The genes secrete proteases, which are known to degrade the proteinaceous component of the ECM, and phenol soluble modulins (psm), which form pores in the biofilm (98, 185). This step is crucial for the bacterial community to disseminate and establish new biofilms at different sites (194).

Under anaerobic growth conditions, *S. aureus* can grow either by anaerobic respiration (using nitrate as a terminal electron acceptor) or by fermentation (195, 196). Regulation of *S. aureus* anaerobic growth is controlled mainly by the SrrAB two-component system (197). Under anaerobic conditions, this system senses reductions in menaquinone in the electron transport chain and causes phosphorylation of the SrrA response regulator to activate genes required for anaerobic growth (197). Although SrrAB is necessary for growth under hypoxic conditions, it also regulates cell lysis and biofilm formation during anaerobic growth. Mashruwala et al showed that hypoxia induces a robust biofilm during fermentative growth and that eDNA is an integral component of the biofilm matrix (198). The high-molecular-weight eDNA is a result of murein hydrolase AtlA-induced lysis, which is transcriptionally upregulated because of decreased respiration. AtlA-induced cell lysis is regulated by SrrAB when it senses the presence of an increased pool of reduced menaquinone, suggesting that biofilm formation under hypoxic conditions requires a programmed cell lysis mechanism regulated by SrrAB (198).

2.2 Cell death of *S. aureus* during the stationary phase

A typical bacterial growth pattern starts with a lag phase, followed by a phase of exponential growth and, finally, a stationary phase (199). During the lag phase, bacterial cells start adjusting to their new nutrient-rich environment (199, 200). These metabolically active cells initiate two cellular processes before entering the exponential phase of growth, where cells are rapidly dividing and the biomass increases (199). As an essential nutrient is depleted in the medium or the bacteria experience an environmental insult, cells cease to grow and prepare to enter the stationary phase (201).

The stationary phase has recently been divided into three phases, [1] stationary phase, [2] death phase, and [3] long-term stationary phase (202). In the stationary phase, death occurs in two stages (202, 203). The first is a rapid loss of viability during the early stationary phase, and the second is during a slow, long-term stationary phase, which can take up to 5 years in standard laboratory conditions without replenishing medium (203). The rapid cell death is considered an altruistic event in which nutrient depletion triggers the cell death mechanism (suicidal mechanism) in a subpopulation of cells for the public good so that siblings can survive famine (202).

The *S. aureus* stationary phase of growth has been investigated in multiple studies so that investigators can understand factors that contribute to stationary phase survival. (204–210). The *cidABC* regulon we described earlier in this chapter contributes to death during the stationary phase through the holin-like protein CidA. Here we will briefly discuss how *cidABC* metabolically drives death in the stationary phase (18, 205). Under aerobic growth conditions with glucose supplementation (35 mM glucose), glucose is metabolized into acetate, which accumulates in the medium and decreases its pH (186). Acetate induces the expression of *cidABC*, subsequently increasing the murein hydrolase activity (186). Thereby, the *cidABC* operon controls cell viability in the stationary phase through acetate-mediated killing by CidC and murein hydrolase-mediated lysis triggered by CidA (205).

The mechanism of stationary phase death mediated by CidC is triggered when acetate accumulates in the growth medium and causes a decrease in the medium's pH so that the pH is nearly the same as the pKa of acetic acid, which is about 4.8 (105, 205). At this level of medium acidification, most of the ionic form of the acetate becomes protonated and can freely diffuse through the bacterial membrane into the cytoplasm, where protons are released and cause cytoplasmic acidification (105). Interestingly, acetate-mediated cell death has exhibited multiple physiological hallmarks of prokaryotic apoptosis, including the presence of ROS, DNA damage, and reduced cellular respiration, suggesting that CidC activity promotes PCD in *S. aureus* as in eukaryotes (105).

The regulation of stationary phase cell death during aerobic growth in *S. aureus* involves multiple players, including CidA, CidB, CidC, CidR, and AlsSD (105, 205, 211, 212). The CidC (pyruvate:menaquinone oxidoreductase) and AlsSD (α -acetolactate synthetase/decarboxylase) activities counteract each other because they compete on the same substrate, pyruvate, for conversion either to acetate (pro-death factor), in the case of CidC, or to acetoin, a more neutral metabolite (prosurvival factor), in the case of AlsSD (105). During overflow metabolism, the LysR-type transcription regulator, CidR, activates the transcription of *cidABC* and *alsSD* to regulate cell death (212). Interestingly, CidA and CidB are known to be membrane-associated proteins, but the mechanism by which they affect stationary phase cell death by modulating levels of acetoin and acetate is not known (212). It has been suggested that CidB increases CidC activity, leading to the production of additional acetate and decreasing the production of acetoin, whereas CidA decreases CidC activity, redirecting the carbon flux toward the AlsSD pathway to generate acetoin. Collectively, stationary phase cell death is driven by CidC and CidB (pro-death factors) and opposed by AlsSD, CidA, and CidR (prosurvival factors) (212). CidB can also promote stationary phase cell death through ROS generation (211), which is known to affect stationary phase survival under the same tested conditions (105).

It is evident that acetate promotes PCD in various organisms. *Saccharomyces cerevisiae*, which is a unicellular yeast, undergoes PCD when exposed to acetic acid, and the dead cells exhibit PCD hallmarks similar to those of eukaryotic PCD (213). Acetic acid also potentiates apoptosis, but not necrosis, in colorectal carcinoma cells, suggesting that acetic acid induces an active cell death process (214). In these cells, caspases are activated in response to acetic acid stress. **Clearly, acetate and ROS are the major factors by which the *cidABC* operon mediates stationary phase cell death under conditions of excess glucose (105, 211). However, the molecular mechanism by which acetate triggers cell death and the advantages of having such an altruistic suicidal trait in the bacterial population are unknown. The aim of the studies described in this dissertation is to explore the molecular events responsible for cell death in *S. aureus* and to add to our understanding of PCD in *S. aureus*.**

Chapter 2: Materials and methods

2.1. Genetic manipulation

The strains and plasmids used in this study are listed in Table 1 and Table 2, respectively. We complemented *clpX*_{I265E} chromosomally with the full-length *clpX* under the control of its native promoter by phage transduction of the SaPI and integration of the plasmid pAQ21, as described previously (215).

To construct the *clpX*_{E188Q} variant using site-directed mutagenesis, the *clpX* gene harboring its native promoter was amplified using the primers listed in Table 3 with an NEB Q5 high-fidelity polymerase from genomic DNA. PCR fragments were resolved on agarose gel, and a pure PCR product was extracted using a DNA gel extraction kit (Thermo Fisher Scientific, USA). Briefly, the two *clpX* fragments were assembled into the PCR-amplified pJC1111 SAPI integrative vector using an NEBuilder HiFi DNA assembly cloning kit (New England Biolabs, Inc., Ipswich, MA, USA), generating a pAQ22 plasmid. Then the constructed plasmid was electroporated into *E. coli* E10B and plated on LB agar containing 100 µg/mL ampicillin for selection. The constructed plasmid was extracted using a Wizard plus SV Minipreps DNA Purification System (Promega, Madison, WI, USA) from E10B grown in LB for 14 to 15 hours with the appropriate antibiotic (100 µg/mL ampicillin); it was then electroporated into the RN4220-containing site-specific SaPI integrase (RN9011) and plated on tryptic soy agar (TSA) plates containing 0.1 mM CdCl₂. The ClpX_{E188Q} variant was transduced into the *clpX* null mutant using ϕ11 phage and plated on 0.1 mM CdCl₂ for selection. The *clpX::clpX*_{E188Q} variant was amplified from genomic DNA and sequenced at the University of Nebraska Medical Center sequencing facility to confirm the point mutation. As described above, complementation of the *clpX* null mutant was accomplished using the primers listed in Table 3, and the construct was integrated into the SAPI site of the *clpX* mutant.

To construct the *trx*B overexpression vector (controlled by *sarA*-P1), the *trx*B gene and pCM29 vector were amplified by PCR, purified with gel extraction, and assembled with the

NEBuilder HiFi DNA Assembly cloning kit to generate pAQ24. The constructed plasmid was extracted as described above and then electroporated into the *S. aureus* RN 4220 intermediate strain. Finally, the pAQ24 was phage transduced into JE2 using ϕ 11, and selection was performed in TSA containing 10 μ g/mL chloramphenicol.

To generate the Δ *spx* markerless deletion, we first used PCR amplification for the *trxB* with sarA-P1 from pAQ24 cloned into pJC1111 to generate pAQ69. Using the same steps described earlier, the plasmid was electroporated into *E. coli* (Luria–Bertani–ampicillin [LB Amp] 100 μ g/mL for selection), then electroporated into *S. aureus* RN9011, and finally transduced into JE2 (0.1 mM CdCl₂ for selection). A size of 1 kb of the up and down arms of the *spx* was amplified by PCR and cloned into the pJB38 allelic exchange vector to generate the pAQ5 plasmid. The plasmid was extracted as described, electroporated into *S. aureus* RN4220, and then phage transduced into JE2::pAQ69. Plates were grown at 30°C on TSA containing 10 μ g/mL of chloramphenicol to maintain plasmid replication. The allelic exchange process started with the streaking of JE2::pAQ69 on TSA (5 μ g/mL of chloramphenicol) and incubated at 43.5°C to force plasmid integration into the chromosome, generating a single recombinant. The single recombinant was regrown in TSB with shaking at 30°C. After three rounds of reinoculation with a 1:3000 dilution, the culture was serially diluted on TSA containing 100 ng/mL anhydrous tetracycline and incubated at 30°C. Visible colonies (tiny in the case of the *spx* mutant) were patched on TSA, TSA containing 10 μ g/mL chloramphenicol, and TSA containing 1 mM diamide to enhance the selection. The Δ *spx* was finally confirmed using the PCR. Complementation of the JE2::pAQ69 Δ *spx* mutant was performed using the low-copy, highly stable plasmid pAQ75. This plasmid was generated by cloning the *spx* with its native promoter into the pKK22 vector. As described above, pAQ75 was electroporated into *E. coli* E10B (LB Amp100 μ g/mL), then electroporated into *S. aureus* RN4220 (trimethoprim 10 μ g/mL), and finally phage transduced into JE2::pAQ69 Δ *spx*. All primers used here are listed in Table 3.

The *spx_{XC10A}* variant was also generated through allelic exchange using pAQ25. Using site-directed mutagenesis, a 2-kb fragment of *spx* containing a single nucleotide change was amplified by PCR and cloned into pJB38. The downstream steps of cloning, allelic exchange, and sequencing were performed as described earlier. The *spx_{XC10A}* variant in the *clpP* mutant background was chromosomally complemented with pAQ26, which is pJC1111 containing the wild-type *spx* driven by a native promoter. All primers used are listed in Table 3.

To construct the ClpP-resistant Spx, Spx^{DDD}, and *Spx*ΔC-HA, we used site-directed mutagenesis with the primers listed in Table 3. PCR fragments of *spx^{DDD}* and *spx*ΔC-HA were cloned into pKK22 and pJC1111, generating pAQ10 and pAQ20, respectively. Extracted plasmids were processed accordingly; pAQ10 was electroporated into *S. aureus* RN4220 (TSA with trimethoprim 10 μg/mL used for selection), whereas pAQ20 was electroporated into *S. aureus* RN9011 (selection was performed on TSA 0.1 mM CdCl₂). Primers are listed in Table 3.

All growth steps after electroporation or transduction were performed aerobically at 37°C with the appropriate antibiotic, except for specific steps during allelic exchange as described.

2.2. Strains and growth conditions

The *S. aureus* strain JE2 and its isogenic mutants used in this study were obtained from the Nebraska Transposon Mutant Library (216) and are listed in Table 1, except for *clpX* and *clpX_{I265E}* (217). Transposon mutants were retransduced into JE2 using ϕ11, and TSA plates containing 5 μg/mL erythromycin were used for selection (215, 216). After retransduction, all transposon mutants were confirmed by PCR using the gene-specific primers listed in Table 3.

To assess stationary phase viability, bacteria were grown aerobically from an initial OD₆₀₀ of 0.06, with agitation at 245 round per minute (rpm) at 37°C in TSB (Difco Laboratories, MI, USA) using a 10:1 (fask:volume) ratio. The TSB was supplemented with 45 mM glucose, either unbuffered or buffered to pH 7.3 with 100 mM 3-(N-morpholino) propanesulfonic acid, 4-morpholinepropanesulfonic acid (MOPS). Cell viability was monitored by subjecting bacterial

cells to serial dilution with 0.9% saline, followed by plating on TSA plates. Plates were then incubated aerobically at 37°C for at least 24 hours before the bacterial colonies were counted; the limit of detection was 10 colony forming units per mL (cfu/mL). To perform experiments involving the cross-substitution of cell-free media, 24-hour-old cultures from the wild-type strain and *clpP* mutant grown as described above were centrifuged at 4100 x g for 10 min in 50-mL conical tubes to obtain pellets of the bacterial cells. Culture supernatants were filtered using 0.2-µm filters (Sartorius, Goettingen, Germany) and cross-substituted into bacterial cell pellets that were washed with 0.9% saline. The pellets were resuspended in the corresponding supernatant, and the stationary phase viability was assessed by counting the colony-forming units per milliliter in serially diluted cultures. Growth curves were performed in 250-mL flasks with a 1:10 ratio in TSB (MilliporeSigma, Burlington, MA, USA) aerobically with shaking at 245 rpm at 37°C. Diamide was prepared in Dimethyl sulfoxide (DMSO) at a concentration of 1 M and added at the time of inoculation to a final concentration of 3 mM.

To assess survival following the antibiotic challenge, overnight bacterial cultures were inoculated in 25 mL of TSB supplemented with 14 mM glucose in a 250-mL flask to a final OD₆₀₀ of 0.06, and cultures were grown at 37°C with shaking at 245 rpm. At 5.5 hours of growth, the colony-forming units were counted as described above (Time 0) and cultures were challenged with chloramphenicol 400 µg/mL, tetracycline 25 µg/mL, trimethoprim 12.5 µg/mL, kanamycin 87.5 µg/mL, erythromycin 200 µg/mL, vancomycin 50 µg/mL, oxacillin 25 µg/mL, or gentamycin 25 µg/mL. Aliquots containing 200 µL of antibiotic-challenged cultures were collected and centrifuged at 16,000 x g, and the pellet was washed by resuspending it in 1 mL of 0.9% saline. After two rounds of thorough washing, the pellets were resuspended in 200 µL of saline, and then they were serially diluted and plated on TSA as described above so the survivors could be counted (218)..

2.3. Protein aggregation

Bacterial cells were grown aerobically in 120 mL of TSB-45 mM glucose with and without MOPS, as previously described for the survival assay. At the specified time points, 5 to 10 mL of the bacterial culture was collected for the isolation of the protein aggregates. The aggregates were isolated from bacterial cells as described by Engman et al. with minor modifications (219). Bacterial cultures were centrifuged at 4000 x g for 10 min, and the cell pellets were washed twice with 1X phosphate-buffered saline (PBS) before storage at -80°C. On the day of the experiment, cells were resuspended in 1 mL of cold 50-mM potassium phosphate buffer at pH 7. Cells were disrupted by shaking with glass beads for four cycles at 4°C with 5-second intervals. Each cycle was programmed for 23 seconds at 6100 rpm in a Precellys Evolution Homogenizer (Bertin Technologies, Montigny-le-Bretonneux, France). Glass beads were pelleted by centrifugation at 200 x g for 10 min. The protein concentration of the crude extract was determined using the Bradford protein assay according to the manufacturer's instructions (Bio-Rad, Hercules, CA, USA). The crude extract containing 250 µg of total protein was transferred into a 1.7-mL Eppendorf tube and centrifuged at 21,000 x g for 40 min at 4°C. The pellet was resuspended in buffer A (50 mM Tris, 150 mM NaCl, pH = 8) with 1% Triton X-100 and incubated at 4°C on a rotating platform for 2 hours, followed by centrifugation at 16,000 x g for 40 min at 4°C. After centrifugation, the pellet was resuspended in buffer A and centrifuged at 16,000 x g for 40 min at 4°C. The resulting pellet was resolubilized in 70 µL of rehydration buffer consisting of 7 M urea, 2 M thiourea, 4% (wt/vol) 3-[(3-cholamidopropyl)-dimethylammonio]-1-propanesulfonate (CHAPS), and 100 mM dithiothreitol (DTT). Thirty microliters of the insoluble fragment was loaded onto 10% SDS polyacrylamide gel, and the resolved protein aggregates were stained with Coomassie blue G-250. The stained gel was imaged and then densitometrically quantified using ImageJ software (National Institutes of Health, Bethesda, MD, USA).

2.4. Protein carbonylation

Bacterial cells were grown in 115 mL of TSB in 1-L flasks, and 2 mL of the culture was collected at the specified time points. Cells were centrifuged at 15,000 x g for 5 min, and the pellet was washed twice with 1 mL of PBS. Washed cells were resuspended in 1.5 mL of PBS with 50 mM DTT and disrupted by glass beads as described above. After centrifugation at 15,000 x g for 10 min, the protein concentration was determined by a NanoDrop 1000 spectrophotometer and 1 mg of protein was used to determine the carbonyl content as follows. The DNA was precipitated using 1% streptomycin sulfate and isolated by centrifugation at 11,000 x g for 10 min. Proteins from the supernatant were precipitated by adding 10% trichloroacetic acid (TCA), vortexed, and incubated for 30 min on ice. Precipitated proteins were centrifuged for 30 min at 12,000 x g at 4°C. Carbonyl-containing proteins were derivatized by incubation with 500 μ L of 10 mM 2,4-dinitrophenylhydrazine (DNPH) dissolved in 2 M HCl for 1 hour with vortexing every 10 to 15 min. After derivatization, samples were mixed with 500 μ L of 20% TCA and centrifuged at 11,000 x g for 3 min. Pellets were washed three times by adding 1 mL of 1:1 ethanol-ethyl acetate, incubating at room temperature for 10 min, and centrifuging at 11,000 x g for 3 min. Finally, the pellets were dissolved in 6 M guanidine in a 20-mM potassium phosphate buffer adjusted to pH 2.3 with trifluoroacetic acid; the absorbance was measured at 370 nm, and the carbonyl content was determined using an extinction coefficient of 22,000 M⁻¹cm⁻¹ (220).

2.5. Quantitative real-time PCR

RNA was extracted using the RNeasy Bacteria Kit according to the manufacturer's instructions (Qiagen, Germantown, MD, USA) from 1 mL of culture for all experiments that required a quantification of gene expression. To lyse the cells, we used the Precellys Evolution Homogenizer as described above, but it was set to two cycles of cell disruption. Following RNA extraction, the cDNA was synthesized using the QuantiTect Reverse Transcription Kit (Qiagen). The quantitative PCR was assessed using the LightCycler 480 SYBR green master mix (Roche) according to the

manufacturer's instructions for 1:20 diluted cDNA. We used the comparative threshold cycle (C_T) method to calculate the relative transcript levels, which were normalized to the amount of the *sigA* transcripts present in RNA samples (221).

2.6. Measurement of competitive fitness

Cultures of JE2 and its isogenic *clpP* or *clpX*_{I265E} mutants grown in TSB-45 mM glucose were used to assess competitive fitness. Following 24 hours of growth in media containing excess glucose, we used $\sim 10^7$ bacteria/mL of each strain for competition experiments. Due to the increased death of the wild-type strain at 72 hours into the stationary phase, competition experiments were initiated from $\sim 10^5$ to $\sim 10^6$ cfu/mL. The bacterial colony-forming units were counted on TSA plates with and without 5 μ g/mL erythromycin immediately after initiation of the competition and at 8 hours between tested strains. The competitive fitness was calculated using the Malthusian parameter (222) for competitors with the following formula: $w = \ln(M_f/M_i) / \ln(W_f/W_i)$, where f and i represent the counts of colony-forming units at the end (8 hours) and beginning (time 0) of the competition assay, respectively. M and W refer to mutant and wild type, respectively.

2.7. Electron paramagnetic resonance (EPR) spectroscopy

We used 10 OD units of 72-hour cultures resuspended in 1 mL KDD buffer (Krebs HEPES buffer, pH 7.4; 99 mM NaCl, 4.69 mM KCl, 2.5 mM CaCl₂, 1.2 mM MgSO₄, 25 mM NaHCO₃, 1.03 mM KH₂PO₄, 5.6 mM D-glucose, 20 mM HEPES, 5 μ M DETC, and 25 μ M deferoxamine) for determination of the ROS production. The bacterial suspensions were mixed with the ROS-sensitive spin probe CMH (working stock ~ 4 mM prepared in KDD buffer) to a final concentration of 200 μ M and incubated at room temperature for 15 min. A Bruker e-scan electron paramagnetic resonance (EPR) spectrometer (Bruker, Billerica, MA, USA) was used with the following acquisition parameters: field-sweep width, 60.0 gauss; microwave frequency, 9.75 kHz; microwave

power, 21.90 mW; modulation amplitude, 2.37 gauss; conversion time, 10.24 ms; time constant, 40.96 ms (Thomas, Chaudhari, Jones, Zimmerman, & Bayles, 2015).

2.8. SOD activity

A 2-mL culture of the wild-type strain and the *clpP* mutant grown in TSB-45 mM glucose was harvested at 24 hours and 72 hours and centrifuged at 16,000 x g for 5 min. The cell pellets were initially washed with saline before finally being resuspended in 0.5 mM KPO₄ buffer at pH 7.3 with 1 X EDTA free protease inhibitor (Roche). Following mechanical lysis of the cells using a bead beater, the clear lysate was retrieved by centrifuging the crude extract at 16,000 x g for 5 min at 4°C. The protein concentration was estimated using the Bradford protein assay (Bio-Rad) as per the manufacturer's instructions, and 10 µg of protein was used to evaluate the superoxide dismutase activity (SOD) activity using a SOD assay kit (Sigma-Aldrich, St. Louis, MO, USA).

The activity of SodA, SodM, and SodAM was evaluated under native conditions. Briefly, 20 µg of the cell lysate from the previous experiment (SOD activity) was resolved on 4% to 20% gradient native gel (Bio-Rad) under native running conditions in an ice-cooled running buffer at 200 v for 2 hours. An amount of 40 mL of solution A (0.05 M potassium phosphate buffer, pH 7, 1 mM EDTA, 0.25 mM NBT [nitro blue tetrazolium chloride]) and 2 mL of solution B (0.5 mM riboflavin) were mixed and submerged in the gel in the dark for 5 min. Excess staining solution was removed, and the gel was wrapped in plastic wrap and subjected to direct sunlight until the desired color developed (223)

2.9. Western blot analysis

Cell lysate from the SOD experiment above was used for the Western blot analysis. Simply, 10 µg protein was resolved on a reducing Tris-glycine SDS-PAGE 4% to 12% gradient gel (Bio-Rad) and transferred using the semidry method by the Pierce Power Blot Cassette system (Thermo Fisher Scientific) onto a nitrocellulose membrane (Schagger, 2006). Antibodies raised against *B. subtilis*

Spx were diluted to 1:1,500 in 5% skim milk in 0.01% PBST (224). Goat antirabbit secondary antibodies (Invitrogen, Carlsbad, CA, USA) were diluted 1:30,000. Immunodetection was performed using the Super Signal West Femto chemiluminescence kit (Thermo Fisher Scientific). Immunoblot images were acquired using the iBright CL1000 (Invitrogen). To detect the SodA, 10 µg of cytoplasmic protein was resolved on 12% SDS-PAGE gel under reducing condition, processed as described above. The SodA antibody was obtained through the NIH Biodefense and Emerging Infections Research Resources Repository, NIAID (Bethesda, MD, USA): Polyclonal Anti-*Bacillus anthracis* Superoxide Dismutase SODA-1 (Locus_Tag:BA_4499), Immunoglobulin G, Rabbit), NR-10506. SodA was used in a concentration of 1:7000 in 5% skim milk in 0.01% PBST. The concentration of secondary antibodies and the development was performed as described above for Spx.

2.10. LC-MS/MS analysis

For proteomics, 100 µg of protein per sample from three biological replicates per group was resuspended in 100 mM ammonium bicarbonate. The samples were digested with Pierce MS-grade trypsin overnight at 37°C following reduction with 10 mM DTT at 56°C for 30 min, and alkylation with 50 mM iodoacetamide was carried out for 20 min in the dark. The resulting peptides were cleaned using PepClean C18 spin columns (Thermo Scientific) and resuspended in a solvent containing 2% acetonitrile (ACN) and 0.1% formic acid (FA). An amount of 500 ng of each sample was loaded onto the trap column Acclaim PepMap 100 75 µm x 2 cm C18 LC Columns (Thermo Scientific) at flow rate of 4 µL/min and then separated with a Thermo RSLC Ultimate 3000 (Thermo Scientific) on a Thermo Easy-Spray PepMap RSLC C18 75 µm x 50 cm C18 2-µm column (Thermo Scientific) with a step gradient of 4% to 25% solvent B (0.1% FA in 80% ACN) for 10 to 100 min and 25% to 45% solvent B for 100 to 130 min at 300 nL/min and 50°C with a 155-min total run time. The eluted peptides were analyzed by a Thermo Orbitrap Fusion Lumos Tribrid (Thermo Scientific) mass spectrometer in a data-dependent acquisition mode. A full-scan

MS survey (from m/z 350 to 1800) was acquired in the Orbitrap with a resolution of 120,000. The AGC target for MS1 was set as 4×10^5 , and the ion filling time was set as 100 ms. The most intense ions with a charge state from 2 to 6 were isolated in a 3-second cycle and fragmented using HCD fragmentation with 35% normalized collision energy and detected at a mass resolution of 30,000 at m/z 200. The AGC target for MS/MS was set as 5×10^4 and the ion filling time of 60-ms dynamic exclusion was set for 30 seconds with a 10-ppm mass window. Protein identification was performed by searching MS/MS data using PEAKS Studio X+ software (Bioinformatics Solutions, Inc., Waterloo, Ontario, Canada) against an in-house database created from the predicted proteins of *S. aureus* USA300 FPR3757. The search was set up for full tryptic peptides with a maximum of two missed cleavage sites. Oxidized methionine was included as a variable modification and the carbamidomethylation of cysteine was set as the fixed modification. The precursor mass tolerance threshold was set at 10 ppm, and the maximum fragment mass error was 0.02 Da. The significance threshold of the ion score was calculated based on a false discovery rate of 1% or less. Qualitative analysis was performed using the Progenesis QI proteomics 4.2 (Nonlinear Dynamics). Statistical analysis was performed using the ANOVA, and the Benjamini–Hochberg (BH) method was used to adjust the p -values for multiple testing using the false discovery rate. The adjusted p -value of .05 or less was considered as significant.

2.11. Flow cytometry

Bacteria were grown in 25 mL of TSB-45 mM glucose or TSB-45 mM glucose supplemented with MOPS in 250-mL flasks as described above, and flow cytometry was performed exactly as previously described (105). All analyses were performed using 24-hour and 72-hour cultures of bacteria on a BD LSRII flow cytometer (Beckton Dickinson, San Jose, CA, USA). Harvested cells were washed twice and diluted to a final concentration of 10^7 cells/mL in PBS. Cells were stained by incubation for 30 min with 5 mM 5-cyano-2,3-ditolyl tetrazolium chloride (CTC) and 15 mM 3-(p -hydroxyphenyl) fluorescein (HPF) followed by FACS analyses at a flow

rate of ~1000 cells/second (225, 226). A total of 10,000 events were collected for each sample. Bacteria were distinguished from the background using a combination of forward-scattered light (FSC) and side-scattered light (SSC). Excitation was at 488 nm using an argon laser. HPF emission at 530 to 630 nm was detected with a 505-nm long-pass mirror, and CTC emission was detected at 695 to 640 nm with a 685-nm long-pass mirror. Raw data were analyzed using FlowJo software (FlowJo LLC, Ashland, OR, USA).

For experiments with rifampicin, *S. aureus* was grown in 25 mL TSB-45 mM glucose in a 250-mL flask as described above. At 24 hours of growth, cells were treated with 200 µg/mL of rifampicin. Cells were collected at 72 hours and subjected to CTC and HPF staining as described above.

2.12. Flow-cell biofilm assay and confocal laser scanning microscopy (CLSM)

Overnight cultures of JE2 and *clpX*_{I265E} grown for 20 hours were adjusted to an OD of 0.002 in 1.5 mL TSB. An amount of 1 mL of each culture was injected into the dual-channel transmission flow-cell system (BioSurface Technologies, Inc., Bozeman, MT, USA) and then incubated statically for 1 hour. After 1 hour, a continuous flow of 10% TSB medium (Millipore) supplemented with 0.2% glucose at a rate of 0.5 mL/min was pumped into each flow chamber. After 24 hours, the medium flow was stopped and the grown biofilm in every flow cell was stained with 3 mL of the cell-permeable fluorophore SYTO-9 at a final concentration of 1.3 µM to stain viable cells, whereas 2 µM of TOTO-3 fluorophore was used to stain dead cells (99).

After 10 min of incubation, the flow cell was imaged using the Zeiss 710 META laser-scanning confocal microscope (Zeiss, Oberkochen, Germany). SYTO-9 was excited with the laser at 488 nm, and the emission was collected at 515 ± 25 nm using a band-pass filter. TOTO-3 was excited with the laser at 633 nm, and the emission was collected at 680 ± 30 nm using a band-pass filter. Z-stack images were taken using a 40X objective analyzed using COMSTAT2 to obtain the

biofilm thickness, biomass (live and dead), and roughness coefficient (Heydorn, 2000 #214; Vorregaard, 2008 #215). Three-dimensional images were constructed using Imaris software (Bitplane, Concord, MA, USA).

2.13. Determination of acetate in the culture supernatant

JE2 and its isogenic mutant *clpP* mutants were grown in 115 mL of either TSB-45 mM glucose or TSB-45 mM glucose buffered with 100 mM MOPS with pH adjusted at 7.3. For the first 12 hours of growth and from 24 h to 120 h, 1.5 mL culture was harvested into 1.7 mL Eppendorf tube and centrifuged at 18,000xg for 5 minutes. The cell free supernatant was transferred into new clean 1.7 mL Eppendorf tube, then stored in – 80C° until the day of experiment. Acetate was measured using commercially available kit (cat#10 148 261 035Roch, Germany) according to the manufactured instruction. Supernatant was diluted 1:10 in if the sample absorbance at 340 nm was above the standard curve. The analysis was performed in 96-well plate and the absorbance was taken using TECAN Infinite 200 PRO (Switzerland).

2.14. RNA-seq analysis

Cultures JE2 wild type and its isogenic mutant *sp_{XC10A}* were grown in TSB 14 mM glucose until they reach 1 optical density units (OD). Each group of three biological replicates were treated with 0.5 mM diamide for 15 minutes then samples were collected for RNA extraction, and untreated controls were collected at the same time. RNA was extracted by Dr. Dorte Frees Lab at Department of Veterinary Disease Biology, University of Copenhagen. The RNA concentration of all samples was measured in duplicate using the Qubit BR RNA assay. The RNA quality and integrity were confirmed for selected samples using TapeStation with RNA ScreenTape (Agilent Technologies). Twelve samples were selected and depleted for rRNA using the Ribo-zero Magnetic kit (Illumina Inc.) according to the manufacturer's instructions. Any potential residual DNA was removed using the DNase MAX kit (MoBio Laboratories Inc.) according to the manufacturer's instructions. After

rRNA depletion and DNase treatment the samples were cleaned and concentrated using the RNeasy MinElute Cleanup kit (QIAGEN) and successful rRNA removal confirmed using TapeStation HS RNA Screentapes (Aligent Technologies). The samples were prepared for sequencing using the TrueSeq Stranded Total RNA kit (Illumina Inc.) according to the manufacturer's instructions. Library concentrations were measured using Qubit HS DNA assay and library size estimated using TapeStation D1000 ScreenTapes (Aligent Technologies). The 22 samples were pooled in equimolar concentrations and sequencing on an Illumina HiSeq2500 using a 1x50 bp Rapid Run (Illumina Inc).

The genome of *S. aureus* USA300 was obtained from the publication (227) website (downloaded through this link). Bioinformatic processing and analysis Raw sequence reads in fastq format were trimmed using USEARCH (v10.0.2132) (228) fastq_filter with the settings -fastq_minlen 45 -fastq_truncqual 20. The trimmed transcriptome reads were depleted of rRNA using BBDuk (229) using the SILVA database as reference database (230). The reads were then mapped to either the genome or sRNAs of *S. aureus* USA300 using minimap2 (v2.8-r672) (231). The count tables were imported to R (232), processed using the default DESeq2 workflow (233) and visualized using ggplot2. PCA analysis of overall sample similarity was done using DESeq2 normalized counts (square root transformed), through the vegan (234) ampvis R packages (235). DNASense ApS | Niels Jernes Vej 10 | DK-9220 | CVR-36036869 | www.dnasense.com 19 KU [CP292].

Table 2-1. List of strains used in this study.

Strain	Description	Source
<i>S. aureus</i> JE2	<i>S. aureus</i> USA300 LAC 13C cured of endogenous plasmids	(216)
JE2 <i>clpP</i>	<i>Bursa aurealis</i> transposon mutant Erm ^R	(216)
JE2 <i>clpC</i>	<i>Bursa aurealis</i> transposon mutant Erm ^R	(216)
JE2 Δ<i>clpX</i>	<i>clpX</i> in-frame deletion, Erm ^R	(217)
JE2 <i>clpP::clpP</i> (<i>clpP</i> comp)	Chromosomal complementation (SaPI site) of <i>clpP</i> mutant, CdCl ₂ and Erm ^R	(236)
JE2 <i>clpX</i>_{1265E}	JE2 expressing ClpX _{1265E} variant, Erm ^R	(217)
JE2 <i>clpX</i>_{1265E}::<i>clpX</i> (<i>clpX</i> comp)	Chromosomal complementation of JE2 ClpX _{1265E} variant, CdCl ₂ ^R , Erm ^R	This study
JE2 <i>sodA</i>	<i>Bursa aurealis</i> transposon mutant, Erm ^R	(216)
JE2 <i>sodM</i>	<i>Bursa aurealis</i> transposon mutant, Erm ^R	(216)
JE2 <i>kata</i>	<i>Bursa aurealis</i> transposon mutant, Erm ^R	(216)
JE2 <i>ahpC</i>	<i>Bursa aurealis</i> transposon mutant, Erm ^R	(216)
JE2 <i>clpPsodA</i>	<i>Bursa aurealis</i> transposon mutant, Tet ^R and Erm ^R	This study
JE2 <i>clpPsodM</i>	<i>Bursa aurealis</i> transposon mutant, Tet ^R and Erm ^R	This study
JE2 <i>clpPkata</i>	<i>Bursa aurealis</i> transposon mutant, Tet ^R and Erm ^R	This study
JE2 <i>clpPahpC</i>	<i>Bursa aurealis</i> transposon mutant, Tet ^R and Erm ^R	This study
JE2 <i>yjbH</i>	<i>Bursa aurealis</i> transposon mutant, Erm ^R	(216)
JE2 <i>spx</i>_{C10A}	JE2 expressing SpxC10A variant chromosomally driven by its native promoter	This study
JE2 <i>spx</i>_{C10A} <i>clpP</i>	<i>Bursa aurealis</i> transposon mutant, Erm ^R in spxC10A generated by allelic exchange	This study
JE2::pAQ69	Chromosomal overexpression (SaPI site) of <i>trxB</i> controlled by the P1 <i>sarA</i> promoter, used as background to generate Δ <i>spx</i> using allelic exchange, CdCl ₂ ^R	This study
JE2::pAQ69 Δ<i>spx</i>	Δ <i>spx</i> deletion generated in JE2::pAQ69 using allelic exchange, CdCl ₂ ^R	This study

JE2::pAQ69 <i>spx</i>_{C10A}	JE2::pAQ69 expressing SpxC10A variant chromosomally driven by its native promoter generated by allelic exchange, CdCl ₂ ^R	This study
JE2::pAQ69 Δ<i>spx</i> pAQ75	In trans complementation of Δ <i>spx</i> deletion using low-copy vector, CdCl ₂ ^R , Tmp ^R	This study
JE2::pAQ69 <i>spx</i>_{C10A} pAQ75	In trans complementation of <i>spx</i> _{C10A} variant using low-copy vector, CdCl ₂ ^R , Tmp ^R	This study
JE2<i>spx</i>_{C10A} <i>clpP</i>::<i>spx</i>	Chromosomal complementation (SapI site) of JE2 <i>spx</i> _{C10A} mutant using <i>spx</i> driven by native promoter, Erm ^R , CdCl ₂ ^R	This study
JE2 pKK22	JE2 harboring the highly stable, low-copy-number plasmid in staphylococci	This study
JE2::<i>spx</i>ΔC-HA	JE2 expressing Spx lacks the C-terminal domain (last 12 amino acids were deleted) from SapI site controlled by the <i>spx</i> native promoter. The Spx variant was tagged with an HA tag at the C-terminal, CdCl ₂ ^R	This study
JE2 <i>spx</i>^{DDD}	JE2 expressing Spx ^{DDD} driven by <i>spx</i> native promoter, coned into pKK22 plasmid, Tmp ^R	This study
JE2 pVT1	JE2 expressing dsRED in trans driven by <i>sarA</i> -P1 promoter, pCM29 backbone, Cm ^R	This study
<i>clpP</i> pVT1	JE2 expressing dsRED in trans driven by <i>sarA</i> -P1 promoter, pCM29 backbone Cm ^R	This study
JE2 <i>trx</i>B	JE2 expressing thioredoxin reductase TrxB controlled by <i>sarA</i> -P1 promoter, pCM29 backbone (Pang, 2010 #213), Cm ^R	This study
JE2::pJC1111	JE2 harboring the SapI integrating vector pJC1111, CdCl ₂ ²	This study
<i>E. coli</i> E10B	Electrocompetent <i>E. coli</i>	Invitrogen
<i>S. aureus</i> RN4220	<i>S. aureus</i> intermediate strain	(215, 237)
<i>S. aureus</i> RN9011	<i>S. aureus</i> intermediate strain specifically used to clone plasmid using the pJC1111 backbone, strain harboring pRN7023 plasmid, Cm ^R	(238)
<i>S. aureus</i> 8325-4	<i>S. aureus</i> strain	(237)
<i>S. aureus</i> 8325-4 Δ<i>spx</i>	<i>S. aureus</i> intermediate strain specifically used to clone plasmid using the pJC1111 backbone, strain harboring pRN7023 plasmid, Cm ^R	(239)

<i>S. aureus</i> 8325-4 Δspx	<i>S. aureus</i> intermediate strain specifically used to clone plasmid using the pJC1111 backbone, strain harboring pRN7023 plasmid, Cm ^R	(239)
--------------------------------------	---	-------

Table 2-2. List of plasmids used in this study

Plasmid	Description	Source
pAQ21	SapI integrating vector carrying <i>clpX</i> gene driven by its native promoter to complement <i>clpX</i> _{I265E} mutant	(217)
pAQ22	SapI integrating vector carrying <i>clpX</i> _{E188Q} gene driven by <i>clpX</i> native promoter	This study
pAQ57	SapI integrating vector carrying <i>clpP</i> gene driven by its native promoter to complement <i>clpP</i> mutant	(236)
pAQ10	Spx ^{DDD} driven by <i>spx</i> native promoter, cloned into pKK22 plasmid backbone	This study
pAQ25	Vector to generate markerless <i>spx</i> deletion using pJB38 backbone (allelic exchange)	This study
pAQ24	<i>trxB</i> overexpression driven by <i>sarA</i> promoter in pCM29 backbone	This study
pAQ75	Low-copy plasmid expressing <i>spx</i> driven by its native promoter	This study
pKK22	Low-copy plasmid	(240)
pAQ69	<i>trxB</i> overexpression driven by <i>sarA</i> promoter cloned into SapI integration vector pJC1111	This study
pAQ26	<i>spx</i> gene driven by native promoter cloned into SapI integration vector pJC1111; for chromosomal <i>spx</i> complementation	This study
pAQ25	Vector to generate <i>spx</i> _{C01A} variant using pJB38 backbone (allelic exchange)	This study
pAQ5	Spx deletion vector to delete <i>spx</i> in pJB38 backbone	This study
pVT1	dsRED cloned into backbone pCM29 to generate <i>sarA</i> -P1 expressing dsRED instead of GFP	—
pAQ20	Encodes ClpP-resistant Spx (<i>spx</i> Δ C-HA) cloned into SapI integration vector pJC1111	This study

Table 2-3. List of primers used in this study

Primer name	Sequence 5'-3'		Source
SaPI1_fwd	gtgcttcaccagcaccacatgctg	Confirm SapI integration	(238)
pJC1111_fwd2	ggattagtttgagctgtcttggtcattga ttgc		This study
ahpC_fwd	tgcttcaggaaactgacg	Confirm transposon	This study
ahpC_rev	aaccaaggctggcaacgaat		
kat_fwd	gtccaattgcaccacat	Confirm transposon	This study
kat_rev	atgccacattctgtgcatg		
sodA_fwd	gttgaccagtcactgcttg	Confirm transposon	This study
sodA_rev	acctcttggcacagactcat		
sodM_fwd	acaatgtacgtacgtgct	Confirm transposon	This study
sodM_rev	acacctttagatgctccac		
clpP_F	ttctacagtattgaacaac	Confirm transposon	This study
clpP_R	tgcagtaagaagtatcacg		
clpC_F	ggtagattaactgagcgtgc	Confirm transposon	This study
clpC_R2	cgctctcaaattcaccacg		
RTPCR spx_F	cctggcttattacgtcgtcca	Real time PCR for <i>spx</i>	This study
RTPCR spx_R	accatacgttggtcttctgt		
RTPCR clpP_F	acaagcgcaagactcagaga	Real time PCR for <i>clpP</i>	This study
RTPCR clpP_R	ccattgatgcagccataccg		
RTPCR clpX_F	ttggtggtgcctttgatggt	Real time PCR for <i>clpX</i>	This study
RTPCR clpX_R	ggcttgcaaattcttctgggc		
RTPCR sodA_F	gttcaggttgggcttggtta	Real time PCR for <i>sodA</i>	This study
RTPCR sodA_R	gcgtgttcccatagctctaaa		
RTPCR ahpC_F	attaacgctgacggaattgg	Real time PCR for <i>ahpC</i>	This study
RTPCR ahpC_R	tccatttagctgggcatac		

JE2 RT sigA_F	aactgaatccaagtgatcttagtg	Real time PCR for <i>sigA</i>	This study
JE2 RT sigA_R	tcacaccttggtcaatacgtttg		
RTPCR trxB_F	caccgtcgtgatgagttacg	Real time PCR for <i>trxB</i>	This study
RTPCR trxB_F	tgacacagaacccactttgc		
pAQ16_seq_f	ggccaacaggtagtggtaaa	Sequencing primers to confirm clpXE188Q mutant	This study
pAQ16_seq_r	ataccatcaaaggcaccacc		
pCM29_fwd	gaattcgtaatcatgtcatagc	Amplify pCM29 backbone for pAQ24	This study
pCM29_rev	aaataatcatcctcctaaggtagcc		
trxB_fwd	ccttaggaggatgattattatgactgaaa tagattttgatatagc	Amplify trxB gene to generate pAQ24 plasmid	This study
trxB_rev	tatgacatgattacgaattcctaagcttgat cgtttaaatg		
YjbH_F2	tatcacctgtaagtaaaatc	Confirm transposon	This study
YjbH_R2	tttaggcatttttagattcc		
pJB38_fwd	aagcaaagtacagggcgatgcatcaag cttattttaattatactctatc	Amplify pJB38 backbone to construct allelic exchange plasmids, pAQ5 and pAQ25	This study
pJB38_rev	tgcttgtaattcatgattcgtagcattcaca aaaataggc		
Spx_fwd	aagcaaagtacagggcgatgaaatgcc tactttcttagtaatatattaataattatc	Amplify spx with its native promoter to construct pAQ20	This study
Spx_rev	tgcttgtaattcatgattcgtaaatcgat cacgttggtgcttcttgtaattg		
Spx_UP_fwd	cctttcgtcttcaagaattccgtctaataat gaaatgaagtttttag	To amplify UP arm for pAQ5	This study
Spx_UP_rev	gttattagtcacggaatgcatgttcttg		

Spx_DN_fwd	gacattccgtgactaataaccatttaacta tgtgtc	To amplify UP arm for pAQ5	This study
Spx_DN_rev	ttgcatgcctgcaggctgactgtctgttg gataagcaaattc		
Spx seq-F1	atacctggcttgtgtcacg	To amplify <i>spx</i> region for sequencing	This study
Spx seq-R1	gtcgaacttgagctgttacg		
pKK22_fwd	cgaatcatgaattacaagcaaaag	To amplify pKK backbone to for pAQ10	This study
pKK22_rev	catcgctgtcactttgc		
pKK22 seqF	gcaacgtatcttatttaaagtgcg	Confirmatory primers for pKK22 cloning	This study
pKK22 seqR	ggtattttaaagtgatcaaaggcg		
spx-HA_tag_fwd	cggccgctgcatgcctgcaggaattcga aatgcctactttc	To amplify <i>spx</i> with its native promoter for pAQ20 cloning	This study
spx-HA_tag_rev	ggatccccgggtaccgag		
pJC1111_fwd	ggatccccgggtaccgag	To amplify pJC1111 backbone for cloning	This study
pJC1111_rev	ctgcaggcatgcagcggc		
pJC1111_UP	ttttgtgatgctcgtcagggg	Confirm cloning into pJC1111 vector	This study
pJC1111_DN	tcaggcgcgcctattctaaa		
pJC1111_seq_fwd	cttttacggttctgcct	Sequencing primer to confirm pJC1111 insert	This study
pJC1111_seq_rev	agtgacacgccttgttgaga		
Spx-HA tag OUT2	gttacaagaacatgacattccgtatacgg agcgta	Confirm integration of pAQ20 and pAQ26, used with SaPI1_fwd	This study
ClpX_fwd	cttcgtcttcaagaattcgtcttcattaat attaaattacaaaaatgag	Primers to amplify <i>clpX</i> with its native promoter to construct pAQ22 (site directed mutagenesis)	This study
ClpX_UP_rev	caattttatcaatttgatctacataaataata ccttttcg		
ClpX_fwd-2	ttatgtagatcaaattgataaaattgcacg taaac	Primers to amplify <i>clpX</i> to construct pAQ22 (site directed mutagenesis)	This study

ClpX_rev	ctgcaggctcgactctagaggtttatattcct cactttttatattctc		
pAQ24_fwd	cggccgctgcatgcctgcaggctagcct gatattttgac	To amplify <i>trxB</i> gene with sarA promoter from pAQ24 to construct pAQ69	This study
pAQ24_rev	agctcgggtacccggggatccttaagctt gatcgtttaaag		
Spx_UP_fwd2	cgaggccctttcgcttcaattttctgttg ggtcttg	To amplify UP arm of <i>spx</i> to construct pAQ25	This study
Spx_UP_rev2	ggcaagatgttgacttggtgaagtaaat aatgttac		
Spx_DN_fwd2	ttaccaagtgaacatcttgccgtaaag cg	To amplify DN arm of <i>spx</i> to construct pAQ25	This study
Spx_DN_rev2	ttgcatgcctgcaggctgaccatcagac atattcatatatcttc		
Spx_fwd 3	cggccgctgcatgcctgcagttaatgc ctactttctagtaatatTTAATAATTATC	To amplify <i>spx</i> gene with native promoter to construct pAQ26	This study
Spx_rev 3	agctcgggtacccggggatccttagtcaa ccatacgttg		

Chapter 3: Staphylococcal ClpXP protease targets the cellular antioxidant system to eliminate fitness-compromised cells in stationary phase

3.1 Introduction

Bacterial pathogens can efficiently switch between growth and non-growing stationary states in response to changes in nutrient status and environmental challenges (241, 242). Often, the entry into stationary phase is triggered by nutrient limitation imposed by the host or due to competition with other microbial cohabitants (243, 244). Multiple stresses, including changes in pH, temperature and osmolarity, can also limit active growth (245). The physiological and adaptive responses to stress that accompany the transition of bacterial cells to a non-growing state are generally optimized for long-term survival (201). These changes enhance persistence in pathogens and make them tolerant to various stressors, including antibiotics and the host immune system (201, 241). However, the fate of bacterial cells within a stationary phase population that undergo stress-induced cellular damage remains unclear. Such cells may become unfit for subsequent growth and may need to be eliminated. Their removal would allow competition for limiting nutrients to be confined to healthier populations and would also ensure that the surviving population is fit for re-entry into the growth cycle under more favorable conditions.

We have previously utilized *Staphylococcus aureus* as a model bacterial pathogen to study stationary phase survival dynamics (105, 212). When grown under conditions of excess glucose, *S. aureus* prematurely enters the stationary phase before glucose is completely exhausted from the media (105). Interestingly, the bacterial cells continue to consume glucose and excrete acetate as a byproduct even though growth is arrested, which suggests that growth and carbon catabolism are uncoupled at this stage. The early entry into the stationary phase under these conditions results from the weak acid properties of acetate. As the pH of the culture shifts towards the pKa of acetate (pH, 4.8) during growth, a net movement of protonated acetate into cells is observed, which results in cytoplasmic acidification (105). This process initiates a series of events during stationary phase

that is not seen when cells are grown under lower glucose concentrations. Notably, cells grown in excess glucose have a lower respiratory potential, produce significant levels of endogenous reactive oxygen species (ROS) and accumulate chromosomal damage. These events culminated in cell death, which progressed throughout the population in stationary phase. Both, the observed decrease in cell viability and the associated hallmarks of cell death could be avoided if acetate production was decreased by the genetic inactivation of *cidC* (pyruvate: menaquinone oxidoreductase) or if the entry of protonated acetate into cells was limited by controlling the decline in extracellular pH with MOPS buffer (pH, 7.4) (105). Thus, acetate-mediated cytoplasmic acidification directly potentiates cell death in stationary phase.

Proteolysis is a conserved process that takes place in all organisms to enforce protein quality control and modulate the intracellular levels of native proteins (246, 247). In bacteria, the ClpP proteases comprise one of the important AAA+ proteolytic machines. *S. aureus* encodes the ClpXP and ClpCP proteases (247). The ClpP subunits assemble as two homo-heptameric rings to form a barrel structure with peptidase activity. The ClpX and ClpC subunits are ATPases that associate with the ClpP barrel as hexameric rings and provide substrate specificity through direct interaction with substrates or specific adaptor proteins (247). Staphylococci that encounter toxic levels of acetate during growth are reported to increase expression of the *clp* genes presumably to maintain protein quality in these cells (248).

Here, we explore the significance of ClpP proteolysis in stationary phase cells that are exposed to acetic acid derived from glucose catabolism. We demonstrate that acetate-mediated intracellular acidification induces protein oxidation and protein aggregation in stationary phase cells. Although the accumulation of oxidized protein aggregates in cells is thought to be cytotoxic, the observed cell death in stationary phase cells do not directly result from passive toxicity arising from protein damage (249, 250). Instead, we demonstrate that damaged cells die from the degeneration of cellular antioxidant capacity catalyzed by the ATP-dependent ClpXP proteolytic machinery. The active process of eliminating cells with extensive protein damage through ClpXP-

dependent proteolysis ensures the survival of the fittest cells in stationary phase. This activation of cell death is not unique to acetate-mediated weak acid stress. Antimicrobials that interfere with protein biosynthesis can also variably induce *clpP* expression and promote ClpXP-dependent cell death in non-growing staphylococci suggesting a broader, more conserved, and beneficial role for ATP-powered cell death processes in bacteria.

3.2 Results

Acetate increases protein oxidation and aggregation under acidic conditions

Since cytoplasmic proteins are sensitive to the oxidation status and pH of their environment, we initially predicted that cell death in stationary phase in response to acetate-mediated intracellular acidification might result from protein damage. To test this hypothesis, we measured the levels of protein oxidation and aggregation under conditions that caused cytoplasmic acidification (105). *S. aureus* JE2 was cultured in media supplemented with excess glucose (45 mM), where acetate accumulated to approximately 37 mM and the extracellular pH remained close to 4.8 throughout the stationary phase measurements (Fig. 3.1A). The protein oxidation status was determined by measuring the carbonyl content of total cytoplasmic protein fraction and protein aggregation was measured as the SDS-insoluble protein fraction from the total cellular protein pools. We observed that the levels of carbonylated proteins and protein-aggregates increased throughout staphylococcal growth as the media acidified (Fig. 3.2A-B and Fig. 3.1A). Additionally, cell viability decreased over 7-logs during stationary phase (Fig. 3.2C and Table. 3.1). Importantly, the levels of protein damage and the rate of cell death were notably lower when cells were grown in media that was buffered to a pH 7.4 with 100 mM MOPS (Fig. 3.2A-C and Table. 3.1), a condition that prevented prolonged exposure of cells to the toxic effects of acetate (Fig. 3.1B) despite the high levels of glucose in the media (105). Acetate mediated cell death in stationary phase could also be prevented by inactivating *ackA*, the major contributor of acetate in *S. aureus*

(Fig. 3.1C-D) (251). However, further analysis of the *ackA* mutant was not attempted due to pleiotropic effects of this mutation on cell physiology. Together, these observations highlight protein oxidation and protein aggregation as important correlates of stationary phase cell death following acetate stress.

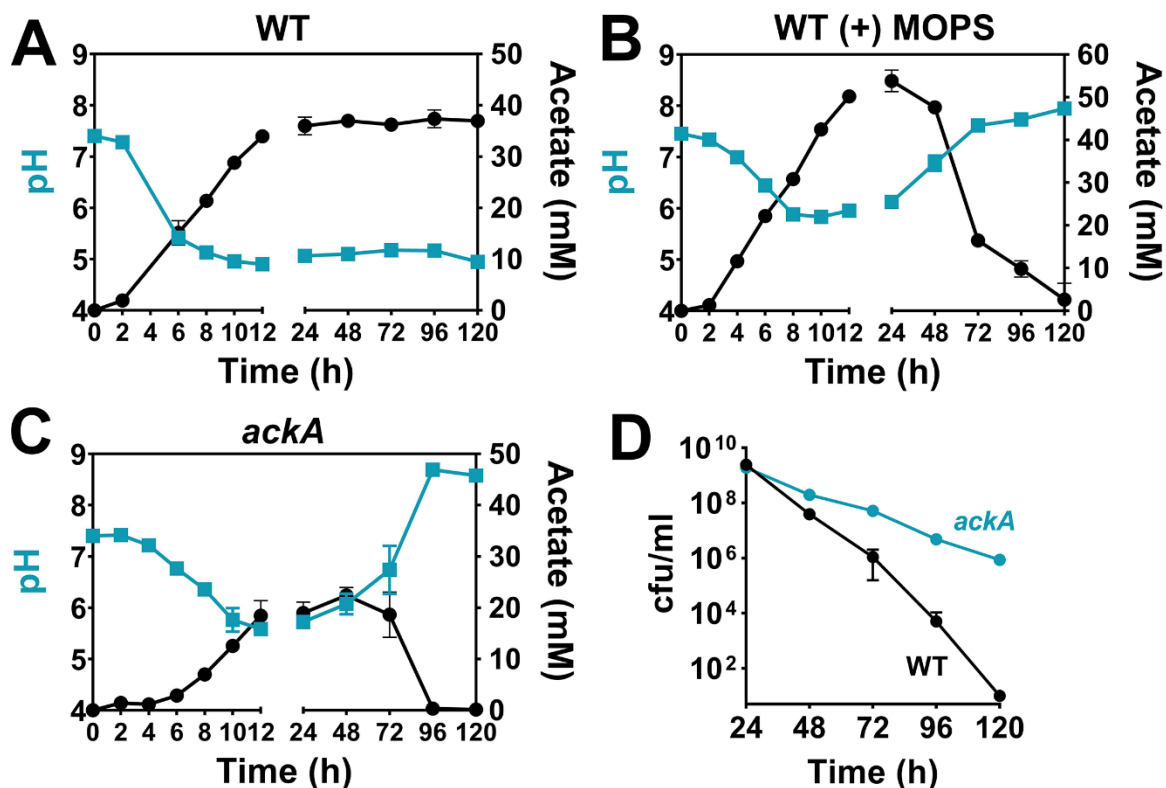


Figure 3.1. Acetate production and pH profile of *S. aureus* .

The extracellular acetate concentrations of culture supernatants (solid circles) from the (A) WT (unbuffered media), (B) WT grown in MOPS buffered media and (C) *ackA* mutant (unbuffered media) were determined over 120 h using a commercially available kit (Roche). The pH (solid squares) was determined using a pH probe (n=3, Mean \pm SD). (D) Cell viability of the WT and *ackA* mutant were measured in stationary phase following growth in TSB-G (n=3, Mean \pm SD).

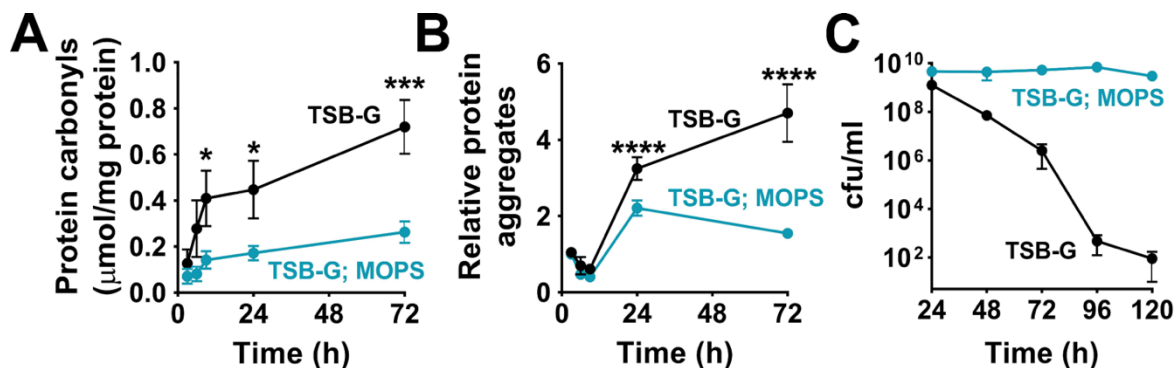


Figure 3.2. Acetic acid induces protein damage and cell death.

The toxicity of acetic acid on staphylococci, was distinguished by growth in MOPS buffered (100 mM, pH 7.3) and unbuffered TSB. Acetic acid remains as charged anions in MOPS buffered media, preventing its entry into cells. (A) Protein oxidation was determined at different stages of growth by measuring the carbonyl content of intracellular proteins ($n=3$, Mean \pm SD). (B) Protein aggregates were measured as the detergent-insoluble fraction of total intracellular proteins. The aggregates were isolated, resolved by SDS-PAGE and quantified using ImageJ software. The fold-differences in protein aggregate levels are relative to those observed at 3 h of growth (mid-exponential phase). ($n=5$, Mean \pm SD). (C) Cell viability in stationary phase was determined by enumeration of total bacterial colony forming units (cfu) following dilution plating. TSB-G, TSB supplemented with 45 mM glucose. Two-way ANOVA with Sidak's multiple comparison post-test; * $P \leq 0.05$, *** $P \leq 0.001$, **** $P \leq 0.0001$.

ClpXP catalyzed proteolysis is essential for acetate-mediated cell death

The accumulation of oxidized proteins and protein-aggregates can themselves have toxic sequelae resulting in the death of the organism (252). In *S. aureus*, ClpP has been described as the major intracellular protease that is involved in protein quality control and is capable of recycling damaged or unneeded proteins (247). Accordingly, we reasoned that the mutation of *clpP* should increase the rate of cell death due to the accumulation of damaged proteins. Upon evaluation of the cytoplasmic protein aggregates and oxidized proteins in the *clpP* mutant, we confirmed an increase in the level of protein damage relative to the parental strain (Fig. 3.3A-B). The increase in protein aggregates over the wild-type strain was primarily observed in the exponential phase (Fig. 3.3B). In comparison, we detected a more notable increase in protein oxidation in the *clpP* mutant over time and into stationary phase (Fig. 3.3A). To determine whether the elevated levels of protein damage following *clpP* mutation increased the rate of staphylococcal cell death, we assessed the survival of a *clpP* mutant over the stationary phase. Unexpectedly, the rate of stationary phase cell death was significantly lower in the *clpP* mutant than the WT strain (Fig. 3.3C and Table. 3.1), which suggested that cell death did not result from protein damage ‘per se,’ but was a consequence of the ClpP activation that followed. Complementation of the *clpP* mutant by introducing the *clpP* allele under the control of its native promoter, within the SaPI chromosomal locus fully restored the rate of cell death in the *clpP* mutant to WT levels (Fig. 3.3C and Table. 3.1), which confirmed a role for ClpP in promoting cell death.

The observed decrease in cell death of the *clpP* mutant did not result from a reduction in extracellular acidification as the concentration of acetate and pH in stationary phase closely matched those of the WT under all tested culture conditions (compare Fig. 3.4A-B and Fig. 3.1A-B). Neither were there any specific extracellular factors excreted by the WT that could induce cell death in the *clpP* mutant, as cross-substitution of cell-free stationary phase culture supernatants between the WT and the *clpP* mutant did not alter the kinetics of cell death of either strain (Fig.

3.4C). This suggested that the ClpP-dependent cell death in the WT strain resulted from endogenous factors.

The proteolytic function of ClpP is dependent on Clp ATPase subunits. In *S. aureus*, the ClpX and ClpC ATPases interact with ClpP (247). Accordingly, we determined the contribution of ClpX and ClpC in acetate-mediated cell death. Although independent mutations of either ATPase subunits exhibited a decreased rate of cell death compared to the WT strain, the *clpX* mutant more fully phenocopied the *clpP* mutant (Fig. 3.3D and Table. 3.1), which suggested that cell death was primarily under the control of the ClpXP protease. This conclusion was confirmed by our observation that acetate-mediated cell death was decreased to a similar extent in a strain expressing a mutant variant of ClpX, ClpX_{I265E}. The ClpX_{I265E} variant retained the ClpX chaperone activity, but not the ClpXP protease function due to a single amino acid substitution in the ClpP recognition motif of ClpX (Fig. 3.3E and Table. 3.1) (217, 253). Additionally, chromosomal complementation of native *clpX* in the *clpX_{I265E}* mutant restored the rate of cell death to WT levels (Fig. 3.3E and Table. 3.1). These observations strongly suggested that the ClpXP proteolytic function was solely responsible for the increase in cell death following acetate-mediated protein damage.

Next, we determined how acetate-mediated intracellular acidification affected ClpXP activity. Previous studies have concluded that Spx is an exclusive substrate of the ClpXP protease (239, 254). Accordingly, the intracellular levels of Spx were used as a proxy for gauging ClpXP activation. In contrast to the Spx levels observed at 24h when WT survival was at its peak, immunoblotting using anti-Spx antibodies revealed that Spx was depleted in the late stationary phase (72 h) when cell viability was actively decreasing (Fig. 3.3F). The depletion of Spx at 72 h was only observed in cultures that had acidified (Fig. 3.3F) and was not due to a decrease in *spx* transcription (Fig. 3.3G). Indeed, Spx levels underwent depletion even though its transcription had dramatically increased (Fig. 3.3F-G). Additionally, we also confirmed that the reduction of Spx at 72 h was dependent on ClpP activity as its inactivation restored Spx levels (Fig. 3.3F). These observations suggest that ClpXP activity is enhanced following acetate-mediated intracellular

acidification. The increased ClpXP activity was also matched with increased expression of both *clpX* and *clpP* following acidification (Fig. 3.3H-I). Collectively, these observations suggest that acetate-mediated protein damage at low pH increases the expression and proteolytic activity of ClpXP, resulting in cell death.

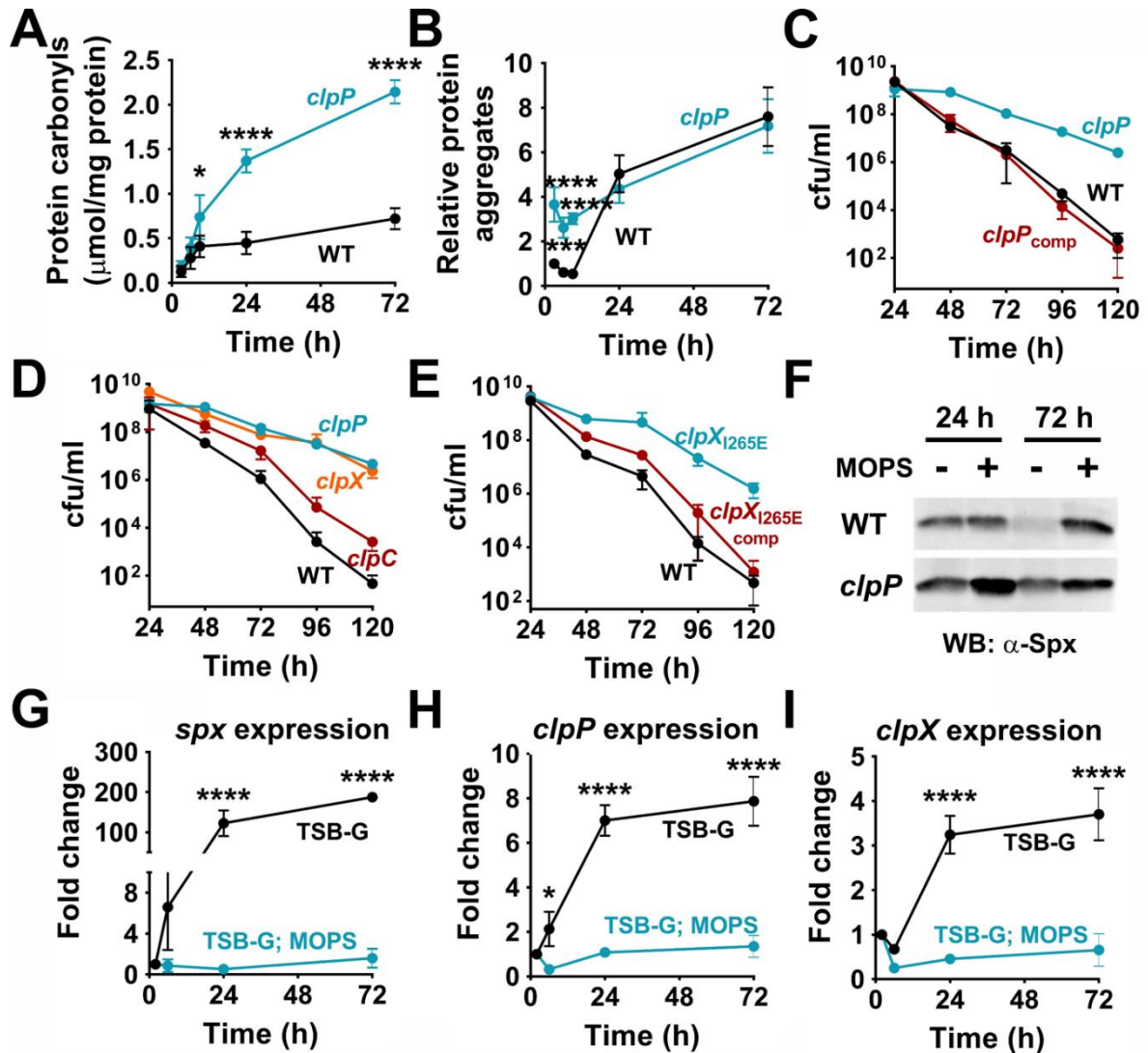


Figure 3.3. The ClpXP proteolytic activity enhances cell death.

(A) Protein oxidation ($n=3$, Mean \pm SD), (B) protein aggregation ($n=5$, Mean \pm SD) and (C) viability of the WT and *clpP* mutants ($n=3$, Mean \pm SD). (D) The cell viabilities of the *clpX*, *clpC* ($n=4$, Mean \pm SD) and (E) *clpX*_{I265E} mutants were determined in stationary phase relative to the WT strain ($n=3$, Mean \pm SD). (F) The intracellular abundance of Spx was used as an indicator of ClpXP proteolytic activity following growth in MOPS buffered (100 mM, pH 7.3) and unbuffered media. *S. aureus* Spx was detected using cross-reactive polyclonal antibodies raised against *B. subtilis* Spx. (G) The fold-change in the expression of *spx*, (H) *clpP* and (I) *clpX* was determined over time during different growth phases by qRT-PCR ($n=3$, Mean \pm SD). Fold-change expression values are relative to 3 h of growth (mid-exponential phase). Two-way ANOVA with Sidak's multiple comparison post-test; * $P \leq 0.05$, *** $P \leq 0.001$, **** $P \leq 0.0001$.

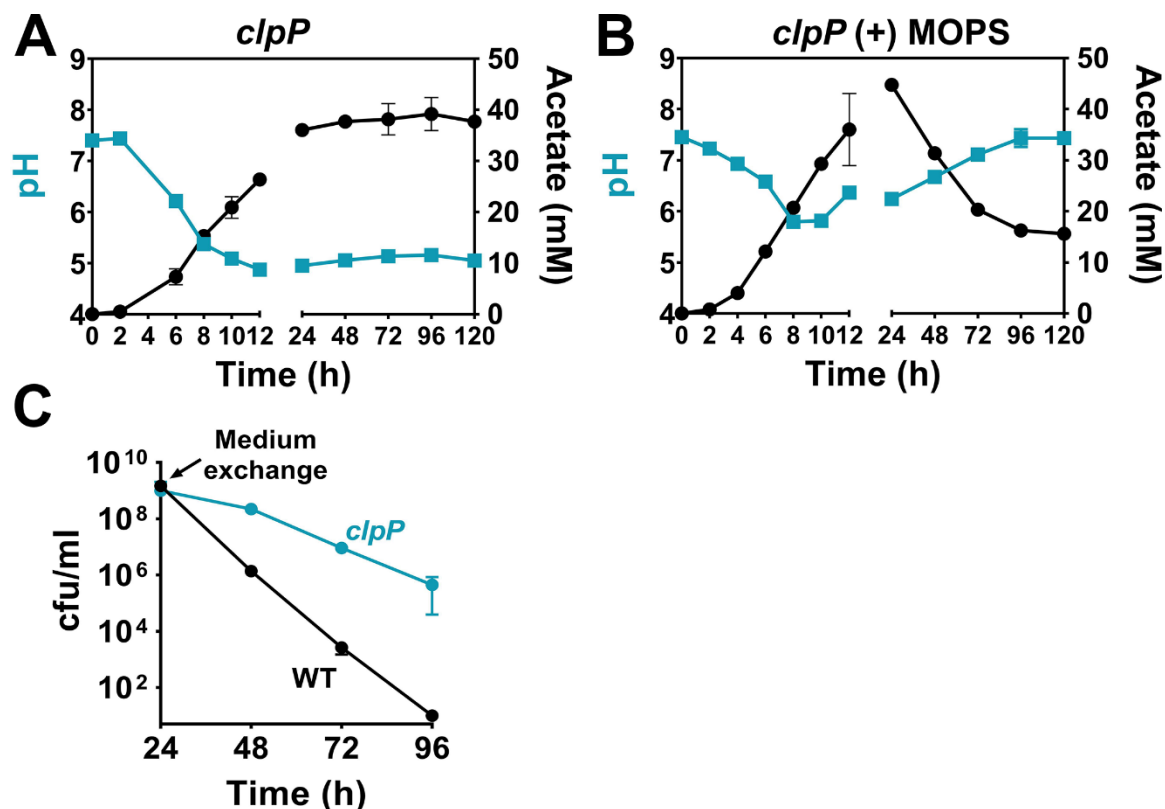


Figure 3.4. Extracellular factors do not contribute to the survival of the *clpP* mutant in stationary phase.

Acetate production (solid circles) and pH profile (solid squares) of the *clpP* mutant following growth in (A) TSB-G (unbuffered media) and (B) TSB-G supplemented with MOPS, pH 7.4 ($n=3$, Mean \pm SD). (C) Stationary phase viability of the WT and *clpP* mutant. Following growth of WT and *clpP* mutant in TSB-G for 24 h, cell-free culture supernatants of both strains were inter-substituted. Cells were washed with sterile saline to remove any traces of original growth media prior to media exchange ($n=3$, Mean \pm SD).

ClpP enhances cell death by diminishing the cellular antioxidant capacity

Thus far, our analyses suggested that ClpXP targeted the degradation of proteins that are important for cell survival in the late stationary phase. To determine potential targets of ClpXP, we initially determined proteomic changes during the transition of WT from 24 h to 72 h in stationary phase. We estimated protein abundance within cells using mass spectrometry. The identified proteins were organized hierarchically into functional classes based on their TIGRFAM annotation and the differences in protein abundance were visualized using Voronoi Treemaps (Fig. 3.5A-B and Fig. 3.6). In general, we observed multiple proteins associated with major cell biosynthetic pathways (protein synthesis, DNA metabolism, purines, pyrimidines, nucleosides and nucleotides, amino acids biosynthesis, biosynthesis of cofactors, prosthetic groups and carriers) to decrease in WT at 72 h relative to 24 h (Fig. 3.5A and Fig. 3.6A-B). Proteins associated with glycolysis were also fewer in abundance during this stage due to the exhaustion of glucose from the media. Instead, proteins involved in alternate pathways of carbon catabolism (amino acid catabolism) and energy metabolism (oxidative phosphorylation) increased at 72 h relative to 24 h of growth (Fig. 3.5A and Fig. 3.6A-B). Similar to the WT, the proteomic profile of the *clpP* mutant also revealed a decrease in proteins associated with various biosynthetic pathways during the same transition period in stationary phase albeit to a lesser degree (compare Fig. 3.5B to 3.5A and Fig. 3.6C, D to Fig. 3.6A-B, respectively). Interestingly, a notable increase in the abundance of proteins associated with anion, cation and amino acid transport were observed in the *clpP* mutant at 72 h relative to 24h (Fig. 3.5B and Fig. 3.6C, D). The *clpP* mutant also produced increased levels of multiple antioxidant enzymes, proteins associated with cysteine homeostasis, pentose phosphate pathway, ATPase and electron transport chain (Fig. 3.5B and Fig. 3.6C, D), suggesting that this mutant may be able to more efficiently undergo oxidative phosphorylation and cope with ROS arising from such metabolism, compared to the WT strain. A direct comparison of the protein abundance between the WT and *clpP* mutant at 72 h confirmed increased levels of antioxidant proteins in the latter mutant (Fig. 3.5C). As opposed to unbuffered conditions, growth of the WT strain in MOPS

buffered media (pH 7.4) resulted in increased abundance of proteins involved in the biosynthetic processes including protein synthesis, DNA metabolism, cofactor biosynthesis and amino acid metabolism (compare Fig. 3.5A to Fig. 3.7A). Proteins associated with central metabolism and energy metabolism were generally more abundant at 72 h relative to 24 h when the WT strain was grown in MOPS buffered conditions as opposed to unbuffered conditions, which suggested an active metabolism for the WT strain even during the late stationary phase (Fig. 3.8A-B). Interestingly, the *clpP* mutant had an overall decrease in most classes of proteins (including biosynthetic and metabolic proteins) at 72 h relative to 24 h when grown in MOPS buffered media (Fig. 3.7B and Fig. 3.8C-D). However, these differences were marginal. Irrespective of these metabolic differences, growth of the *clpP* mutant in MOPS buffered media reduced the levels of antioxidant enzymes relative to unbuffered culture conditions (Fig. 3.7C). These findings are consistent with the hypothesis that the *clpP* mutant may be able to survive longer in the stationary phase following acetate stress by modulating their metabolism and controlling the level of intracellular ROS.

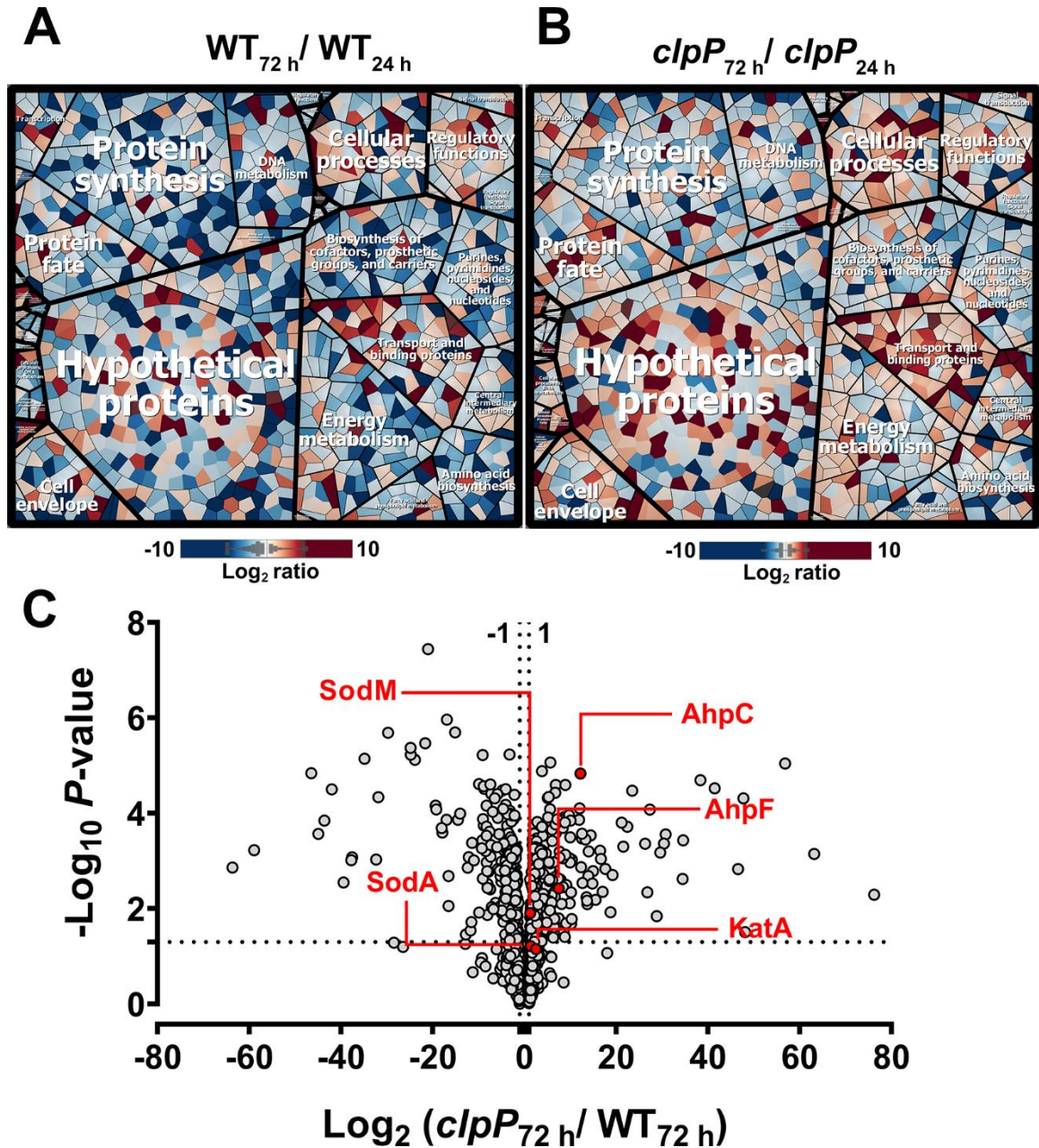
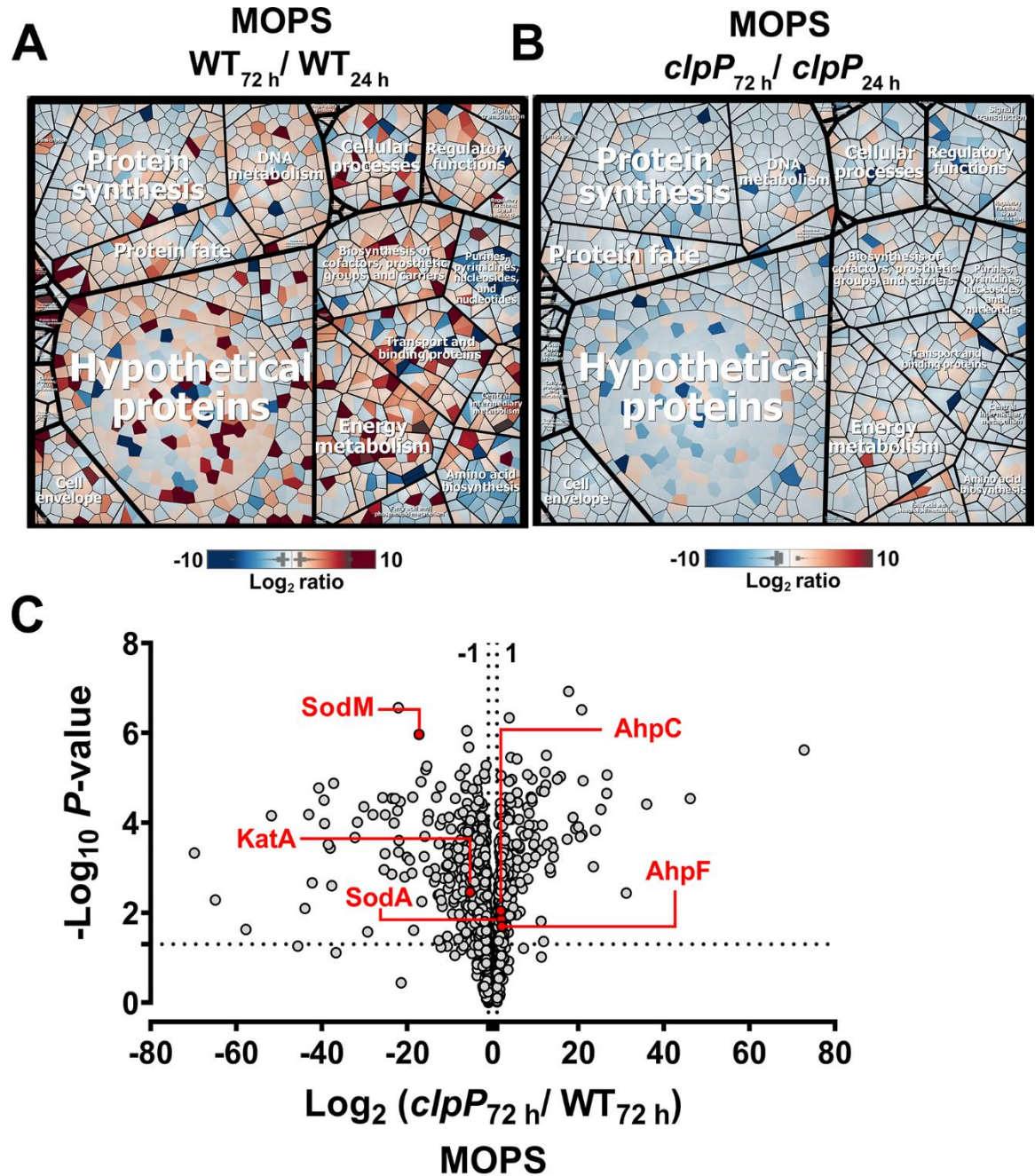


Figure 3.5. Altered proteome of stationary phase cells undergoing acetate stress.

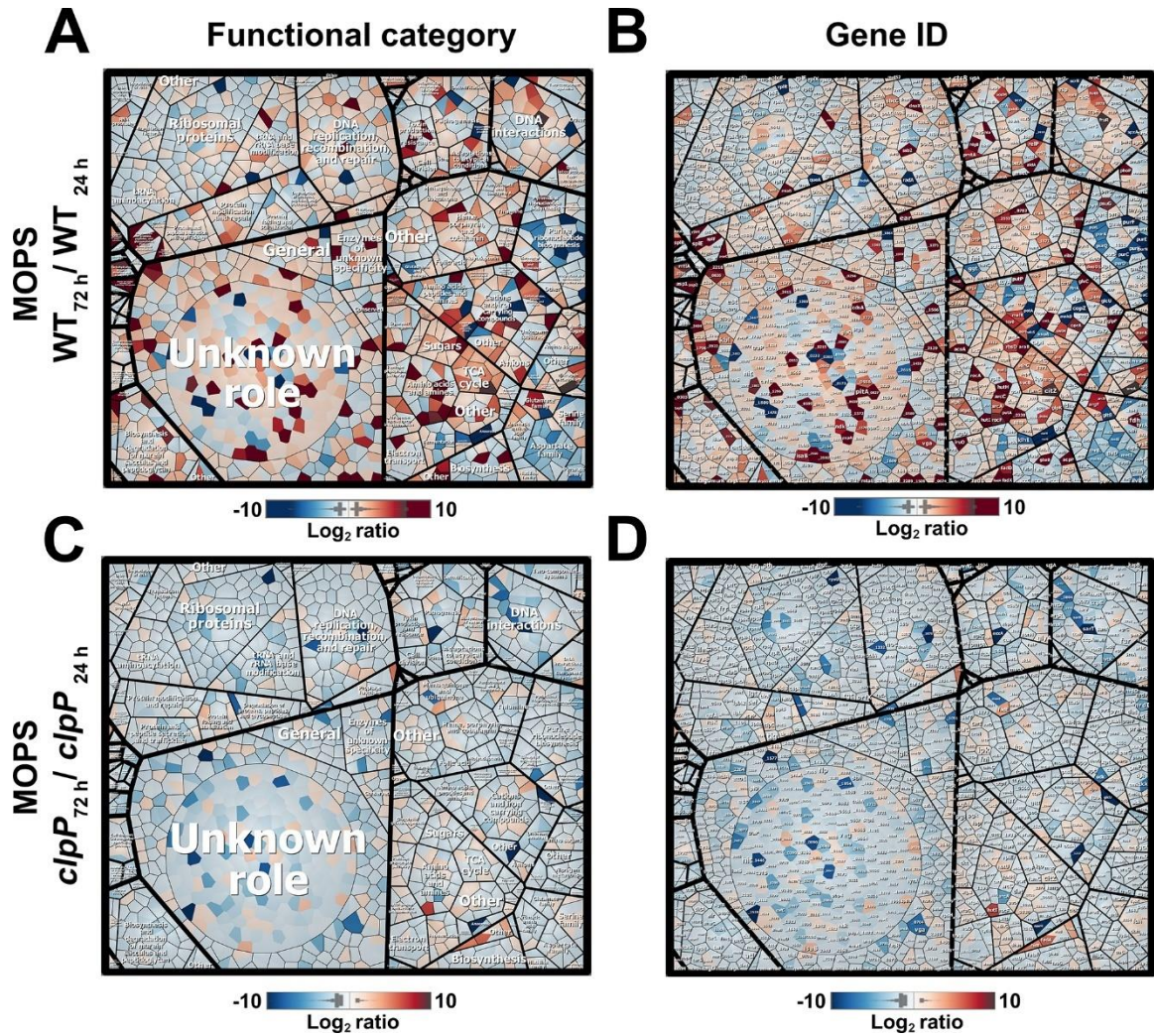
(A) Voronoi Treemaps of WT and (B) *clpP* mutant were generated from Log₂ ratios of their respective intracellular proteins at 72 h and 24 h of growth in TSB-G. Proteins with altered ratios were clustered based on the TIGRFAM annotations and depicted as functional categories. Further subcategories and gene ID annotations are indicated in *SI Appendix*, Fig. 3.6 (C) Volcano plot of the intracellular proteins in stationary phase cells. Each data point represents individual proteins organized according to their mean *clpP* / WT Log₂ fold-change ratios (y-axis) following 72 h of growth in TSB-G. The horizontal dotted line indicates the cut-off for proteins that showed significantly altered abundance ($P \leq 0.05$).

Figure 3.6. Proteomic profiling of stationary phase cells undergoing acetate stress. (A, B) Voronoi Treemaps of WT and (C, D) *clpP* mutant were generated from Log₂ ratios of their respective intracellular proteins at 72 h and 24 h of growth in TSB-G. Proteins with altered ratios were clustered based on the TIGRFAM annotations and depicted as functional categories. (A, C) represent functional sub-categories and (B, D) represent the corresponding gene IDs/ protein names. SAUSA300_XXXX locus tags are annotated as _XXXX in Voronoi Treemaps.



3.7. Altered proteome of stationary phase cells grown in MOPS buffered TSB-G media, pH 7.4

(A) Voronoi Treemaps of WT and (B) *clpP* mutant were generated from Log₂ ratios of their respective intracellular proteins at 72 h and 24 h of growth in TSB-G. Proteins with altered ratios were clustered based on the TIGRFAM annotations and depicted as functional categories. Further subcategories and gene ID annotations are indicated in *SI Appendix*, Fig. 3.8 (C) Volcano plot of the intracellular proteins in stationary phase cells. Each data point represents individual proteins organized according to their mean *clpP*/ WT Log₂ fold-change ratios (y-axis) following 72 h of growth in TSB-G supplemented with MOPS, pH 7.4. The horizontal dotted line indicates the cut-off for proteins that showed significantly altered abundance ($P \leq 0.05$).



3.8. Proteomic profile of stationary phase cells grown in MOPS buffered TSB-G media, pH 7.4

Voronoi Treemaps of WT and (C, D) *clpP* mutant were generated from Log₂ ratios of their respective intracellular proteins at 72 h and 24 h of growth in TSB-G supplemented with MOPS, pH 7.4. Proteins with altered ratios were clustered based on the TIGRFAM annotations and depicted as functional categories. (A, C) represent functional sub-categories and (B, D) represent the corresponding gene IDs/ protein names. SAUSA300_XXXX locus tags are annotated as _XXXX in Voronoi Treemaps.

To determine whether inactivation of *clpP* affected ROS production in the stationary phase, we performed EPR spectroscopy on WT and *clpP* mutant samples collected at 72 h of growth using CMH as a ROS-specific spin probe (255). EPR spectroscopy demonstrated that the *clpP* mutant produced lower levels of ROS than the WT strain (Fig. 3.9A). ROS production in stationary phase was undetected when WT and the *clpP* mutant was grown in media buffered with MOPS, pH 7.4 (Fig. 3.9A). *S. aureus* has multiple enzymes that control the endogenous production of ROS. Specifically, SodA and SodM dismutate superoxide ($O_2^{\bullet-}$) to hydrogen peroxide (H_2O_2) (Fig. 3.9B). Subsequently, catalase and AhpC converts H_2O_2 to water and limits the formation of toxic hydroxyl radical (OH^{\bullet}) (Fig. 3.9B). Given that the abundance of these enzymes was increased in the *clpP* mutant (Fig. 3.5C), we hypothesized that they might individually or collectively aid cell survival by enhancing endogenous ROS detoxification. To test this hypothesis, we determined the individual contribution of each enzyme to enhancing the survival of the *clpP* mutant. Although mutation of *sodA* did not change the kinetics of cell death in the WT strain, its mutation in the *clpP* background (*clpP**sodA*) completely abrogated survival of the *clpP* mutant to WT levels (Fig. 3.9C and Table 3.1). Separately, inactivation of *sodM* had no noticeable effect on the death kinetics in either the WT or *clpP* mutant backgrounds (Fig. 3.9D and Table 3.1). Furthermore, consistent with a role for *sodA* in the survival of the *clpP* mutant, we observed that the total superoxide dismutase activity was elevated in the *clpP* mutant but not in WT, *sodA* and *clpP**sodA* mutants at 24 h and 72 h into stationary phase (Fig. 3.9E). Notably, the observed differences in SodA enzyme activity did not result from differences in *sodA* expression (Fig. 3.9F), which suggested that SodA is likely to be a substrate of the ClpXP protease under these conditions. Indeed, western blot analysis using anti-SodA antibodies revealed a ClpP-dependent decrease in SodA levels (by ~ 44%) in the WT strain at 72 h relative to 24 h in stationary phase (Fig. 3.9G). The decrease in SodA abundance (Fig. 3.9G) is consistent with the observed decrease in SOD activity (> 40%) when WT transitioned from 24 h to 72 h (Fig. 3.9E). Unlike *sodA*, the transcription of *ahpC* was increased over 8-fold in the *clpP* mutant at 72 h (Fig. 3.9F). The *clpP**ahpC* double mutant exhibited a decreased survival

compared to the *clpP* mutant (Fig. 3.9H and Table 3.1). However, the *ahpC* mutant itself exhibited an increased rate of cell death relative to the WT strain (Fig. 3.9H and Table 3.1). This suggested that although *ahpC* is essential for stationary phase survival, its contribution towards the survival of the *clpP* mutant is likely to be modest. We did not observe a role for *kata* in increasing the survival of the *clpP* mutant (Fig. 3.9I and Table 3.1). Together, these observations suggest that under acetic acid stress, the targeted degradation of SodA and the reduction of *ahpC* expression by ClpP in the stationary phase could trigger cell death.

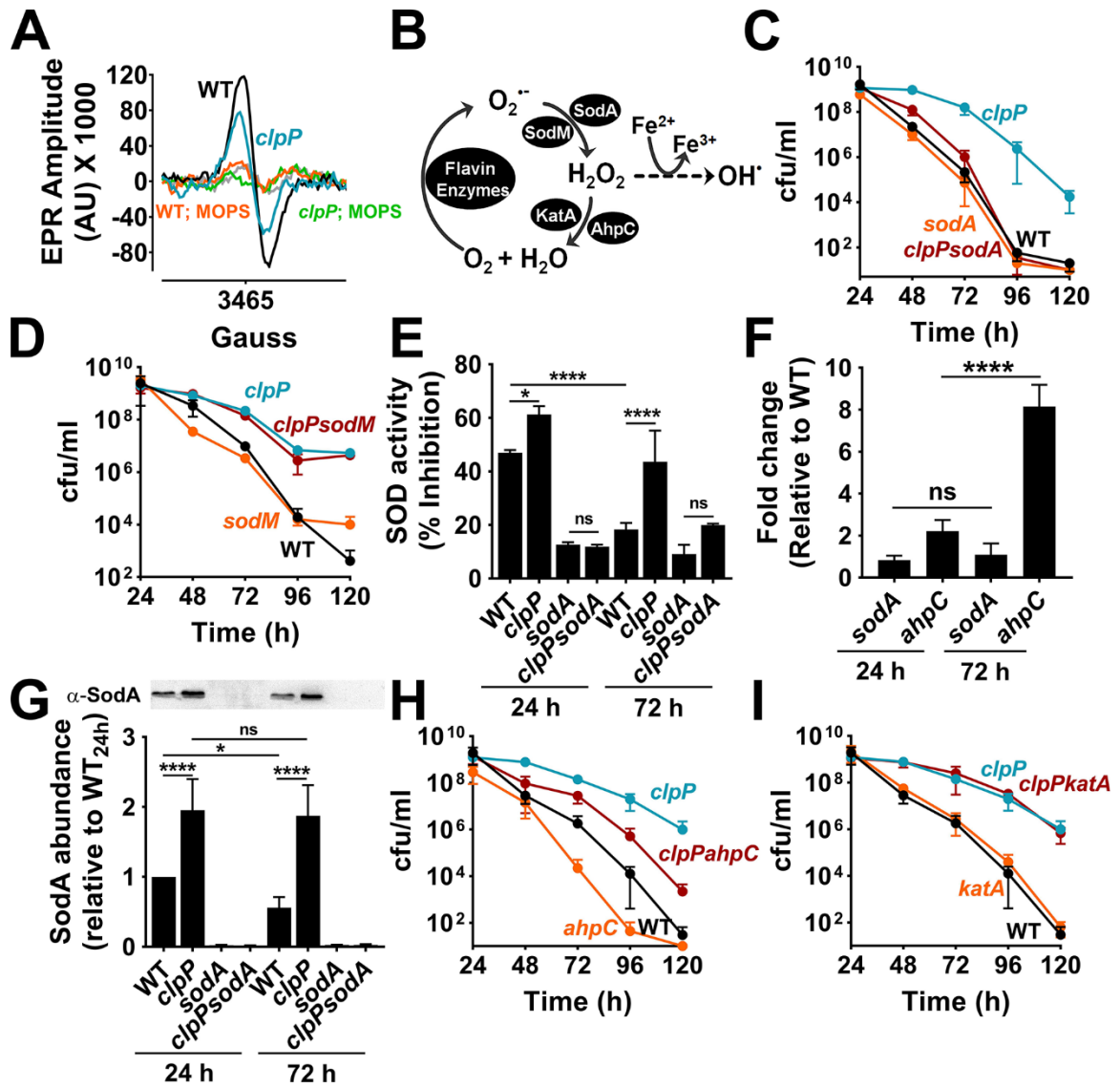


Figure 3.9. ClpXP targets SodA to subvert the antioxidant capacity of cells.

(A) Representative electron paramagnetic resonance (EPR) spectroscopic trace of ROS derived from whole cells in stationary phase (72 h). ROS was detected using the spin probe, CMH. (B) Schematic of the antioxidant enzymes of *S. aureus* and their target ROS. SodA/ SodM, Mn-dependent superoxide dismutases; KatA, catalase; AhpC, alkylhydroperoxidase subunit. (C) Stationary phase viability of *sodA* and (D) *sodM* mutants relative to WT and *clpP* mutant strains (n=3, Mean \pm SD). (E) SOD activity of cell extracts at 24 h and 72 h were determined as the percent inhibition of WST-1 reduction by superoxide using a commercially available kit (Sigma). WST-1, water-soluble tetrazolium salt (n=3, Mean \pm SD). (F) The fold-change in expression of *sodA* and

ahpC were determined at 24 h and 72 h in the *clpP* mutant. The fold-change expression values were calculated relative to the expression of these target genes in WT strain at identical time-points (n=3, Mean \pm SD). (G) The intracellular levels of SodA were detected in various mutants by western blot analysis using cross-reactive polyclonal antibodies raised against *B. anthracis* SodA (top panel). Densitometric quantification was performed by Image J (bottom panel) (H) Cell viability of *ahpC* and (I) *katA* mutants in stationary phase (n=3, Mean \pm SD). Two-tailed unpaired t-test; ** $P \leq 0.01$, *** $P \leq 0.001$, **** $P < 0.0001$.

ClpP-dependent cell death enhances the competitive fitness potential of staphylococci

The necessity of mechanisms that activate cell death in single-cell organisms like *S. aureus* are counterintuitive. Hence, we suspected that the benefits of ClpP-dependent cell death might exist at the population rather than the single-cell level. Since the accumulation of damaged proteins was likely to affect growth, we hypothesized that the enhanced survival of the *clpP* mutant during the stationary phase might come at the cost of maintaining the overall competitive fitness potential of the population. To test this hypothesis, we harvested the WT and *clpP* mutant before the onset of cell death when cell viability for both strains was highest (24 h growth) and at a subsequent time point when cell viability of the WT (but not the *clpP* mutant) was declining (72 h) (Fig. 3.10A). We performed competition assays of the *clpP* mutant and WT strains derived from each time point. We assessed their mean competitive fitness (w) as a ratio of their Malthusian parameters over an 8 h growth period (222). Although the *clpP* mutant isolated from 24 h old cultures exhibited only a modest decrease in fitness relative to the WT strain ($w_{24} = 0.87$), the mean competitive fitness of the *clpP* mutant was significantly diminished when the competition was initiated from 72 h old cultures ($w_{72} = 0.365$) (Fig. 3.10B). We observed a similar trend when the competition was conducted between *clpX_{I265E}* and the WT strain ($w_{24} = 1.03$ vs. $w_{72} = 0.673$) (Fig. 3.10C). To test whether the observed competitive fitness defect of the *clpP* mutant resulted from increased SodA activity rather than pleiotropic effects of the *clpP* mutation, we performed co-culture competition

of the *clpPsodA* double mutant with its isogenic *sodA* parent strain following 72 h growth. We observed that the competitive defect of the *clpP* mutant was reversed (Fig. 3.10D), if *sodA* was inactivated in that background (*clpPsodA*). These results strongly suggest that ClpXP-dependent decrease in SodA activity initiates cell death and is essential for maintaining the overall competitive fitness potential of staphylococcal populations undergoing stress in stationary phase.

We next asked if the evolutionary pressure to maintain competitive fitness through regulated cell death could be triggered by antimicrobial compounds that interfere with protein homeostasis and induce *clpP* expression. To test this hypothesis, we treated the WT strain with different classes of antibiotics at the post-exponential phase (25X MIC). We also assessed their ability to induce *clpP* expression (Fig. 3.10E) and induce ClpP-dependent cell death (Table 3.2). Our analysis revealed that different antibiotics were able to differentially activate *clpP* expression by 24 h relative to untreated control at the same time-point; notably, aminoglycosides that interfered with protein synthesis were most prominent in this regard (Fig. 3.10E). Importantly, we also observed a strong positive correlation between the ability of antibiotics that induce *clpP* expression, to also promote *clpP*-dependent cell death (Pearson coefficient (r)= 0.7612, r^2 = 0.5794, P =0.0282) (Fig. 3.10E and Table 3.2). Collectively, our findings strongly suggest that non-dividing populations with irreparable protein damage are targeted for elimination in a ClpXP-dependent manner to sustain population fitness.

3.3 Discussion

The evolutionary selection of energy-dependent cell death processes in bacteria may have its origins in niches where interspecies competition and antimicrobial warfare are commonly observed. Antimicrobial compounds and metabolic byproducts such as weak acids that interfere with protein homeostasis are frequently produced by competing bacterial species (256, 257). Such interactions could adversely bias fitness outcomes of target bacterial populations that are affected by the harmful effects of these metabolites (258). While bacteria may transition to non-growing

states under these conditions and become more tolerant, the continued stress from these antimicrobials is likely to increase the number of damaged cells in the population (259). The elimination of unfit cells through an active self-destruction program could improve the competitive fitness of the bacterial population when cells re-enter growth under more favorable conditions.

How are unfit cells eliminated? Studies have shown that stress-induced oxidized protein aggregates in the cytoplasm can be lethal (252). However, our findings demonstrate that this is not the case in staphylococci that enter stationary phase following acetate stress. Indeed, the *clpP* mutant accumulated more oxidized proteins that aggregated at a faster rate than the wild type strain but still survived significantly better in stationary phase.

According to our model (Fig. 3.11), cells that accumulate damaged proteins in stationary phase induce ClpXP expression and activity in response. The extent of intracellular protein damage following stress may dictate the fate of cells. When cell division halts and cells enter stationary phase, protein quality control is critical because cells can neither dilute damage through cell division nor diverge all energy to protein repair as resources are scarce during stationary phase. If the damage is beyond repair and affects the competitive fitness of the population, the fitness-compromised cells must undergo cell death. Our findings suggest that ClpXP potentiates cell death by targeting the degradation of SodA. The resulting inability to efficiently detoxify superoxide triggers cell death. Several lines of evidence cumulatively support this model. First, acetate mediated cytoplasmic acidification increased the expression of both *clpX* and *clpP* in stationary phase. Consistent with this phenotype, an increase in ClpXP-dependent proteolytic activity could be deduced from the degradation of Spx, a ClpXP-specific substrate, and more broadly from the profound ClpP-dependent changes in the intracellular proteome of the WT strain during late stationary phase. Second, the observed cell death was not related to the chaperone function of ClpX in *S. aureus* (253) as the *clpX*_{I265E} mutant was unable to initiate cell death in response to acetic acid stress. This reconfirmed the role of the ClpXP protease as the primary mediator of cell death. Finally, although the abundance of multiple intracellular proteins decreased upon ClpP activation,

those involved in countering oxidative stress and redox balance were prominent. SodA activity was significantly reduced in the late stationary phase in a ClpP-dependent manner. Furthermore, inactivation of *sodA* in the *clpP* mutant restored the kinetics of cell death back to WT levels, thus highlighting SodA as a target of ClpXP for the induction of cell death in stationary phase. It is worth noting that SodA was previously identified as a critical factor for long term-survival of *S. aureus* in stationary phase (260). Thus, ClpXP induces cell death by targeting established proteins involved in maintaining cell viability.

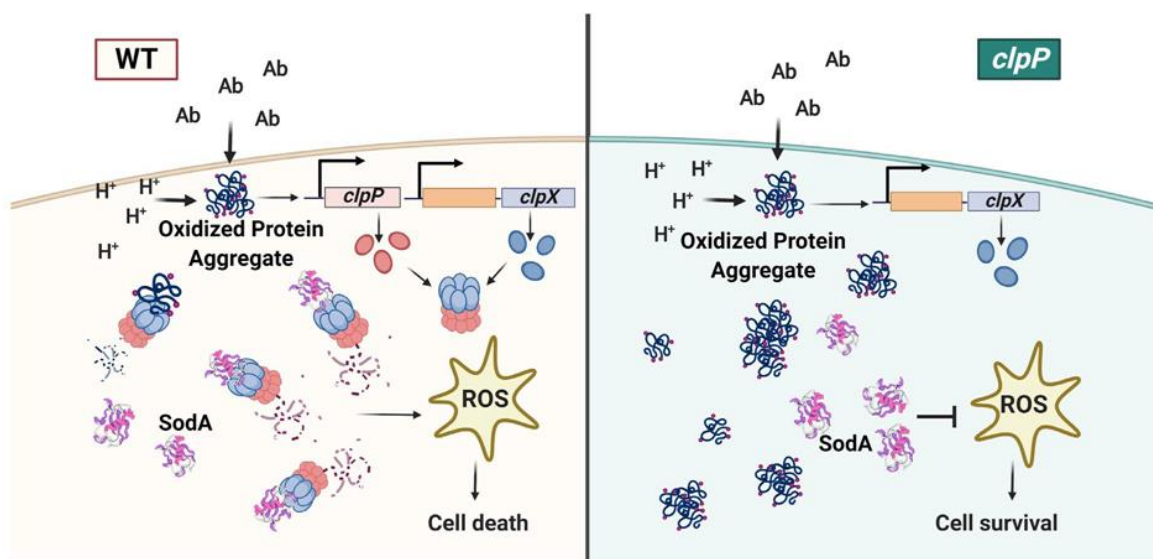


Figure 3.10. Model of the ClpXP mediated cell death pathway in *S. aureus*

S. aureus accumulates oxidized protein aggregates and turns on the expression of *clpX* and *clpP* when they encounter antibiotic [Ab] stress or undergo intracellular acidification [H⁺]. In rapidly dividing cells that can dilute the effect of damaged proteins through cell division, the ClpXP protease may be sufficient to recycle protein aggregates and restore fitness of cells. However, non-dividing populations that contain protein aggregates undergo cell death to maintain population fitness (left panel). To initiate cell death, the ClpXP protease targets the degradation of SodA which results in lethal oxidative damage due to sustained superoxide production. In the *clpP* mutant (right panel), the lack of protein turnover results in the retention of proteins that are highly susceptible to oxidation and aggregation. However, the increased levels and activity of SodA promotes cell survival due to decreased ROS mediated killing. This image was created with BioRender.com.

The toxicity of superoxide is well documented and involves damage to macromolecules and metal centers in enzymes that are important for cell viability (261). Irreparable DNA double-stranded breaks due to Fenton chemistry and oxidation of essential proteins could result in permanent loss of replicative ability, resulting in cell death (262). Alternatively, intracellular oxidation may activate the Cid and Lrg proteins, which have been previously shown to modulate cell death in *S. aureus* (17). Although recent evidence suggests that these proteins are involved in the transport of metabolites across the cell membrane (263), oxidative stress may trigger their oligomerization and pore formation in the cell membrane resulting in cell death (45). Proteomic analysis revealed altered levels of several proteins involved in various cellular functions when cell death is triggered following stress. Thus, the involvement of additional pathways independent of SodA in the regulation of cell death cannot be ruled out.

While ClpXP can turnover native proteins and control their intracellular abundance (246, 264), the specific signals that mark SodA for degradation in unfit cells is not known. Similarly, the sources of cellular ROS in stress-induced damaged cells remain to be identified. However, the ability of ClpXP to regulate cell death appears to be conserved in prokaryotes and eukaryotes. In a recent study, the *B. subtilis* ClpXP protease was shown to eliminate defective sporulation cells by degrading SpoIVA and inducing lysis (89). Such a mechanism in *B. subtilis* was proposed to select

against the loss of a sporulation program (89). In *E. coli*, it was demonstrated that the ClpPA protease ultimately promotes survival during starvation and phage infection by inducing toxin-antitoxin (MazEF)-mediated programmed cell death in a subpopulation of cells. Accordingly, it was shown that the ClpPA targets the anti-toxin MazE for degradation, thus freeing the MazF toxin to inhibit the translation of essential proteins by cleaving mRNA (23). In eukaryotes, the mitochondrial ClpXP protease was found to restrict the lifespan of the fungus *P. anserine* (265). Interestingly, the human ortholog of *clpP* was also able to reduce the extended lifespan of the *P. anserine clpP* mutant when heterologously expressed in that organism (265), suggesting functional conservation of ClpP in controlling cell death and lifespan across the Kingdoms of life.

Like the *clpX* mutation, the inactivation of *clpC* also increased survival of stationary phase cells that had undergone protein damage; albeit this was a modest increase in our model. The importance of the staphylococcal ClpCP protease in promoting cell death in stationary phase has been described in multiple studies (206). The increased survival of the *clpC* mutant was attributed to a greatly reduced TCA cycle activity resulting from poor aconitase function in this mutant. Consequently, the lower cellular energy available to the *clpC* mutant was hypothesized to prevent entry of cells into the energy-dependent death phase (209, 266). Independently, the reduced TCA cycle activity and low respiratory potential in the *clpC* mutant could also result in less ROS production and increased stationary phase survival (206, 267). More recently, the ClpCP protease was shown to modulate intracellular survival by targeting the MazEF toxin-antitoxin system in *S. aureus* (268). The degradation of the MazE antitoxin by the ClpCP protease resulted in MazF toxin mediated bacterial stasis (268).

Previously, Dwyer et al. demonstrated that antibiotic-stress induced several hallmarks of apoptosis in *E. coli* and enabled the destruction of cells similar to programmed cell death in eukaryotes (90). Remarkably, the ClpXP protease was shown to play a significant role in antibiotic-induced bacterial cell death in addition to RecA and members of the SOS response regulon (90). Our findings also highlight a link between certain classes of antibiotics and ClpXP-dependent cell

death. Notably, we observed increased *clpP* expression and ClpP-dependent cell death when antibiotics that target bacterial ribosomes like gentamicin, kanamycin, and erythromycin were used against *S. aureus*. These antibiotics primarily disrupt protein homeostasis by blocking protein synthesis (269, 270). Although some of these antibiotics are thought to be bacteriostatic (271, 272), at high concentrations, most of these antibiotics may become bactericidal due to indirect effects from protein damage (269, 273). Our finding that antibiotic-mediated killing can be alleviated by inactivating *clpP* indicates a significant contribution for ClpP proteolysis in cell death during antibiotic stress.

In conclusion, our findings suggest that the activation of ClpXP in non-dividing stationary phase cells that are subject to stress will deteriorate cellular antioxidant capacity and ultimately result in cell death. This process eliminates unfit cells that accumulate damaged proteins in the cytoplasm. We propose that the ClpXP-dependent cell death program in bacteria is evolutionarily selected to maintain competitive fitness during growth transition.

Table 3-1. Stationary phase death rates (k_{\max}^{\dagger}).

[‡] k_{\max} values were calculated using GInaFiT (274).

Statistical significance for Fig. 3.2C was determined using two-tailed Student's *t*-test.

Figure	Strain	K_{\max}	Significance			Regression model
Fig. 3.2C	WT in TSB-G	0.193 ± 0.015	** *** **			Log-linear regression
	WT in TSB-G;MOPS	0.002 ± 0.0001				
Fig. 3.3C	WT	0.159 ± 0.017	** **	ns		Log-linear regression
	<i>clpP</i>	0.066 ± 0.001				
	<i>clpP:clpP</i>	0.175 ± 0.027				
Fig. 3.3D	WT	0.183 ± 0.0152	** *** **	** *** **		Log-linear regression
	<i>clpP</i>	0.066 ± 0.005				
	<i>clpC</i>	0.146 ± 0.005				
	<i>clpX</i>	0.076 ± 0.005				
Fig. 3.3E	WT	0.173 ± 0.230	** **	ns		Log-linear regression
	<i>clpX_{I265E}</i>	0.083 ± 0.005				
	<i>clpX_{I265E}::clpX</i>	0.166 ± 0.025				
Fig. 3.7C	WT	0.217 ± 0.028	** **	ns	ns	Log-linear regression
	<i>clpP</i>	0.125 ± 0.023				
	<i>sodA</i>	0.235 ± 0.023				
	<i>clpP</i> <i>sodA</i>	0.240 ± 0.031				
Fig. 3.7D	WT	0.183 ± 0.025	** *** **	*	** *** **	Log-linear regression
	<i>clpP</i>	0.066 ± 0.003				
	<i>sodM</i>	0.140 ± 0.010				
	<i>clpP</i> <i>sodM</i>	0.070 ± 0.010				
Fig. 3.7H	WT	0.185 ± 0.010	** *** **	ns	** **	Log-linear regression
	<i>clpP</i>	0.079 ± 0.010				
	<i>ahpC</i>	0.207 ± 0.023				
	<i>clpP</i> <i>ahpC</i>	0.135 ± 0.016				
Fig. 3.7I	WT	0.185 ± 0.010	** *** **	ns	ns	Log-linear regression
	<i>clpP</i>	0.079 ± 0.010				
	<i>katA</i>	0.178 ± 0.008				
	<i>clpP</i> <i>katA</i>	0.072 ± 0.013				

Statistical significance for Fig. 3.3C-4H was determined using one-way ANOVA and Tukey's multiple comparisons test (* $p \leq 0.05$, ** $p \leq 0.01$, *** $p \leq 0.001$, **** $p < 0.0001$).

Table 3-2. Stationary phase death rates ($k_{\max}^{\#}$) following antibiotic treatment.

Antibiotic	Strain	k_{\max}	Significance	Regression model
Kanamycin	WT	0.223 ± 0.011	**	Log-linear +
	<i>clpP</i>	0.175 ± 0.013		shoulder
Gentamicin	WT	0.223 ± 0.011	*	Log-linear +
	<i>clpP</i>	0.176 ± 0.015		shoulder
Erythromycin	WT	0.049 ± 0.017	ns	Log-linear
	<i>clpP</i>	0.028 ± 0.002		regression
Trimethoprim	WT	0.032 ± 0.001	*	Log-linear
	<i>clpP</i>	0.019 ± 0.007		regression
Tetracycline	WT	0.025 ± 0.005	ns	Log-linear
	<i>clpP</i>	0.027 ± 0.001		regression
Chloramphenicol	WT	0.086 ± 0.015	*	Log-linear +
	<i>clpP</i>	0.120 ± 0.010		shoulder
Vancomycin	WT	0.040 ± 0.0003	ns	Log-linear
	<i>clpP</i>	0.040 ± 0.004		regression
Oxacillin	WT	0.096 ± 0.015	ns	Log-linear +
	<i>clpP</i>	0.083 ± 0.005		shoulder

[#] k_{\max} values were calculated using GInaFiT (274)

Statistical significance was determined using two-tailed Student's *t*-test (* $p \leq 0.05$, ** $p \leq 0.01$, *** $p \leq 0.001$, **** $p < 0.0001$).

Chapter 4: The role of Spx in the survival of *Staphylococcus aureus* in stationary phase

4.1 Introduction

Most of the successful human pathogens, including *Staphylococcus aureus*, have the ability to withstand immune defenses. It not only produces a plethora of virulence factors that affect the immune system but it also resists killing by immune effectors (275, 276). Reactive oxygen species (ROS) and reactive nitrogen species (RNS) are potent antimicrobial molecules used by cells of the innate immune system (primarily neutrophils and macrophages) to kill phagocytized *S. aureus* (276). NADPH oxidase, myeloperoxidase, and nitric oxide synthase are the main enzymes that produce the superoxide anion ($O_2^{\cdot-}$), hypochlorous acid (HOCl), and nitric oxide (NO^{\cdot}), respectively (276). Hydrogen peroxide (H_2O_2), hydroxyl radical (OH^{\cdot}), and peroxynitrite are also formed during the oxidative burst (276, 277). *S. aureus* has multiple detoxifying enzymes to help it cope with oxidative and nitrosative stress, and they are generated either endogenously or exogenously (197, 278–281). Superoxide is detoxified by superoxide dismutase A (SodA) and superoxide dismutase M (SodM) to H_2O_2 and O_2 , respectively (260, 282, 283), and then H_2O_2 is detoxified by either catalase (KatA) or alkyl hydroperoxide reductase (AhpC) before it interacts with free iron to produce OH^{\cdot} through the Fenton reaction (277, 284). These enzymes are considered the first line of defense for detoxifying these reactive molecules, and the second line of defense consists of low-molecular-weight thiol (bacillithiol), staphyloxanthin, Coenzyme A, and the thioredoxin repair system (279, 285, 286). All of the previously discussed oxidative stress components are fine-tuned through a complex network of oxidant sensors to ensure a reduced intracellular environment in *S. aureus* (276, 279, 287).

Spx (suppressor of ClpP and ClpX) is a highly conserved transcription regulator in low-GC gram-positive bacteria that regulates multiple components of the oxidative stress response, including bacillithiol (BSH) biosynthesis, cysteine metabolism, and the activity of the thioredoxin

system (288). It is a unique transcription regulator in the sense that it does not bind DNA but it does interact with DNA and is co-purified with RNA polymerase (RNAP) (289, 290). Spx interacts with the RNAP alpha-subunit, C-terminal domain upstream of the -35 box (at -43/-44 in *B. subtilis*) (291). This interaction with RNAP directly regulates 275 genes, which are either repressed or activated by Spx (291). The Spx regulon is mainly triggered by thiol stress, which activates the redox-sensitive CXXC motif (redox-sensing switch) (292). The thiol–disulfide switch at the N-terminus enhances the central domain’s interaction with the C-terminal domain of the RNAP alpha subunit, causing increased transcription of bacillithiol biosynthesis and the thioredoxin system (286, 288, 289, 293). These observations are mainly reported in *B. subtilis*; studies of *S. aureus* are extremely limited. However, *S. aureus* Spx shares a great deal of homology with *B. subtilis* Spx, suggesting that the functions of Spx in *S. aureus* and *B. subtilis* are similar (239).

Spx has been recognized as a specific ClpXP protease substrate in *S. aureus* and *B. subtilis* (254, 294). Under specific conditions, the ClpCP of *B. subtilis* can contribute to Spx degradation (295). ClpXP recognizes a specific amino acid sequence at the C-terminal domain of Spx, and the YjbH adaptor protein tethers Spx to ClpX to facilitate degradation by the ClpXP complex (296, 297). Thus, inactivation of *S. aureus* *clpP*, *clpX*, or *yjbH* causes increased accumulation of Spx compared with the wild type strain (217, 239, 296). Inactivation of *spx* in *S. aureus* renders the bacterial cells sensitive to various stressors, including extremely high and low temperatures, thiol stress, and peroxide stress, and it induces biofilm formation because of the induction of the polysaccharide intercellular adhesin (PIA) locus, *icaABCD* (239). Proteomic analysis revealed that disruption of *spx* induces a dramatic change in its proteome (239). Yet, we still do not have enough studies to understand the role of Spx in *S. aureus* physiology.

Previous observations and our previous study in Chapter 3 suggest that stationary phase cell death in *S. aureus* is a ClpXP-regulated mechanism that exhibits PCD hallmarks resembling those of apoptosis in eukaryotic cells. These hallmarks are, possibly, downstream effects of changes in stationary phase cell physiology. In this study we aimed to explore whether Spx is part of the

ClpXP-mediated cell death mechanism and how it affects cell physiology in the stationary phase. Our results indicate that Spx is not only essential for stationary phase survival but also is a good target at which ClpXP can aim to kill the cell. We also determined that the adaptor protein, YjbH, acts as an accelerator of cell death by enhancing Spx degradation. Our results demonstrate that the redox-sensing switch of Spx plays a central role in promoting stationary phase survival by activating the thioredoxin system to maintain a reduced intracellular environment.

4.2 Results

Spx is necessary for stationary phase survival under oxidative stress

Previously, we showed that growth in conditions of excess glucose triggers ClpXP-mediated cell death, in which native proteins that are important for stationary phase survival under acid stress are targeted. Multiple substrates were of interest because of their roles in combating oxidative stress, which drives cell death in addition to cytoplasmic acidification. One of these identified substrates is Spx, which we used previously as a proxy to evaluate the activity of ClpXP in the stationary phase. Spx was clearly detected on a western blot at 24 hours of growth (Fig. 3.3F) but not at 72 hours, and these observations indicate that Spx is probably connected to the stationary phase cell death network. Given that Spx is essential for *S. aureus* viability (298), we hypothesized that ClpXP targets essential proteins, such as Spx, to regulate stationary phase cell death.

Because of how essential Spx is for cell viability, we used a Δ spx mutant that was successfully generated in the *S. aureus* 8325-4 strain (239) to evaluate the role of Spx for stationary phase cell survival following aerobic growth in Tryptic Soy Broth (TSB) supplemented with 45 mM of glucose. The stationary phase survival of the Δ spx mutant was severely compromised compared with that of the *S. aureus* 8325-4 wild-type strain. It showed diminished viability at 48 hours of growth in TSB-45 mM glucose (Fig. 4.1A, Table. 5.1). Chromosomal complementation of the Δ spx under the control of its native promoter restored the stationary phase survival similar

to that in the *S. aureus* 8325-4 wild-type strain (Fig. 4.1A Table. 5.1); this suggested that the phenotype was not a result of the suppressor mutations reported in this strain (298). Given that increased ROS and decreased cellular respiration are hallmarks of PCD during *S. aureus* stationary phase cell death following growth in TSB supplemented with excess glucose (105), we hypothesized that the increased cell death of the Δ *spx* mutant was due to an increased accumulation of ROS following cytoplasmic acidification. To test this hypothesis, the *S. aureus* 8325-4 wild-type strain, Δ *spx*, and Δ *spx*-Comp were grown in TSB-45 mM glucose and cells were harvested at 24 hours and 72 hours to assess cellular respiration and ROS in the stationary phase using flow cytometry. The cell-permeable 5-Cyano-2,3-ditolyl tetrazolium chloride (CTC) redox dye was used to detect cellular respiration, and the hydroxyphenyl fluorescein (HPF) cell-permeable fluorescent reporter, which detects hydroxyl radicals, was used as a proxy to evaluate ROS accumulation (225, 226). It was not surprising to see that all strains had similar respiring populations at 24 hours and decreased cellular respiration at 72 hours on CTC staining (Fig. 4.1B) since these are trends that have been reported before (105). However, the HPF-positive population was negligible at 24 hours in all strains, whereas at 72 hours there were 15% more HPF stained cells in the Δ *spx* mutant compared with the *S. aureus* 8325-4 wild-type strain (Fig. 4.1B), a phenotype that was successfully complementable (Fig. 4.1B). These results indicate that Spx is important for stationary phase survival and that the ClpXP-dependent degradation of Spx causes increased ROS in the stationary phase of growth.

Given that growth in TSB-45 mM glucose buffered with MOPS at pH 7.3 inhibits stationary phase cell death and prevents a high Spx turnover rate by ClpXP (Fig. 3.2C and 3.2F), we explored the role of Spx in stationary phase survival. The viability of *S. aureus* 8325-4 wild-type cells grown in TSB-45 mM glucose with 100 mM MOPS was completely rescued in the stationary phase (Fig. 4.1C, Table. 5.1). However, buffering the medium with MOPS only partially rescued the cell death of Δ *spx* (Fig. 4.1C, Table. 5.1). Accordingly, cells of the wild-type strain and the Δ *spx* mutant stained with HPF and CTC to evaluate cellular respiration and ROS accumulation

showed no difference at 24 hours (Fig. 4.1D), whereas the Δspx mutant exhibited decreased respiration and increased ROS at 72 hours of growth (Fig. 4.1D). These interesting observations indicate that Spx possibly prevents ROS-dependent inactivation of cellular respiration. These results indicate that Spx is critical for *S. aureus* stationary survival and plays a role in maintaining the intracellular environment in a reduced state to survive stationary phase (Fig. 4.1D).

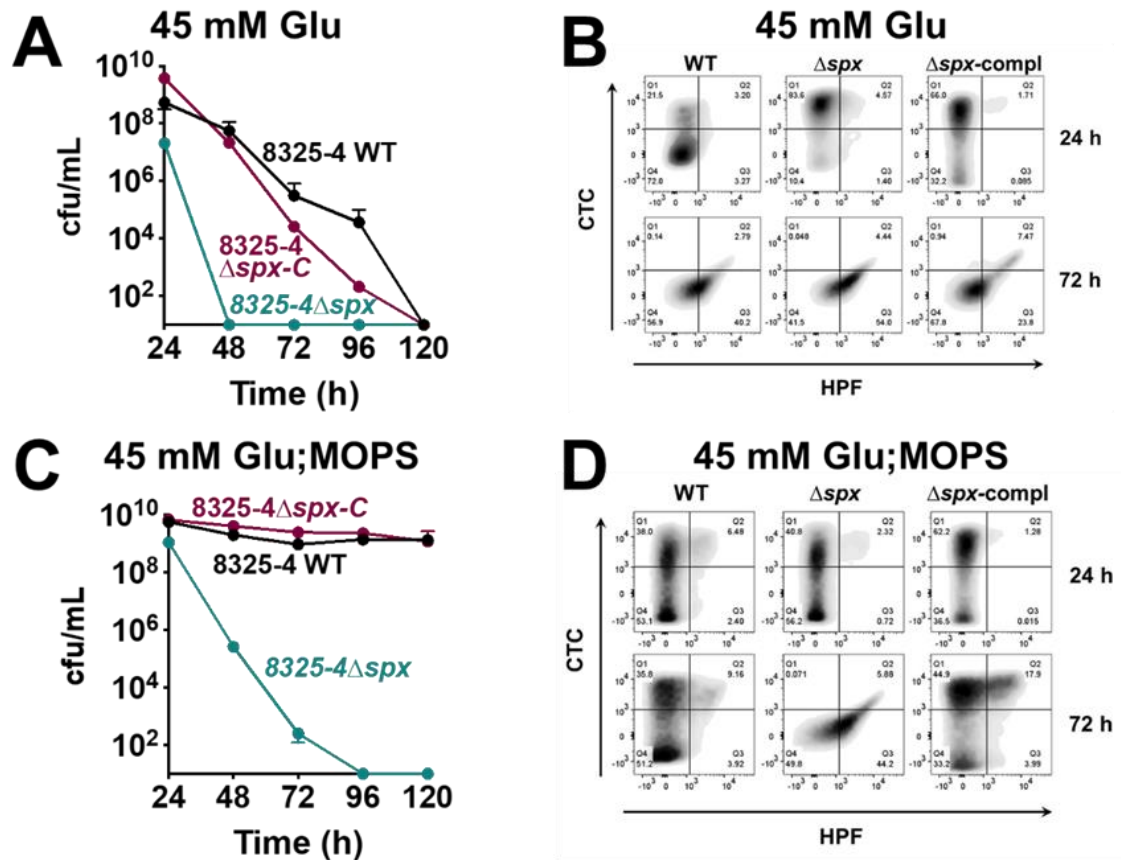


Figure 4.1. Spx enhances stationary phase survival under stress and non-stress conditions
 (A) Survival assay of *S. aureus* 8325-4 and its isogenic Δspx and Δspx complemented strain (Δspx -C) in TSB-45 mM glucose. Survival was monitored over a period of 120 hours. (B) Flow cytometry of *S. aureus* 8325-4, Δspx , and Δspx -C cells stained with CTC and HPF harvested at 24 hours and 72 hours of growth in TSB-45 mM glucose. (C) Survival assay of *S. aureus* 8325-4, Δspx , and Δspx -C in TSB-45 mM glucose supplemented with 100 mM MOPS (pH 7.3). (D) CTC- and HPF-stained 8325-4, Δspx , and Δspx -C cells grown in TSB-45 mM glucose supplemented with 100 mM MOPS (pH 7.3). Cells were collected at 24 hours and 72 hours of growth and analyzed using flow cytometry. (n = 3, mean \pm SD.)

The redox-sensing switch of Spx is not essential for *S. aureus* viability

Spx interaction with the C-terminal domain of RNA polymerase changes when disulfide bonds form between the redox-active cysteine residues at position 10 and position 13 of the Spx (289). Oxidation of the CXXC motif (redox-sensing switch) of Spx activates or represses the Spx regulon under oxidative stress (289). Given that we showed that Spx is critical for stationary phase survival, we investigated whether the oxidation/reduction of the CXXC motif mediates stationary phase survival. Multiple attempts to generate *spx* deletion in the *S. aureus* USA300 JE2 strain were unsuccessful, and this confirmed the essential status of the *spx* gene across different backgrounds of *S. aureus* strains. Work by Villanueva et al showed that bypassing the essentiality of *spx* can be achieved by overexpressing one of two known targets of Spx, the genes encoding thioredoxin (TrxA) or thioredoxin reductase (TrxB), in trans under the control of an Spx-independent promoter (298). Thus, to generate an *spx* deletion in JE2, we expressed TrxB chromosomally at the SapI site under the control of the constitutive promoter *sarA* to form the strain, JE2::pAQ69 (Fig. 4.2A). Using allelic exchange, we were able to delete *spx* in this background, generating the JE2::pAQ69 Δ *spx* strain. The goal of expressing TrxB constitutively from a single copy on the chromosome is to avoid plasmid loss during long stationary phase survival experiments and to express TrxB enough to make the cell viable only upon the loss of *spx*. Interestingly, a substitution of one amino acid of Cys (Cysteine) at position 10 to Ala (Alanine) to block the intramolecular disulfide bond between Cys at 10 and Cys at 13 was easily generated using allelic exchange, and it led to the formation of *spx*_{C10A} in the JE2 background. This clearly suggests that the oxidation of Spx is not essential for *S. aureus* cell viability. In other words, reduced Spx can express enough *trxA* and *trxB* to keep cells viable.

To evaluate the role of Spx and Spx_{C10A} in the support of aerobic growth, JE2::pAQ69, JE2::pAQ69*spx*_{C10A}, and JE2::pAQ69 Δ *spx* were grown in TSB and growth was monitored spectrophotometrically. Interestingly, JE2::pAQ69*spx*_{C10A} grew at the same rate as the JE2::pAQ69 wild-type background, exhibiting no growth defect, suggesting that the CXXC motif of Spx is

dispensable for *S. aureus* growth under standard aerobic growth conditions (Fig. 4.2B). In contrast, JE2::pAQ69 Δ *spx* grew poorly compared with JE2::pAQ69 or JE2::pAQ69*spx*_{C10A}. Importantly, the growth defect in JE2::pAQ69 Δ *spx* was complemented in trans, indicating that Spx is necessary for the growth of *S. aureus* independent of its oxidation state under these tested conditions (Fig. 4.2B). In addition, since Spx is known for its role in combating thiol stress (288, 292, 299), we aimed to evaluate the role of Spx and its oxidation state in growth under thiol stress. Locking Spx into a reduced state increased the sensitivity of *S. aureus* to the thiol-oxidizing agent diamide, where JE2::pAQ69*spx*_{C10A} had an increased growth defect compared with the JE2::pAQ69 wild-type strain (Fig. 4.2C). However, JE2::pAQ69 Δ *spx* was more sensitive to thiol stress than JE2::pAQ69*spx*_{C10A} (Fig. 4.2C). Therefore, we subjected JE2 and *spx*_{C10A} to 0.5 mM diamide during exponential growth and cells were collected for RNA-seq analysis to investigate how cells lacking the Spx redox-sensing switch adapt to thiol stress in comparison to the wild type strain. Interestingly, under non-stress conditions, the transcriptome of the *spx*_{C10A} mutant at exponential phase of growth resembles that of the wild type strain (Fig. 4.3A), and three hypothetical genes were slightly upregulated in the wild type strain compared to that of the *spx*_{C10A} mutant (Fig. 4.3A). However, the transcriptome of diamide treated strains revealed that 373 genes were expressed in both the wild type strain and *spx*_{C10A} mutant, 497 genes were unique to wild type, and 328 were unique to the *spx*_{C10A} mutant (Fig. 4.3B). Although the genes expressed in both strains indicate similar Spx-independent responses to thiol stress, the lack of the Spx redox-sensing switch in the *spx*_{C10A} mutant dramatically increased the magnitude of the response, suggesting the presence of increased thiol stress in the *spx*_{C10A} mutant compared to the wild type strain (Fig. 4.3C). Accordingly, it was not surprising to see that the highest upregulated genes in the *spx*_{C10A} mutant were genes involved in protein quality control, including the CtsR regulon (*clpP*, *clpC*, *clpB*, *mcsA*, and *mcsB*) and the heat shock proteins (*groES*, *groEL*, and *dnaK*), and the potential-diamide reducing enzyme (*azoR*), because these are common bacterial responses to thiol stress (300–304). The 497 unique genes differentially expressed in the wild type strain (Fig. 4.3D) indicated that these genes are directly or indirectly regulated by the

oxidized form of Spx. Enrichment analysis indicated that these unique genes are part of multiple cellular processes (Fig. 4.3F), suggesting a global regulatory role for the Spx redox-sensing switch under thiol stress. Interestingly, most of the 328 unique genes expressed in the *spx_{C10A}* mutant falls in the same category of cellular processes as those expressed only in the wild type strain (Fig. 4.3G). However, the number of genes in each functional category was generally less compared to those expressed only in the wild type strain (compare Fig. 4.3G to Fig. 4.3F, see Appendix Table. S1 and S2). These results suggest that Spx is critical for maintaining the intracellular environment in a reduced state and that the ability of Spx to sense the redox status maximizes the response against thiol stress.

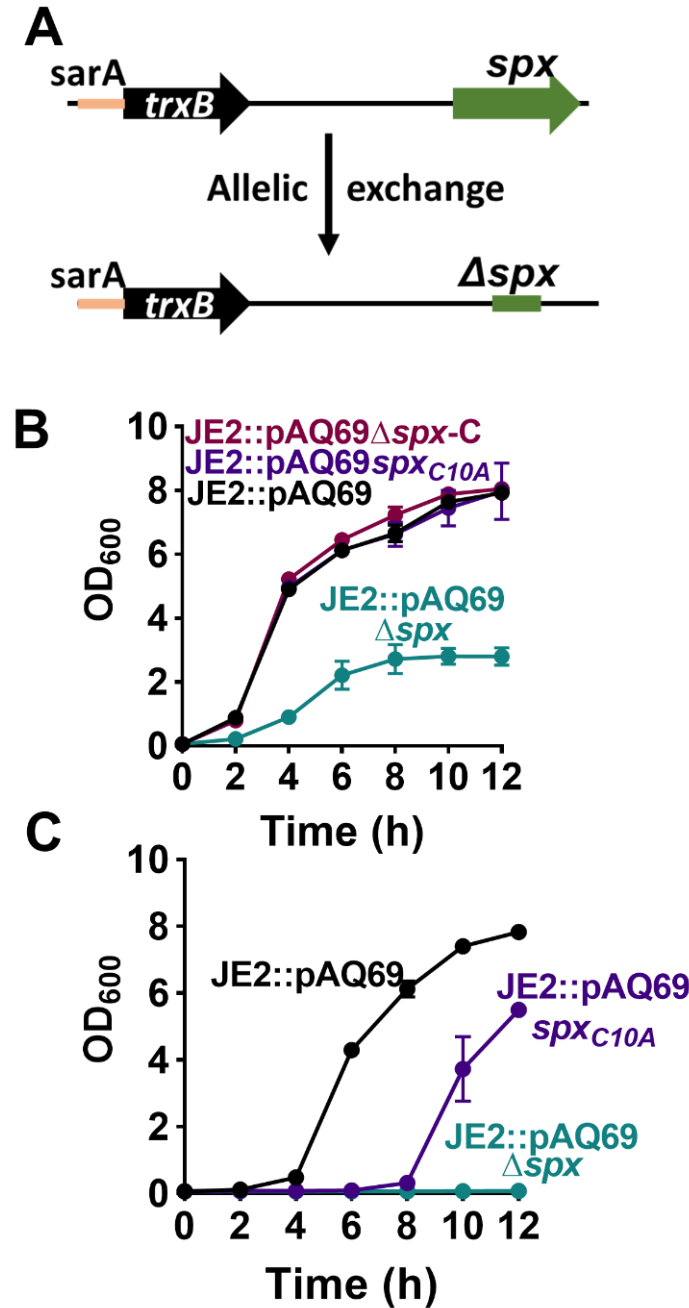


Figure 4.2. Spx is required for *S. aureus* growth independent of its redox-sensing switch

(A) Diagram demonstrates experimental workflow of allelic exchange process to generate *spx* mutant. Single copy of *trxB* driven by *sarA* promoter is integrated at the chromosomal SapI site of wild type JE2, generating JE2::pAQ69, which is subsequently used for allelic exchange. (B) Growth curve of JE2::pAQ69 and its isogenic mutants JE2::pAQ69 Δspx and JE2::pAQ69 spx_{C10A} , and JE2::pAQ69 Δspx -C (in trans complementation) in TSB (C) Growth curve of JE2::pAQ69 and its isogenic mutants JE2::pAQ69 Δspx and JE2::pAQ69 spx_{C10A} in TSB containing 3 mM diamide. Growth curve was plotted as a measure of turbidity at OD₆₀₀. (n = 3, mean \pm SD.)

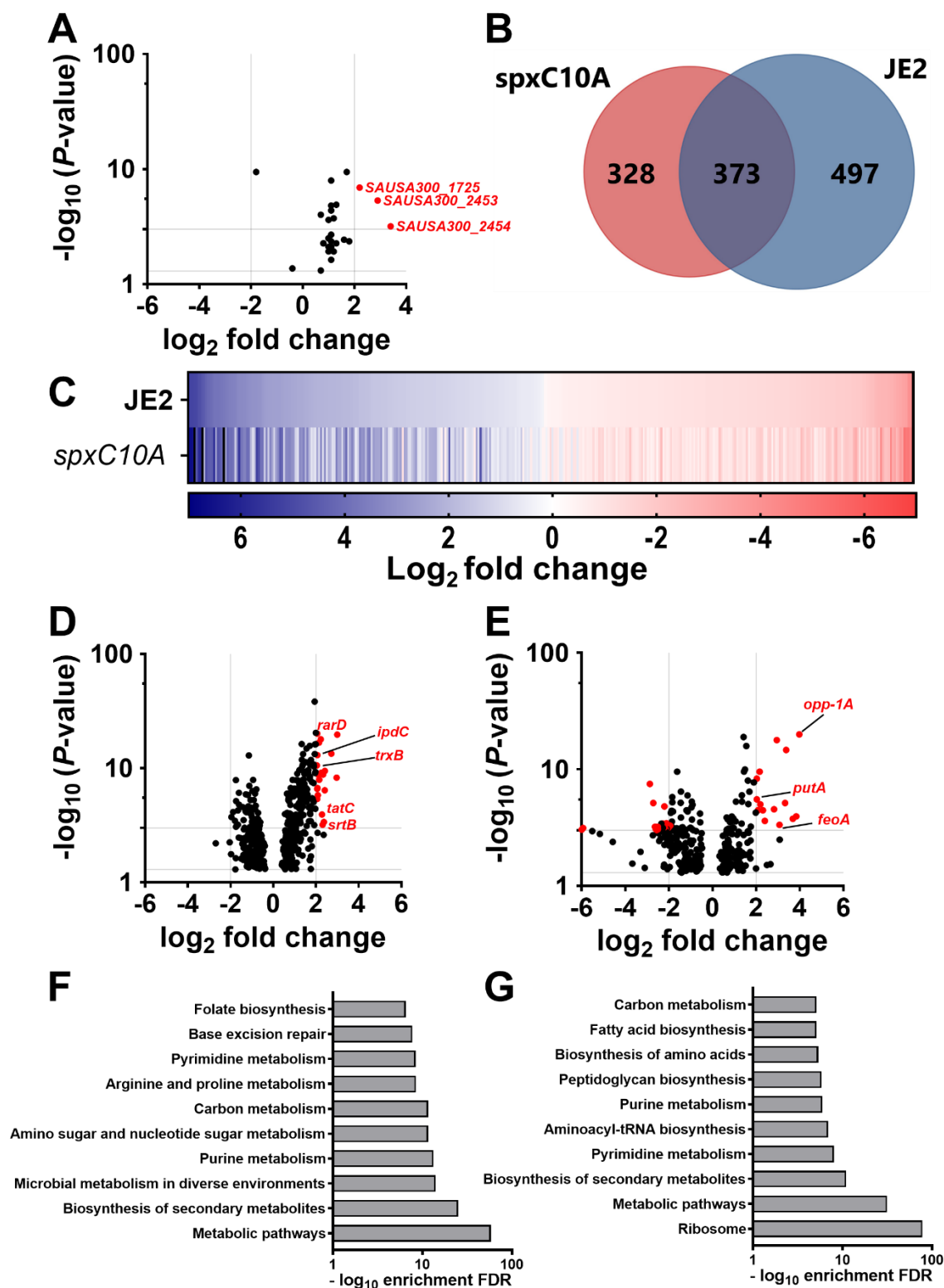


Figure 4.3 Transcriptomic analysis of after thiol stress

(A) Volcano plot representing transcriptome of JE2 compared to *spxC10A* mutant grown aerobically in TSB without stress, 15 minutes after cells reached 1 OD unit. (B) Venn diagram

representation of the common and unique genes that are differentially expressed after exposure to 0.5 mM diamide for 15 minutes after reaching 1 OD unit of growth. (C) Heatmap representing the commonly upregulated and downregulated genes in the wild type and *spxC10A* mutant after diamide stress. Volcano plots representing all the uniquely expressed genes in (D) wild type and (E) *spxC10A* mutant after diamide challenge. ShinyGo V0.060 (305) enrichment analysis of the top ten cellular pathways were affected from (F) wild type and (G) *spxC10A* mutant unique genes. The enrichment analysis was performed using KEGG pathways source. Volcano plot cut off was set to P -value ≤ 0.05 and \log_2 fold change ≥ 2.0 .

The redox-sensing switch of Spx enhances stationary phase survival

We have shown that Spx is important for stationary phase survival in the *S. aureus* 8325-4 strain. The question to be answered now is does Spx-mediated stationary phase survival require a functional redox-sensing switch of Spx? To answer this question, we first evaluated the stationary phase survival of JE2::pAQ69 and its isogenic mutant, JE2::pAQ69 Δ spx, grown in TSB-45 mM glucose. JE2::pAQ69 Δ spx lost viability at a faster rate than JE2::pAQ69, confirming the role of Spx in JE2 *S. aureus* stationary phase survival (Fig. 4.4A, Table. 4.1). Interestingly, the *spx_{C10A}* mutant, which only expresses a reduced form of Spx, exhibited a rate of cell death similar to that of the wild type (Fig. 4.4B, Table. 4.1). This observation may not be conclusive for evaluating the role of the Spx redox-sensing switch in stationary phase survival, because SpxC10A is most likely to be completely degraded by day 3, as in the wild-type Spx variant; this is an observation that we have validated by western blot (Fig. 3.3F). Therefore, this experiment can only be achieved if we use a mutant that will not be able to degrade Spx. We have shown that inactivation of the *clpP* enhances stationary phase survival and prevents degradation of Spx (Fig. 3.3F and Fig. 3.3C). Blocking the formation of the intramolecular disulfide bond of Spx in the *clpP**spx_{C10A}* mutant dramatically increased stationary phase death of the *clpP* mutant, as in the wild type and *spx_{C10A}* (Fig. 4.4C, Table. 4.1). Furthermore, expressing the native *spx* gene from a single copy on the chromosome controlled by its native promoter restored the viability of the *clpP**spx_{C10A}* mutant, suggesting that survival of the *clpP* mutant requires not only Spx but also a functional Spx redox-sensing switch (Fig. 4.4C, Table. 4.1). These results demonstrate that Spx is critical for stationary phase survival and that it enhances survival when it is activated by the oxidation of its redox-sensing switch.

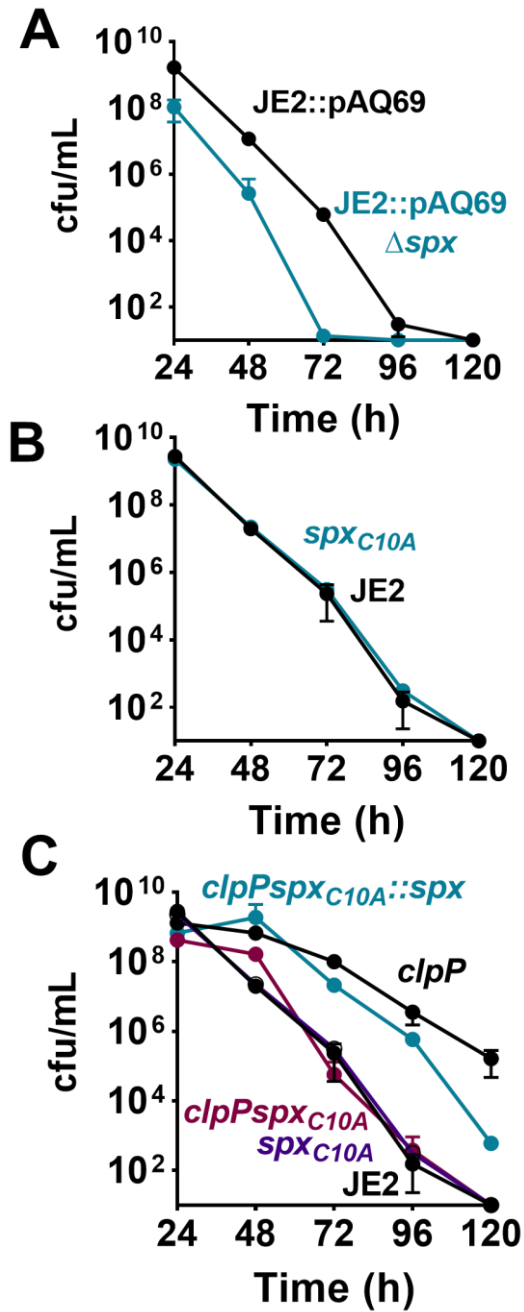


Figure 4.4. Redox-sensing switch of Spx enhances survival of *clpP* mutant

Long-term survival assay of (A) JE2::pAQ69 and its isogenic mutant JE2::pAQ69 Δ spx. (B) JE2 and JE2spx_{C10A}. (C) JE2 and its isogenic mutants *clpP*, spx_{C10A}, *clpP*spx_{C10A}, and *clpP*spx_{C10A}::spx (chromosomally complemented with *spx*) grown in TSB-45 mM. Cell viability was evaluated every 24 hours for 120 hours on TSA plates. (n = 3, mean \pm SD.)

YjbH is a partial contributor to ClpP-mediated cell death

ClpP-dependent proteolysis requires the AAA+ chaperones to recognize a substrate, unfold it, and then pass it to the proteolytic chamber of ClpP to start hydrolysis (306). This process sometimes is mediated by specific adaptor proteins that help in the recognition of the substrate's degron, which is a degradation signal located at the C-terminus or N-terminus of a protein (80, 307). The Spx degron is located at the C-terminus of the protein that the YjbH adaptor protein recognizes and exposes to facilitate the degradation process by ClpXP (308). Given that the ClpXP-dependent degradation of Spx causes cell death, we hypothesized that the inactivation of the gene encoding YjbH will slow the turnover rate of Spx, thus, decreasing stationary phase death.

To test this hypothesis, JE2 and its isogenic mutants *clpP* and *yjbH* were grown in TSB-45 mM glucose and the cell viability was evaluated every day for 5 days. Survival of the *yjbH* mutant had an intermediate phenotype between the wild type and the *clpP* mutant, suggesting that slowing Spx degradation decreases the rate of cell death mediated by ClpXP (Fig. 4.5A, Table. 4.1). If YjbH truly mediates cell death with ClpXP through Spx, but not due to other unknown effects, then the intermediate survival phenotype should correlate with the Spx-dependent effect on ROS in the stationary phase. To evaluate ROS accumulation in the *yjbH* mutant in comparison with the wild type strain and the *clpP* mutant, cells were stained with HPF at 24 hours and 72 hours of growth in TSB-45 mM glucose. As expected, the results demonstrate no differences in HPF-positive cells at 24 hours of growth between all the tested strains (Fig. 4.5B). At 72 hours of growth, the wild type had more HPF-positive cells than the *clpP* mutant, whereas the *yjbH* mutant had a number of HPF-positive cells that was intermediate between the wild type and the *clpP* mutant (Fig. 4.5B); this phenotype correlated with a modest increase in *yjbH* mutant survival (Fig. 4.5A). These observations indicate that YjbH enhances ClpXP-mediated cell death by facilitating Spx degradation, subsequently increasing the formation of ROS and, presumably, damage to macromolecules.

YjbH partially mediates the ClpXP-mediated degradation of Spx by interacting with the last two amino acids at the C-terminus, and deleting 12 amino acids of the Spx C-terminus renders the protein resistant to degradation by ClpXP and abolishes the binding of YjbH to Spx yet keeps it a transcriptionally active protein (308). Therefore, we hypothesized that blocking the interaction of YjbH with Spx would partially rescue ClpXP-mediated cell death. Cells expressing the Spx Δ C-HA (Spx lacking the C-terminal domain and tagged with HA-tag) variant from a single copy at the SapI site controlled by its native promoter were grown in TSB-45 mM glucose, and survival was monitored as described above. Indeed, expressing Spx lacking the degradation signal enhanced survival of JE2::Spx Δ C-HA compared with the JE2:pJC1111 wild-type strain (Fig. 4.5C, Table. 4.1). Another approach to slow the cooperative degradation of Spx by ClpXP and YjbH is to modify the last two amino acids in the C-terminus degradation signal from Ala (Alanine) and Asn (Asparagine) to two Asp (Aspartic acid) (308). This strategy was successful in *B. subtilis*, generating ClpP-resistant Spx (308). Interestingly, the native *S. aureus* Spx already has one Asp at the C-terminus (Fig. 4.4D). Because changing any of the last three amino acids at the C-terminus to Asp reduces recognition of the degradation signal by ClpXP (309), we generated a gene encoding an Spx variant with three Asp residues at the C-terminus (Spx^{DDD}) and introduced it into the stable low-copy vector, pKK22, driven by its native promoter, aiming to make a more stable and functional Spx. Expressing Spx^{DDD} in JE2 significantly increased its stationary phase survival (Table. 4.1), compared with that of JE2:pKK22 when grown in TSB-45 mM glucose (Fig. 4.5D, Table. 4.1). Collectively, these results indicate that recognition of the Spx through the C-terminal degradation signal is required for ClpXP/YjbH-mediated cell death of *S. aureus*.

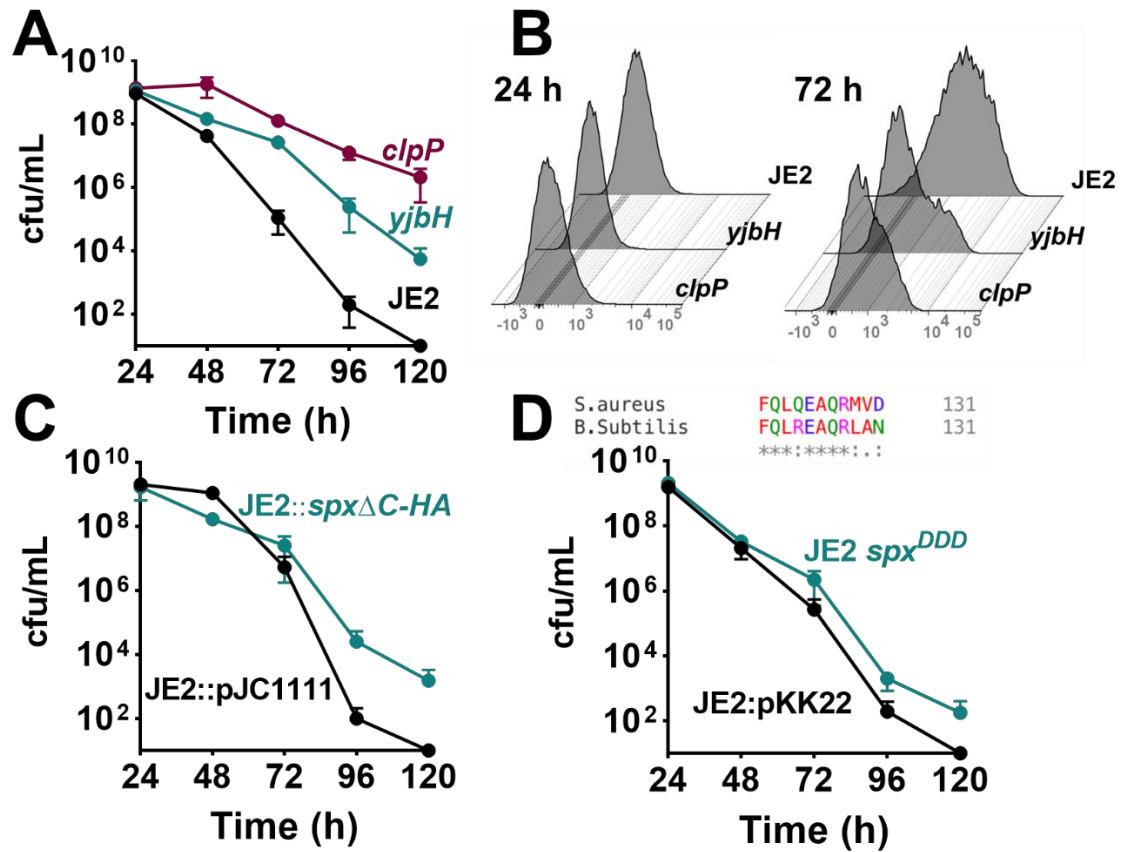


Figure 4.5. YjbH contributes to cell death by enhancing Spx degradation

(A) Survival assay of the wild-type JE2, *yjbH*, and *clpP* mutants in TSB-45 mM glucose. (B) Histogram of JE2, *yjbH*, and *clpP* cells stained with HPF at 24 hours and 72 hours of growth in TSB-45 mM glucose and analyzed using flow cytometry. (C) and (D) 120-hour survival assay of cells expressing ClpP-resistant Spx variants in comparison with their corresponding wild type, grown in TSB-45 mM glucose. JE2::*spx*ΔC-HA strain expresses Spx lacking the C-terminal from single copy in the chromosome driven by its native promoter. JE2 Spx^{DDD} is expressed from low-copy plasmid under the control of *spx* native promoter. Cell viability was evaluated every 24 hours for 120 hours on TSA plates. (n = 3, mean ± SD.)

Spx increases stationary phase survival independent of superoxide dismutase

How does Spx enhance stationary phase survival? We have shown that ClpXP mediates cell death by targeting the antioxidant capacity of *S. aureus*, causing increased ROS and, subsequently, damage to macromolecules (Fig. 3.2 A-B and Fig. 3.7A) (105). Given that the inactivation of *spx* increases cell death because of an increased accumulation of ROS (Fig. 4.1B-D), we aimed to explore the role of Spx in controlling the antioxidant capacity of *S. aureus* in the stationary phase. We concluded that SodA is the major antioxidant enzyme required for stationary phase survival of the *clpP* mutant (Fig. 3.7A-F) and that the functional redox-sensing switch of Spx enhances *clpP* mutant survival (Fig. 4.4C). Therefore, we investigated the SOD activity in *clpPspxC10A* mutant and compared it with that of the *clpP* mutant to evaluate the role of Spx in controlling SodA activity. The wild-type, *clpP*, *spxC10A*, and *clpPspxC10A* strains were grown in TSB-45 mM glucose, and cells were harvested at 24 and 72 hours to determine the intracellular activity of SodA, SodM, and the SodA/M hybrid using a zymogram. At 24 hours of growth, the SOD activity of the *clpP* mutant was significantly higher compared with that in the wild type, whereas the *clpPspxC10A* strain had slightly higher SOD activity compared with that of the wild-type or *spxC10A* strain. However, at 72 hours of growth, *clpPspxC10A* maintained comparable SodA activity with that in the *clpP* mutant despite an increase in death (Fig. 4.6 and Fig. 4.4C). These observations suggest that the redox-sensing switch of Spx decreases ROS and enhances *clpP* mutant survival independent of SodA.

Spx plays a significant role in maintaining intracellular redox homeostasis in *B. subtilis* by controlling the expression of thioredoxin and thioredoxin reductase and the low-molecular-weight bacillithiol biosynthetic genes (288). Although bacillithiol synthesis is controlled by Spx, the redox-sensing switch is not required to activate the transcription of the biosynthetic operon (288). However, a basal level of Spx is required to transcribe the *trxA* and *trxB* genes, yet a high induction of the thioredoxin system requires the redox-sensing switch of Spx under thiol stress (288). We observed similar results in *S. aureus spxC10A* challenged with diamide (Fig. 4.3D&F). Thus, we

hypothesize that Spx and its redox-sensing switch enhance stationary phase survival by inducing activity of the thioredoxin system. Given that *trxA* and *trxB* are essential genes in *S. aureus*, we placed *trxB* under the control of the constitutive *sarA* promoter so that it is expressed in the wild type strain independent of Spx, which is degraded by ClpXP. We grew the JE2trxB, *clpPpVT1*, and JE2pVT1 strains in TSB-45 mM glucose, and the cell viability was monitored for 96 hours. As expected, overexpression of thioredoxin reductase enhanced the survival of the JE2trxB strain compared with the JE2pVT1 control strain (Fig. 4.7A, Table. 4.1). However, the JE2trxB strain did not survive to the level of the *clpPpVT1* strain, suggesting that additional factors, primarily ROS detoxifying enzymes, are still compromised by ClpXP that targets the antioxidant capacity of the cell to induce death (Fig. 4.7A, Table. 4.1). To investigate whether the thioredoxin system contributes to *clpP* mutant survival as a result of active Spx, the expression of *trxA* in the wild type and the *clpP* mutant grown in TSB-45 mM glucose was evaluated using the real-time polymerase chain reaction. At 6 hours of growth, *trxA* was significantly higher in the *clpP* mutant than in the wild type strain, whereas at 24 hours *trxA* expression was increased by only 1.2-fold in the *clpP* mutant compared to that of the wild type (Fig. 4.7B). The proteomic analysis from Chapter 3 (Fig 3.5B and 3.6C&D) indicated that no difference was found in the TrxB or TrxA protein levels in the *clpP* mutant relative to the JE2 strain at 24 hours of growth in TSB-45 mM glucose. However, at 72 hours of growth in TSB-45 mM glucose, TrxA and TrxB were significantly higher in the *clpP* mutant compared to the wild type strain (2.97-fold and 2.31-fold; *p*-value = 0.008 and 0.005, respectively). These results indicate that Spx enhances stationary phase survival by maintaining the intracellular redox environment in a reduced state.

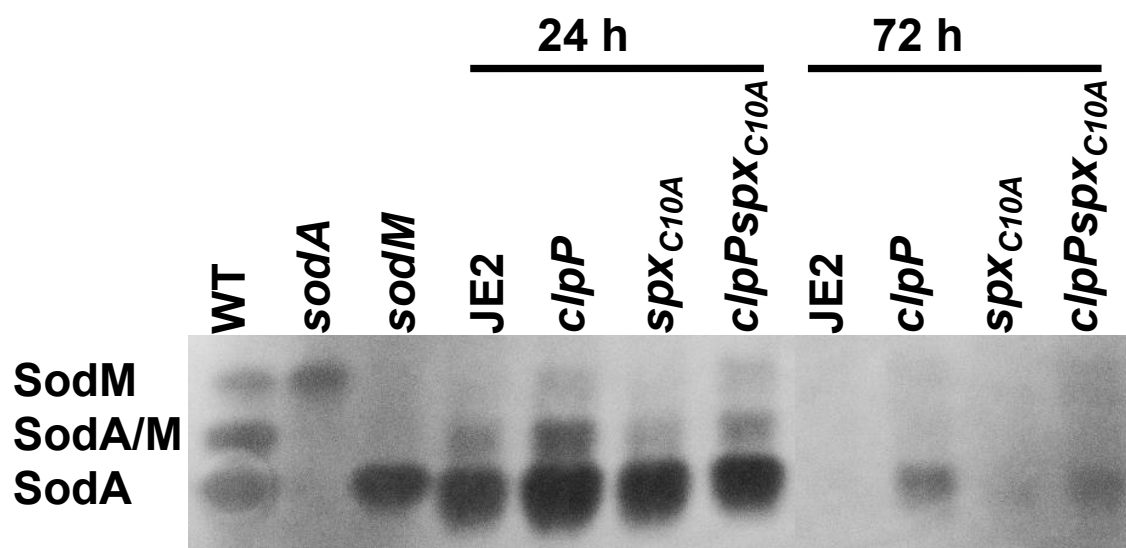


Figure 4.6. Spx does not enhance survival by increasing activity of SOD

Zymography representing the intracellular activity of SodA, SodM, and SodA/M hybrid at 24 hours and 72 hours of JE2 and *clpP*, *spx_{C10A}*, and *clpPspxC_{10A}* mutant cells grown in TSB-45 mM glucose. An amount of 50 µg of cellular lysate protein was resolved on a 4% to 20% gradient native gel and then developed using riboflavin as an O_2^- generator in the presence of light (sun or fluorescent lamp). O_2^- is reduced with nitro blue tetrazolium to formazan, forming dark blue color. Picture color was inverted for easier visualization.

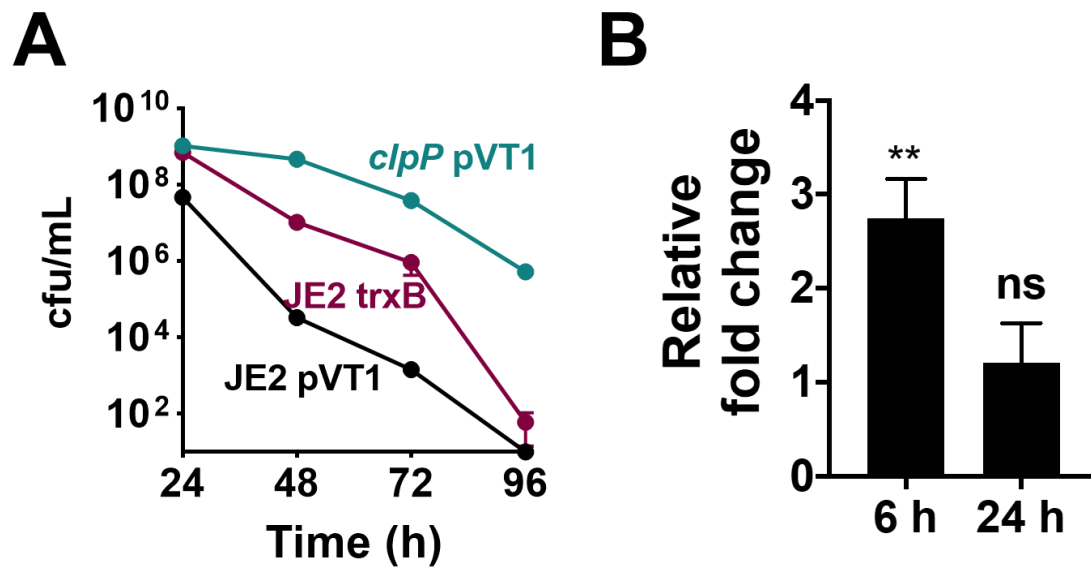


Figure 4.7. Expression of thioredoxin reductase independent of Spx enhances survival

(A) Survival assay of the wild-type *S. aureus* expressing thioredoxin reductase constitutively from P1 *sarA* promoter (JE2*trxB*), JE2 pVT1, and *clpP*pVT1 in TSB-45 mM glucose over a period of 120 hours. Viable cells were counted on TSA plates after track dilution, as described in the section Materials and Methods. (B) Real-time PCR representing gene expression of *trxB* in *clpP* mutant relative to the wild-type JE2 strain evaluated at 6 hours and 24 hours from cells grown in TSB-45 mM glucose. (n = 3, mean \pm SD.) Statistical analysis was determined using two-tailed Student's *t*-test. (* $p \leq .05$, ** $p \leq .01$, *** $p \leq .001$).

Table 4-1. Stationary phase death rates ($k_{\max}^{\#}$).

Figure	Strain	K_{\max}	Significance			Regression model
Fig. 4.1A	8325-4WT	0.195 ± 0.020	***	ns		Log-linear regression
	8325-4 Δspx	0.302 ± 0.002				
	8325-4 Δspx -C	0.212 ± 0.002				
Fig. 4.1C	8325-4WT	0.013 ± 0.001	***	ns		Log-linear regression
	8325-4 Δspx	0.196 ± 0.001				
	8325-4 Δspx -C	0.021 ± 0.001				
Fig. 4.3A	JE2::pAQ69	0.211 ± 0.004				Log-linear regression
	JE2::pAQ69 Δspx	0.304 ± 0.054				
Fig. 4.3B	JE2	0.211 ± 0.001	ns			Log-linear regression
	JE2 spx_{C10A}	0.207 ± 0.001				
Fig. 4.3C	JE2	0.210 ± 0.001	***	ns	ns	Log-linear regression
	<i>clpP</i>	0.100 ± 0.014				
	JE2 spx_{C10A}	0.207 ± 0.001				
	JE2 <i>clpP</i> spx_{C10A}	0.203 ± 0.006				
	JE2 <i>clpP</i> spx_{C10A} :: <i>spx</i>	0.146 ± 0.008				
Fig. 4.4H	JE2	0.204 ± 0.004	***	***		Log-linear regression
	<i>clpP</i>	0.134 ± 0.012				
	<i>yjbH</i>	0.076 ± 0.008				
Fig. 4.4C	JE2:: pJC1111	0.233 ± 0.011	**			Log-linear regression
	JE2:: <i>spx</i> Δ C-HA	0.1567 ± 0.005				
Fig. 4.4D	JE2 pKK22	0.208 ± 0.006	*			Log-linear regression
	JE2 <i>spx</i> ^{DDD}	0.1783 ± 0.011				
Fig. 4.8A	JE2 pVT1	0.216 ± 0.004	***	***		Log-linear regression
	<i>clpP</i> pVT1	0.070 ± 0.006				
	JE2 <i>trxB</i>	0.140 ± 0.009				

[#] k_{\max} values were calculated using GInaFiT (274).

Statistical significance for Fig. 4.3B was determined using two-tailed Student's *t*-test.

Statistical significance for Fig. 4.1A-4.8A was determined using Ordinary one-way ANOVA and Dunnett's multiple comparisons test (* $p \leq 0.05$, ** $p \leq 0.01$, *** $p \leq 0.001$, **** $p < 0.0001$).

4.3 Discussion

ClpXP regulates cell death to enhance the fitness of a population by selectively killing fitness-compromised cells. We previously have identified multiple potential substrates that were affected by ClpXP and this study focused on unveiling the importance of the essential protein Spx for stationary phase survival. We discovered that Spx is not only important for growth but also for survival in the stationary phase in TSB-45 mM glucose and TSB-45 mM glucose buffered medium. This suggests that there is a strong correlation between redox homeostasis and stationary phase survival. Spx was critical for survival, and its redox-sensing switch contributed significantly to its ability to promote survival. Our previous observations pointed to a potentially fast turnover of Spx by ClpXP when cytoplasmic acidification occurred, and here we established that the YjbH adaptor enhances ClpXP-mediated cell death by facilitating the degradation of Spx. Thus, the inactivation of *yjbH* rescued the process of ClpXP-mediated cell death and decreased the process of ROS accumulation, and the manipulation of the C-terminus degradation signal, which interacts with YjbH, enhanced stationary phase survival. Our observations indicated that the primary role of Spx in stationary phase survival is to maintain redox homeostasis and minimize ROS accumulation. Although the intracellular concentration of bacillithiol (BSH) reaches 5 mM in *B. subtilis* (310) and its biosynthetic genes are controlled by Spx (288), *S. aureus* has redundant redox-buffering molecules, such as cysteine and coenzyme A (CoASH), which can compensate for the loss of BSH (279, 299, 311). Thus, we conclude that Spx mediates survival by maintaining a reduced intracellular environment through the thioredoxin system, and BSH biosynthesis may not contribute to the process.

The results of this study also demonstrate that the accumulation of Spx in *S. aureus* adversely affects bacterial growth (312–314) and the inactivation of the *spx* gene is detrimental to cell viability (298). Thus, generating ClpP-resistant Spx was a challenging step because too much Spx was toxic to the cells and survival assays did not produce conclusive data. Partial rescue was only observed when Spx was expressed from a single copy on the chromosome or a low-copy-

number plasmid (Fig. 4.5C&D). Although Spx expression increases dramatically under acetic acid stress starting from post exponential phase of growth through the stationary phase (Fig. 3.3G), it is likely that ClpXP and YjbH can manage to degrade native or ClpP-resistant Spx at a faster rate. Additionally, a better survival trend was observed with *trxB* overexpression when it was under the control of a constitutive promoter (Fig. 4.7A). We believe that plasmid loss in the stationary phase is inevitable with a 5-day survival assay under acetic acid stress, which contributes to the short period of enhanced survival of JE2*trxB* (Fig. 4.7A).

YjbH contributes to Spx degradation continuously as part of the posttranscriptional regulation of Spx in firmicutes (296, 308). Under nonstress conditions, YjbH is soluble and interacts with Spx to facilitate degradation; however, when exposed to stress, YjbH immediately aggregates (219, 315). Thus, the inactivation of *yjbH*, or thiol stress, oxidative stress, and antibiotics, can cause an accumulation of Spx inside a cell of *S. aureus* or *B. subtilis* despite the presence of active ClpXP (219, 296, 315). Interestingly, although *S. aureus* YjbH contains four cysteine residues, YjbH aggregation and Spx degradation occur independent of the YjbH cysteine residues (296). It is intriguing to observe that YjbH maintains its activity and mediates cell death despite acidification of the cytoplasm, which caused the increased accumulation of protein aggregates (Fig. 3.2B&C). Given that YjbH interaction with Spx is inhibited by the anti-adaptor YirB in *B. subtilis* (297), there may be conditions where Spx is in high demand but YjbH is not aggregating to decrease Spx degradation. We speculate that under our testing conditions with high levels of glucose, YjbH was not aggregating, and the antiadaptor, which has not been identified in *S. aureus*, was not inhibiting YjbH.

How does the thioredoxin system promote survival and reduce ROS? TrxA mediates the reduction of intermolecular or intramolecular disulfides in proteins, and TrxB reductase reduces oxidized TrxA, using nicotinamide adenine dinucleotide phosphate (NADPH) as an electron donor (316). The thioredoxin system repairs disulfides of proteins that are formed as a result of oxidative stress or during the catalysis of some enzymes, such as ribonucleotide reductase and methionine

sulfoxide reductase (316, 317). Multiple studies have tried to identify the thioredoxin system substrates using multiple approaches in vitro and in vivo (317, 318). Comprehensive and thorough studies in *E. coli* have identified more than 260 thioredoxin substrates, which include some of the ROS detoxifying enzymes, such as KatG, AhpC, and SodB (317, 318). We speculate that Spx reduces ROS accumulation by maintaining an active thioredoxin system that keeps AhpC active, which is suspected to be reduced by the thioredoxin system (317, 319). Additionally, cysteine residues in AhpC are critical for enzyme activity; substitution of Cys residues near the active site negatively affects the enzymatic activity of AhpC (320, 321). Given that the HPF staining we used to evaluate the presence of ROS in *spx* and *yjbH* mutants detects primarily hydroxyl radicals (225), and SodA is active in *clpP**spx*_{C10A}, we speculate that when O₂⁻ is detoxified by SodA, H₂O₂ accumulates and is converted into the hydroxyl radical (OH[•]) through Fenton chemistry (261, 262). The hydroxyl radical is a highly reactive ROS and it is extremely potent compared with other ROS (277, 322). The only way by which H₂O₂ can be detoxified under our testing condition is through AhpC because KatA did not have a role in survival as its inactivation in *clpP* mutant background did not increase cell death (Fig. 3.7H&I). Thus, overexpression of TrxB most likely promoted survival by maintaining an active AhpC to scavenge H₂O₂ before it was converted to OH[•].

In conclusion, acetate-mediated cell death in *S. aureus* starts with the metabolism of excess glucose into acetate, which induces expression of the cell death operon, *cidABC* (205). The carbon-overflow metabolic pathway CidC is activated, and acetate is generated from pyruvate, leading to a buildup of acetate in the medium (205). Consequently, the pH of the medium approaches the pK_a of acetate, which becomes protonated and neutrally charged (105). At this point, acetate can passively diffuse across the bacterial membrane, and as a result, protons are released into the cytoplasm, causing cytoplasmic acidification (105). Cytoplasmic acidification is followed by PCD hallmarks, including increased ROS and decreased respiration and viability (105). Our work indicates that cells undergo irreparable protein damage during weak acid stress. In response, ClpXP compromises two independent cellular processes to eliminate the damaged cells and maintain

overall population fitness. First, it targets the antioxidant enzymes, causing increased cellular ROS and damage to macromolecules. Second, it targets the degradation of Spx which controls transcription of the essential *trxA* and *trxB* genes. The latter process is likely to promote the ROS-mediated death of unfit cells by reducing the thiol buffering capacity of the cell.

Chapter 5: Concluding remarks

5.1. Main findings

Using genetic, physiological, and biochemical techniques, we provided multiple lines of evidence that ClpXP regulates cell death in *S. aureus*. Protein damage is well known to have detrimental effects on cell viability (11, 323, 324). Yet, we concluded that acetic acid-induced cell death is not due to the passive toxicity of damaged proteins. Counterintuitively, cell death is mediated by the protease that should eliminate protein damage, ClpP, with the help of the AAA+ chaperone ClpX and the adaptor YjbH. We propose that three components cooperatively target native proteins instead of damaged proteins to disrupt cellular processes that are important for stationary phase survival. Transcriptional and posttranscriptional modulation of ROS detoxification enzymes by ClpXP causes increased ROS accumulation and, subsequently, cell death. Additional observations indicate that the effect of ClpXP is not exclusive to ROS. We found that the thioredoxin system is also affected because of Spx posttranscriptional modulation with the help of the adaptor protein YjbH. Thus, rescuing Spx degradation either by inactivation of *clpP*, *clpX*, or *yjbH* or by generation of ClpP-resistant Spx variants promotes survival. Stable Spx is critical for survival in the stationary phase to maintain the intracellular environment reduced by upregulating expression of the thioredoxin system, and this only occurs if the Spx redox switch is activated through the formation of a disulfide bond in the CXXC motif. These sequential events occur as a result of cytoplasmic acidification, where cells accumulate damage over time that affects their ability to replicate (replicative fitness) when stress is alleviated. As cells gradually lose their replicative fitness because of damage accumulation, a ClpXP suicidal mechanism is activated to preserve the population's fitness by eliminating unfit cells (Fig. 5.1).

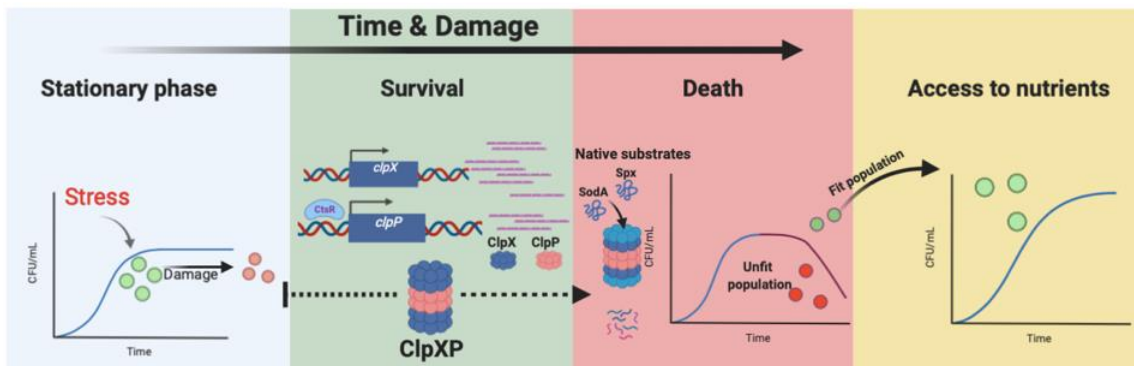


Figure 5.1. Proposed cell death model

Maintaining replicative fitness is critical for the bacterial population to ensure the existence of the species in a harsh environment. Here, we propose that during stationary phase survival, ClpXP protease eliminates damaged or unfit cells from the population to enhance the selection of the fittest cells. Our proposed model demonstrates that under a continuous mild protein homeostasis stress because of acid or antibiotic stress, ClpP with the help of ClpX are highly expressed to maintain protein homeostasis and protein quality. At this stage, protein quality control is critical because cells can neither dilute damage through cell division nor diverge all energy to protein repair as resources are scarce during stationary phase. If the damage is beyond repair and affects the replicative fitness of the population, damaged cells commit suicide by self-digesting native proteins through ClpXP. Illustration was generated using Biorender.com

5.2. Is ClpXP-mediated death an active process?

Distinguishing active cell death (regulated) from passive cell death (accidental) requires a great deal of work. For example, active cell death should be genetically encoded; it should exhibit physiological and morphological hallmarks and require energy; it should be capable of being blocked or inactivated; and it should have meaning for the whole organism (1). Previous work and our study strongly indicate that acetate-mediated cell death in the stationary phase is an active, regulated cell death mechanism. This statement is based on the following evidence.

As cells die they exhibit PCD hallmarks, including increased ROS and DNA damage, decreased respiration and cell viability, and the loss of membrane potential (105). Irreparable damage is an important factor in passive cell death, including protein damage that affects multiple cellular processes. However, it is not the cause of the stationary phase cell death because surviving mutants have increased damage compared with wild-type strains. Multiple genetic determinants regulating cell death were identified, including *cidABC* and *cidR*, and in this study we identified *clpP*, *clpX*, and *yjbH* as potential downstream cell death effectors. Additionally, the cell death process requires a continuous synthesis of cell death mediators. This was clearly observed when a wild-type culture grown for 24 hours in TSB-45 mM glucose was treated with a high concentration of rifampicin to block mRNA synthesis. At 72 hours of growth, cells treated with rifampicin and untreated cells were co-stained with CTC and HPF to evaluate cellular respiration and ROS, respectively (Fig. 5.2A). The untreated cells exhibited few of the PCD hallmarks, such as ROS accumulation and loss of cellular respiration (Fig. 5.2B). However, the cells treated with rifampicin were CTC positive and HPF negative, and this indicates that the cells were respiring (metabolically active) and did not accumulate ROS. This strongly suggests that the generation of ROS and decreased cellular respiration are mediated by proteins that have to be synthesized from transcribed mRNA during the death phase, which usually starts at 48 hours of growth in TSB-45 mM glucose.

Finally, the active cell death process (apoptosis) in eukaryotes requires energy for execution (325), and the ClpXP protease is known to be an energy-dependent intracellular protease

(246). ATP is hydrolyzed in the Walker-B motif of ClpX to power protein unfolding and translocation, and the *clpX*_{E185Q} mutation (Glutamic acid 185 to Glutamine) in the Walker domain slowed ATP hydrolysis dramatically in *E. coli* (326). To test whether ClpXP-mediated cell death required energy to initiate the cell death process, a *clpX*_{E188Q} variant (Glu was at position 188 in *S. aureus*) that does not hydrolyze ATP or the wild-type ClpX was expressed in the $\Delta clpX$ mutant background in a single copy at the SapI site driven by a native promoter. Both variants were grown in TSB-45 mM glucose to assess cell viability. The *clpX*_{E188Q} variant had a higher survival rate than the wild-type *clpX* (Fig. 5.2C). Thus, ClpXP-mediated cell death in *S. aureus* is an energy-dependent process similar to the active apoptotic cell death process in eukaryotes.

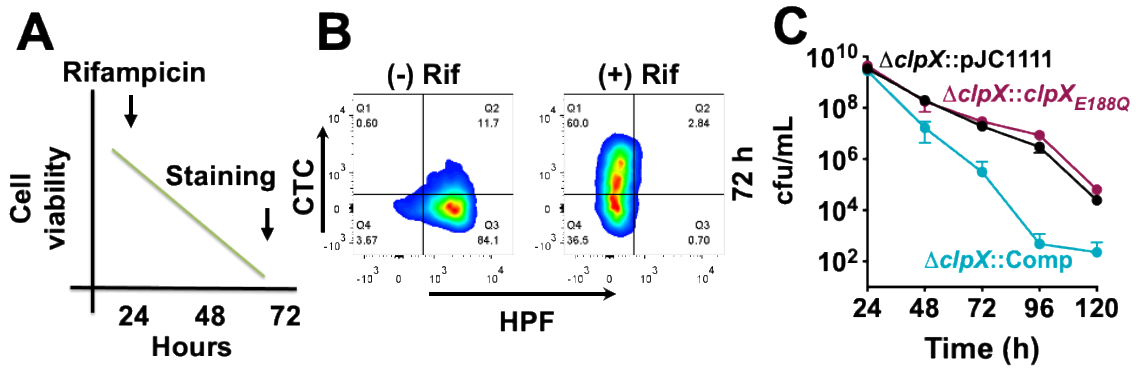


Figure 5.2. ClpXP-mediated cell death is an active cell death process

(A) Cartoon of the experimental workflow to block mRNA synthesis with addition of 200 μ g/mL rifampicin at 24 h of growth in TSB-45 mM glucose. (B) CTC and HPF stained cells from rifampicin and untreated cultures at 72 h of growth analyzed using flowcytometry. (C) Survival assay of $\Delta clpX::pJC1111$, $clpX_{E188Q}$, and $\Delta clpX::Comp$ in TSB-45 mM glucose. Cell viability was determined by track dilution on TSA plates. (n=3, mean \pm SD).

5.3. Does ClpXP-mediated cell death contribute to biofilm development?

We discussed in Chapter 1 how cell death benefits the whole bacterial population in different settings. Cell death during *S. aureus* biofilm development is undoubtedly necessary for normal biofilm development (49, 98). Our data indicate that ClpXP-mediated cell death enhances the replicative potential in the stationary phase. However, does ClpXP-mediated cell death provide other benefits under different physiological growth conditions. Because of the pleiotropic effect of *clpP* or *clpX* inactivation on growth and biofilm phenotypes (82), we used *clpX_{I265E}* to assess biofilm development under conditions of continuous flow. Wild-type and *clpX_{I265E}* strains were stained with CYTO-9 and TOTO-3 to evaluate live and dead cells, respectively, within the biofilm. Interestingly, confocal microscopy images revealed that *clpX_{I265E}* had a distorted biofilm structure compared with that of the wild type, which formed a typical mushroom-like structure (tower) containing a significant number of dead cells (red indicates the TOTO-3 stain) (Fig. 5.3A-B). Subsequent COMSTAT analysis indicated that the *clpX_{I265E}* mutant exhibited decreased biofilm thickness, percentage of dead biomass, and roughness coefficient compared with the normally developed biofilm of the wild type strain (Fig. 5.3C-E). These phenotypes could be the result of decreased ClpXP-mediated cell death, based on our knowledge that acetic acid likely triggers cell death in biofilm microcolonies (105). Thus, we propose that ClpXP-mediated cell death in *S. aureus* can be triggered in different environments, benefitting the population in different ways.

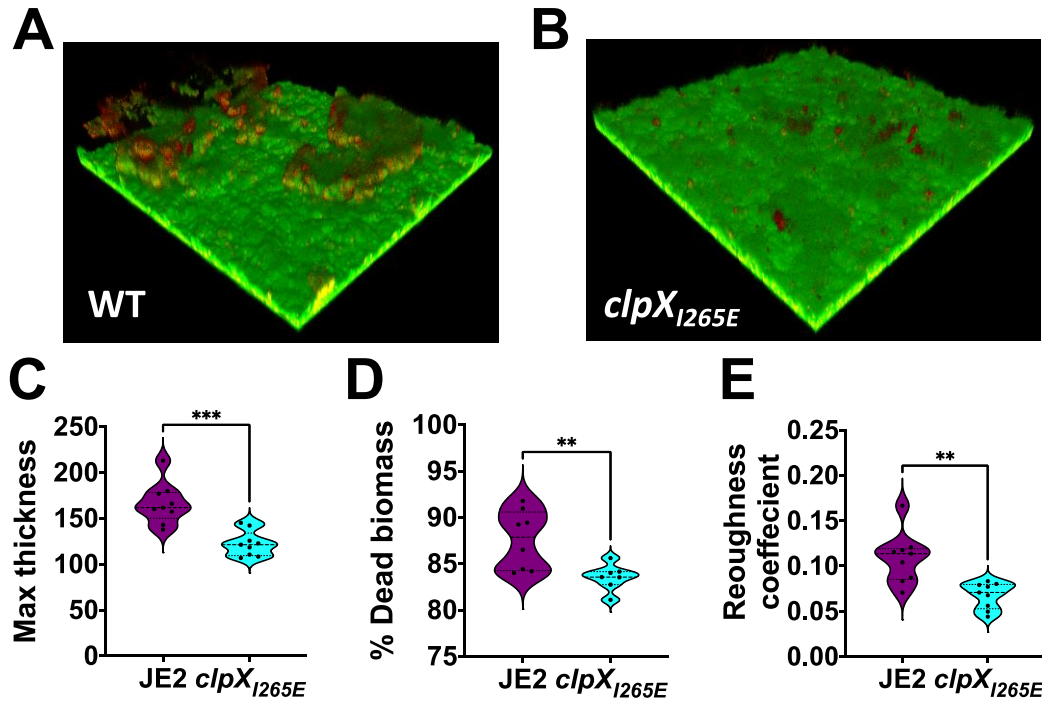


Figure 5.3. ClpP is required for biofilm maturation and development

3D CLMS image of (A) JE2 (B) *clpX*_{1265E} biofilms stained with life and dead stains, SYTO-9 and TOTO-3. (C) Biofilm thickness (D) % dead biomass (E) roughness coefficient of JE2 and *clpX*_{1265E} were analyzed using COMSTAT. Pictures were generated using Imaris software. (n≥7, mean ± SD). Statistical analysis was determined using two-tailed Student's *t*-test. (* p≤0.05, ** p≤0.01, *** p≤0.001).

5.4. Is ClpXP protease a pro-survival or pro-death protein?

The primary function of ClpXP is the maintenance of protein homeostasis to promote survival and growth; however, does it have a role in cell death? In general, ATP-dependent proteases recognize substrates through protease recognition motifs that are located at the C-terminus or N-terminus of a given protein or peptide. Not all signals are accessible for recognition by ClpXP, but these motifs usually become exposed to degradation because of protein denaturation or aggregation (327). We assume that the increased detection of ClpXP recognition motifs on damaged proteins may serve as a signal for ClpXP protease to evaluate the damage. If the damage is overwhelming and detrimental to the cell, then ClpXP initiates cell death. Another possible mechanism is the presence of specific adaptor proteins that are only expressed or become active at the onset of death to mediate the ClpXP interaction with particular substrates for degradation.

ClpP is part of the CtsR regulon, which is known to be critical for protein quality control in the staphylococci. Although it has not been reported how CtsR responds to protein aggregation, the CtsR regulon is induced when cells are exposed to a stress that disrupts protein homeostasis, such as heat, ROS, a low pH, and certain classes of antibiotics, including kanamycin, erythromycin, and gentamicin. Derepression of the CtsR operon occurs as a result of weakened CtsR–DNA binding or degradation of the repressor, which in both cases alleviates the repression of the CtsR regulon. Under the testing conditions used here, it is speculated that a combination of ROS, cytoplasmic acidification, and protein damage induced *clpP* expression. These factors drive the continuous ClpP-dependent degradation of CtsR and, subsequently, the uncontrollable expression of *clpP* during the stationary phase. Increased ClpP abundance and protein damage trigger a quick turnover of native proteins that are essential for stationary phase survival. In conclusion, what triggers the pro-survival or pro-death ClpXP remains critical component of the mechanism that we do not fully understand.

Appendix

S. 1. ShinyGo V.0.60 Enrichment analysis of uniquely expressed genes in wild type after diamide stress using KEGG pathway database (305).

(-) LOG Enrichment FDR	Genes in list	Total genes	Functional Category	Genes
57.97209	59	442	Metabolic pathways	<i>cap5e cap5n ipdc ipk cyse hisc murb rocd pgi menb qoxd qoxc qoxa purk purs muri arcb gmk rpoz coabc pgsa lysa suca fola bira zwf gnd accc accb cdd dgka hola nadd aroe apt folc coae pola glta dnae acka menc mene fumc alda2 ilva atpd upp rpoe glmm moaa moad moae urea ureb urec galu gntk arca</i>
25.10448	28	223	Biosynthesis of secondary metabolites	<i>cap5e cap5n ipk naga hisc gcvh rocd pgi menb purk purs arcb lysa suca zwf gnd accc accb aroe glta menc mene fumc alda2 ilva galu gntk arca</i>
13.95176	16	128	Microbial metabolism in diverse environments	<i>cyse pgi lysa suca zwf gnd accc accb glta acka fumc alda2 urea ureb urec gntk</i>
13.2454	12	57	Purine metabolism	<i>purk purs gmk rpoz hola apt pola dnae rpoe urea ureb urec</i>
11.57557	9	29	Amino sugar and nucleotide sugar metabolism	<i>cap5e cap5n cap5o naga murb pgi crr glmm galu</i>
11.55087	12	80	Carbon metabolism	<i>cyse pgi suca zwf gnd accc accb glta acka fumc ilva gntk</i>
8.422442	7	27	Arginine and proline metabolism	<i>rocd arcb alda2 urea ureb urec arca</i>
8.395707	8	44	Pyrimidine metabolism	<i>trxb rpoz cdd hola pola dnae upp rpoe</i>
7.701941	5	10	Base excision repair	<i>ung nth tag pola muty</i>
6.523614	5	16	Folate biosynthesis	<i>fola folc moaa moad moae</i>
5.946859	5	21	Homologous recombination	<i>pria recg hola pola dnae</i>
5.946859	4	9	Sulfur relay system	<i>mnma moaa moad moae</i>
4.740898	4	17	Glycerophospholipid metabolism	<i>pgsa glpd gpsa dgka</i>

4.722349	5	37	Pyruvate metabolism	<i>accc accb acka fumc alda2</i>
4.570725	7	104	Biosynthesis of amino acids	<i>cyse hisc arcb lysa aroe glta ilva</i>
4.529499	4	20	Pentose phosphate pathway	<i>pgi zwf gnd gntk</i>
4.506842	3	7	Nucleotide excision repair	<i>mfd uvrc pola</i>
4.491261	4	21	Propanoate metabolism	<i>accc accb acka alda2</i>
4.429971	4	22	Oxidative phosphorylation	<i>qoxd qoxc qoxa atpd</i>
4.375554	3	8	Ubiquinone and other terpenoid-quinone biosynthesis	<i>menb menc mene</i>

S. 2. ShinyGo V.0.60 Enrichment analysis of uniquely expressed genes in *spxC10A* mutant after diamide stress using KEGG pathway database (305).

(-) LOG Enrichment FDR	Genes in list	Total genes	Functional Category	Genes
77.88206	42	56	Ribosome	<i>rpsf rpsr rplk rpla rplj rpll rpsl rpmf rpsp rpls rpsb rpsa rpsn rpma rplu rpsd rplm rplq rpsk rpsm rpmj rplo rpmf rpse rplr rplf rpsb rple rplx rpln rpsq rpmc rplp rpsc rplv rpsa rplb rplw rpld rplc rpsj rpmh</i>
31.47277	41	442	Metabolic pathways	<i>dnan ggt pflb mete gltb gltd tmk hpt mvk mvad nrdf fabh fabf mend pyrbr pyrc cara plsx fabd fabg succ glpk femb murg cmk lpda hemd hema pyk pfka murc puta ilva murf ddl luxs lacd rpoa adk moac sdaaa</i>
11.00388	17	223	Biosynthesis of secondary metabolites	<i>mete gltb gltd hpt mvk mvad mend succ lpda hemd hema pyk pfka puta ilva adk sdaaa</i>
8.038425	8	44	Pyrimidine metabolism	<i>dnan tmk nrdf pyrbr pyrc cara cmk rpoa</i>
6.910465	6	24	Aminoacyl- tRNA biosynthesis	<i>sers trps pros alas thr leus</i>
5.92915	7	57	Purine metabolism	<i>dnan hpt nrdf arcc pyk rpoa adk</i>
5.843765	5	20	Peptidoglycan biosynthesis	<i>femb murg murc murf ddl</i>
5.340568	8	104	Biosynthesis of amino acids	<i>mete gltb gltd pyk pfka ilva luxs sdaaa</i>
5.133305	4	13	Fatty acid biosynthesis	<i>fabh fabf fabd fabg</i>
5.133305	7	80	Carbon metabolism	<i>arcc succ lpda pyk pfka ilva sdaaa</i>
4.639145	4	18	Alanine, aspartate and glutamate metabolism	<i>gltb gltd pyrbr cara</i>
4.639145	4	18	Fatty acid metabolism	<i>fabh fabf fabd fabg</i>
4.390121	4	21	Homologous recombination	<i>dnan ssb recr reca</i>
3.935047	7	128	Microbial metabolism in diverse environments	<i>gltb gltd arcc succ lpda pyk pfka</i>
3.617282	3	13	Nitrogen metabolism	<i>gltb gltd arcc</i>

3.27867	3	17	DNA replication	<i>dnan ssb rnhc</i>
	3	21	Cysteine and methionine metabolism	<i>mete luxs sdaaa</i>
3.023146				
	3	31	Glycine, serine and threonine metabolism	<i>lpda ilva sdaaa</i>
2.542759				
	3	37	Pyruvate metabolism	<i>pflb lpda pyk</i>
2.34271				
	2	11	Biotin metabolism	<i>fabf fabg</i>
2.3199				

Reference

1. Galluzzi L, Bravo-San Pedro JM, Vitale I, Aaronson SA, Abrams JM, Adam D, Alnemri ES, Altucci L, Andrews D, Annicchiarico-Petruzzelli M, Baehrecke EH, Bazan NG, Bertrand MJ, Bianchi K, Blagosklonny M V., Blomgren K, Borner C, Bredesen DE, Brenner C, Campanella M, Candi E, Cecconi F, Chan FK, Chandel NS, Cheng EH, Chipuk JE, Cidlowski JA, Ciechanover A, Dawson TM, Dawson VL, De Laurenzi V, De Maria R, Debatin KM, Di Daniele N, Dixit VM, Dynlacht BD, El-Deiry WS, Fimia GM, Flavell RA, Fulda S, Garrido C, Gougeon ML, Green DR, Gronemeyer H, Hajnoczky G, Hardwick JM, Hengartner MO, Ichijo H, Joseph B, Jost PJ, Kaufmann T, Kepp O, Klionsky DJ, Knight RA, Kumar S, Lemasters JJ, Levine B, Linkermann A, Lipton SA, Lockshin RA, López-Otín C, Lugli E, Madeo F, Malorni W, Marine JC, Martin SJ, Martinou JC, Medema JP, Meier P, Melino S, Mizushima N, Moll U, Muñoz-Pinedo C, Nuñez G, Oberst A, Panaretakis T, Penninger JM, Peter ME, Piacentini M, Pinton P, Prehn JH, Puthalakath H, Rabinovich GA, Ravichandran KS, Rizzuto R, Rodrigues CM, Rubinsztein DC, Rudel T, Shi Y, Simon HU, Stockwell BR, Szabadkai G, Tait SW, Tang HL, Tavernarakis N, Tsujimoto Y, Vanden Berghe T, Vandenabeele P, Villunger A, Wagner EF, Walczak H, White E, Wood WG, Yuan J, Zakeri Z, Zhivotovsky B, Melino G, Kroemer G. 2015. Essential versus accessory aspects of cell death: Recommendations of the NCCD 2015. *Cell Death Differ* 22:58–73.
2. Tang D, Kang R, Berghe T Vanden, Vandenabeele P, Kroemer G. 2019. The molecular machinery of regulated cell death. *Cell Res* 29:347–364.
3. Wyllie A. H. CARKJFR. 1972. Apoptosis: A Basic Biological Phenomenon with Wideranging Implications in Tissue Kinetics. *Br J Cancer* 26:239–257.
4. Galluzzi L, Aaronson SA, Abrams J, Alnemri ES, Andrews DW, Baehrecke EH, Bazan NG, Blagosklonny M V., Blomgren K, Borner C, Bredesen DE, Brenner C, Castedo M, Cidlowski JA, Ciechanover A, Cohen GM, De Laurenzi V, De Maria R, Deshmukh M, Dynlacht BD, El-Deiry WS, Flavell RA, Fulda S, Garrido C, Golstein P, Gougeon ML, Green DR, Gronemeyer H, Hajnóczky G, Hardwick JM, Hengartner MO, Ichijo H, Jäättelä M, Kepp O, Kimchi A, Klionsky DJ, Knight RA, Kornbluth S, Kumar S, Levine B, Lipton SA, Lugli E, Madeo F, Malorni W, Marine JCW, Martin SJ, Medema JP, Mehlen P, Melino G, Moll UM, Morselli E, Nagata S, Nicholson DW, Nicotera P, Nuñez G, Oren M, Penninger J, Pervaiz S, Peter ME, Piacentini M, Prehn JHM, Puthalakath H, Rabinovich GA, Rizzuto R, Rodrigues CMP, Rubinsztein DC, Rudel T, Scorrano L, Simon HU, Steller H, Tschopp J, Tsujimoto Y, Vandenabeele P, Vitale I, Vousden KH, Youle RJ, Yuan J, Zhivotovsky B, Kroemer G. 2009. Guidelines for the use and interpretation of assays for monitoring cell death in higher eukaryotes. *Cell Death Differ* 16:1093–1107.
5. Peeters SH, de Jonge MI. 2018. For the greater good: Programmed cell death in bacterial communities. *Microbiol Res* 207:161–169.
6. Durand PM, Ramsey G. 2019. The Nature of Programmed Cell Death. *Biol Theory* 14:30–41.
7. Claessen D, Rozen DE, Kuipers OP, Søgaard-Andersen L, Van Wezel GP. 2014. Bacterial solutions to multicellularity: A tale of biofilms, filaments and fruiting

- bodies. *Nat Rev Microbiol* 12:115–124.
8. Lewis K. 2000. Programmed Death in Bacteria. *Microbiol Mol Biol Rev* 64:503–514.
9. Shapiro JA. 1998. Thinking about bacterial populations as multicellular organisms. *Annu Rev Microbiol* 52:81–104.
10. Huettenbrenner S, Maier S, Leisser C, Polgar D, Strasser S, Grusch M, Krupitza G. 2003. The evolution of cell death programs as prerequisites of multicellularity. *Mutat Res - Rev Mutat Res* 543:235–249.
11. Nyström T. 2001. Not quite dead enough: On bacterial life, culturability, senescence, and death. *Arch Microbiol* 176:159–164.
12. Cheng WC, Hardwick JM. 2007. A Quorum on Bacterial Programmed Cell Death. *Mol Cell* 28:515–517.
13. Smith RP, Barraza I, Quinn RJ, Fortoul MC. 2020. The mechanisms and cell signaling pathways of programmed cell death in the bacterial world *International Review of Cell and Molecular Biology*, 1st ed. Elsevier Inc.
14. Ameisen JC. 2002. On the origin, evolution, and nature of programmed cell death: A timeline of four billion years. *Cell Death Differ* 9:367–393.
15. Nedelcu AM, Driscoll WW, Durand PM, Herron MD, Rashidi A. 2011. On the paradigm of altruistic suicide in the unicellular world. *Evolution (N Y)* 65:3–20.
16. Rice KC, Bayles KW. 2003. Death's toolbox: Examining the molecular components of bacterial programmed cell death. *Mol Microbiol* 50:729–738.
17. Bayles KW. 2014. Bacterial programmed cell death: Making sense of a paradox. *Nat Rev Microbiol* 12:63–69.
18. Rice KC, Bayles KW. 2008. Molecular Control of Bacterial Death and Lysis. *Microbiol Mol Biol Rev* 72:85–109.
19. Ogura T, Hiraga S. 1983. Mini-F plasmid genes that couple host cell division to plasmid proliferation. *Proc Natl Acad Sci U S A* 80:4784–4788.
20. Van Melder L, Bernard P, Couturier M. 1994. Lon-dependent proteolysis of CcdA is the key control for activation of CcdB in plasmid-free segregant bacteria. *Mol Microbiol* 11:1151–1157.
21. Naito T, Kusano K, Kobayashi I. 1995. Selfish behavior of restriction-modification systems. *Science (80-)* 267:897–899.
22. Yarmolinsky M. 1995. Programmed cell death in bacterial populations. *Science (80-)* 267:836–837.
23. Aizenman E, Engelberg-Kulka H, Glaser G. 1996. An *Escherichia coli* chromosomal “addiction module” regulated by 3',5'-bispyrophosphate: A model for programmed bacterial cell death. *Proc Natl Acad Sci U S A* 93:6059–6063.
24. Fraikin N, Goormaghtigh F, Van Melder L. 2020. Type II Toxin-Antitoxin Systems: Evolution and Revolutions. *J Bacteriol* 202:1–14.
25. Amitai S, Yassin Y, Engelberg-Kulka H. 2004. MazF-mediated cell death in *Escherichia coli*: A point of no return. *J Bacteriol* 186:8295–8300.
26. Zhang Y, Zhang J, Hoeflich KP, Ikura M, Qing G, Inouye M. 2003. MazF cleaves cellular mRNAs specifically at ACA to block protein synthesis in *Escherichia coli*. *Mol Cell* 12:913–923.
27. Amitai S, Kolodkin-Gal I, Hananya-Meltabashi M, Sacher A, Kulka HE. 2009. *Escherichia coli* MazF leads to the simultaneous selective synthesis of both ““death

- proteins” and “ ‘survival proteins.’” *PLoS Genet* 5.
28. Pedersen K, Christensen SK, Gerdes K. 2002. Rapid induction and reversal of a bacteriostatic condition by controlled expression of toxins and antitoxins. *Mol Microbiol* 45:501–510.
 29. Christensen SK, Pedersen K, Hansen FG, Gerdes K. 2003. Toxin-antitoxin loci as stress-response-elements: ChpAK/MazF and ChpBK cleave translated RNAs and are counteracted by tmRNA. *J Mol Biol* 332:809–819.
 30. Allocati N, Masulli M, Di Ilio C, De Laurenzi V. 2015. Die for the community: An overview of programmed cell death in bacteria. *Cell Death Dis* 6:1–10.
 31. Mutschler H, Gebhardt M, Shoeman RL, Meinhart A. 2011. A novel mechanism of programmed cell death in bacteria by toxin-antitoxin systems corrupts peptidoglycan synthesis. *PLoS Biol* 9.
 32. Lioy VS, Martín MT, Camacho AG, Lurz R, Antelmann H, Hecker M, Hitchin E, Ridge Y, Wells JM, Alonso JC. 2006. pSM19035-encoded ζ toxin induces stasis followed by death in a subpopulation of cells. *Microbiology* 152:2365–2379.
 33. Camacho AG, Misselwitz R, Behlke J, Ayora S, Welfle K, Meinhart A, Lara B, Saenger W, Welfle H, Alonso JC. 2002. In vitro and in vivo stability of the $\epsilon 2\zeta 2$ protein complex of the broad host-range *Streptococcus pyogenes* pSM19035 addiction system. *Biol Chem* 383:1701–1713.
 34. Janion C. 2008. Inducible SOS response system of DNA repair and mutagenesis in *Escherichia coli*. *Int J Biol Sci* 4:338–344.
 35. Cohen SE, Foti JJ, Simmons LA, Walker GC. 2008. The SOS Regulatory Network. *EcoSal Plus* 3.
 36. Cohen SE, Foti JJ, Simmons LA, Walker GC. 2008. The SOS Regulatory Network. *EcoSal Plus* 3.
 37. Lee H, Lee DG. 2019. Programmed cell death in bacterial community: Mechanisms of action, causes and consequences. *J Microbiol Biotechnol* 29:1014–1021.
 38. Erental A, Kalderon Z, Saada A, Smith Y, Engelberg-Kulka H. 2014. Apoptosis-Like Death, An extreme SOS response in *Escherichia Coli*. *MBio* 5:1–15.
 39. Erental A, Sharon I, Engelberg-Kulka H. 2012. Two programmed cell death systems in *escherichia coli*: An apoptotic-like death is inhibited by the mazef-mediated death pathway. *PLoS Biol* 10.
 40. Dewachter L, Verstraeten N, Fauvart M, Michiels J. 2016. The bacterial cell cycle checkpoint protein obg and its role in programmed cell death. *Microb Cell* 3:255–256.
 41. Wang JYJ. 2001. DNA damage and apoptosis. *Cell Death Differ. Nature Publishing Group*.
 42. Desvaux M. 2012. Contribution of holins to protein trafficking: Secretion, leakage or lysis? *Trends Microbiol* 20:259–261.
 43. Park T, Struck DK, Deaton JF, Young R. 2006. Topological dynamics of holins in programmed bacterial lysis. *Proc Natl Acad Sci U S A* 103:19713–19718.
 44. Saier MH, Reddy BL. 2015. Holins in bacteria, eukaryotes, and archaea: Multifunctional xenologues with potential biotechnological and biomedical applications. *J Bacteriol* 197:7–17.
 45. Ranjit DK, Endres JL, Bayles KW. 2011. *Staphylococcus aureus* CidA and LrgA

- proteins exhibit holin-like properties. *J Bacteriol* 2011/03/18. 193:2468–2476.
46. Rice KC, Firek BA, Nelson JB, Yang SJ, Patton TG, Bayles KW. 2003. The *Staphylococcus aureus* *cidAB* operon: Evaluation of its role in regulation of murein hydrolase activity and penicillin tolerance. *J Bacteriol* 185:2635–2643.
 47. Rice KC, Mann EE, Endres JL, Weiss EC, Cassat JE, Smeltzer MS, Bayles KW. 2007. The *cidA* murein hydrolase regulator contributes to DNA release and biofilm development in *Staphylococcus aureus*. *Proc Natl Acad Sci U S A* 104:8113–8118.
 48. Massimi I, Park E, Rice K, Müller-Esterl W, Sauder D, McGavin MJ. 2002. Identification of a novel maturation mechanism and restricted substrate specificity for the SspB cysteine protease of *Staphylococcus aureus*. *J Biol Chem* 277:41770–41777.
 49. Bayles KW. 2007. The biological role of death and lysis in biofilm development. *Nat Rev Microbiol* 5:721–726.
 50. Pang X, Moussa SH, Targy NM, Bose JL, George NM, Gries C, Lopez H, Zhang L, Bayles KW, Young R, Luo X. 2011. Active Bax and Bak are functional holins. *Genes Dev* 25:2278–2290.
 51. Claverys JP, Håvarstein LS. 2007. Cannibalism and fratricide: Mechanisms and raisons d'être. *Nat Rev Microbiol*. Nature Publishing Group.
 52. Ramisetty BCM, Sudhakari PA. 2020. 'Bacterial Programmed Cell Death': cellular altruism or genetic selfism? *FEMS Microbiol Lett* 367:10–13.
 53. Qi F, Kreth J, Lévesque CM, Kay O, Mair RW, Shi W, Cvitkovitch DG, Goodman SD. 2005. Peptide pheromone induced cell death of *Streptococcus mutans*. *FEMS Microbiol Lett* 251:321–326.
 54. Thomas VC, Hiromasa Y, Harms N, Thurlow L, Tomich J, Hancock LE. 2009. A fratricidal mechanism is responsible for eDNA release and contributes to biofilm development of *Enterococcus faecalis*. *Mol Microbiol* 72:1022–1036.
 55. Kolodkin-Gal I, Engelberg-Kulka H. 2008. The extracellular death factor: Physiological and genetic factors influencing its production and response in *Escherichia coli*. *J Bacteriol* 190:3169–3175.
 56. Kolodkin-Gal I, Sat B, Keshet A, Engelberg-Kulka H. 2008. The communication factor EDF and the toxin-antitoxin module *mazEF* determine the mode of action of antibiotics. *PLoS Biol* 6:2774–2785.
 57. Kumar S, Kolodkin-Gal I, Engelberg-Kulka H. 2013. Novel quorum-sensing peptides mediating interspecies bacterial cell death. *MBio* 4:1–12.
 58. Kolodkin-Gal I, Hazan R, Gaathon A, Carmeli S, Engelberg-Kulka H. 2007. A linear pentapeptide is a quorum-sensing factor required for *mazEF*-mediated cell death in *Escherichia coli*. *Science* (80-) 318:652–655.
 59. Thomas VC, Hancock LE. 2009. Suicide and fratricide in bacterial biofilms. *Int J Artif Organs*. Wichtig Editore s.r.l.
 60. Leung V, Dufour D, Lévesque CM. 2015. Death and survival in *Streptococcus mutans*: Differing outcomes of a quorum-sensing signaling peptide. *Front Microbiol* 6:1–6.
 61. Dufour D, Lévesque CM. 2013. Cell death of *Streptococcus mutans* induced by a quorum-sensing peptide occurs via a conserved streptococcal autolysin. *J Bacteriol* 195:105–114.

62. Perry JANN. 2009. Study of the physiological and molecular mechanisms underlying peptide-induced cell death and biofilm formation in *Streptococcus mutans*. Univ Toronto 169.
63. Piñas GE, Cortes PR, Albarracín Orio AG, Echenique J. 2008. Acidic stress induces autolysis by a CSP- independent ComE pathway in *Streptococcus pneumoniae*. *Microbiology* 154:1300–1308.
64. Lemme A, Gröbe L, Reck M, Tomasch J, Wagner-Döbler I. 2011. Subpopulation-specific transcriptome analysis of competence-stimulating-peptide-induced *Streptococcus mutans*. *J Bacteriol* 193:1863–1877.
65. Eldholm V, Johnsborg O, Haugen K, Ohnstad HS, Havastein LS. 2009. Fratricide in *Streptococcus pneumoniae*: Contributions and role of the cell wall hydrolases CbpD, LytA and LytC. *Microbiology* 155:2223–2234.
66. Perry JA, Jones MB, Peterson SN, Cvitkovitch DG, Lévesque CM. 2009. Peptide alarmone signalling triggers an auto-active bacteriocin necessary for genetic competence. *Mol Microbiol* 72:905–917.
67. Kint CI, Verstraeten N, Wens I, Liebens VR, Hofkens J, Versées W, Fauvart M, Michiels J. 2012. The *Escherichia coli* GTPase ObgE modulates hydroxyl radical levels in response to DNA replication fork arrest. *FEBS J* 279:3692–3704.
68. Dewachter L, Verstraeten N, Monteyne D, Kint CI, Versées W, Pérez-Morga D, Michiels J, Fauvart M. 2015. A single-amino-acid substitution in obg activates a new programmed cell death pathway in *Escherichia coli*. *MBio* 6:1–6.
69. Dewachter L, Verstraeten N, Jennes M, Verbeelen T, Biboy J, Monteyne D, Pérez-Morga D, Verstrepen KJ, Vollmer W, Fauvart M, Michiels J. 2017. A mutant isoform of ObgE causes cell death by interfering with cell division. *Front Microbiol* 8:1–12.
70. Dewachter L, Verstraeten N, Fauvart M, Michiels J. 2018. An integrative view of cell cycle control in *Escherichia coli*. *FEMS Microbiol Rev* 42:116–136.
71. Hirano Y, Ohniwa RL, Wada C, Yoshimura SH, Takeyasu K. 2006. Human small G proteins, ObgH1, and ObgH2, participate in the maintenance of mitochondria and nucleolar architectures. *Genes to Cells* 11:1295–1304.
72. Kirstein J, Molière N, Dougan DA, Turgay K. 2009. Adapting the machine: Adaptor proteins for Hsp100/Clp and AAA+ proteases. *Nat Rev Microbiol* 7:589–599.
73. Tyedmers J, Mogk A, Bukau B. 2010. Cellular strategies for controlling protein aggregation. *Nat Rev Mol Cell Biol* 11:777–788.
74. Davies KJA, Lin SW. 1988. Degradation of oxidatively denatured proteins in *Escherichia coli*. *Free Radic Biol Med* 5:215–223.
75. Gur E, Biran D, Ron EZ. 2011. Regulated proteolysis in Gram-negative bacteria-how and when? *Nat Rev Microbiol* 9:839–848.
76. Jastrab JB, Darwin KH. 2015. Bacterial Proteasomes. *Annu Rev Microbiol* 69:109–127.
77. Konovalova A, Søgaaard-Andersen L, Kroos L. 2014. Regulated proteolysis in bacterial development. *FEMS Microbiol Rev* 38:493–522.
78. Olivares AO, Baker TA, Sauer RT. 2015. Mechanistic insights into bacterial AAA+ proteases and protein-remodelling machines. *Nat Rev Microbiol* 14:33–44.
79. Krüger E, Zühlke D, Witt E, Ludwig H, Hecker M. 2001. Clp-mediated proteolysis

- in Gram-positive bacteria is autoregulated by the stability of a repressor. *EMBO J* 20:852–863.
80. Striebel F, Kress W, Weber-Ban E. 2009. Controlled destruction: AAA+ ATPases in protein degradation from bacteria to eukaryotes. *Curr Opin Struct Biol* 19:209–217.
 81. Reeves A, Gerth U, Völker U, Haldenwang WG. 2007. ClpP modulates the activity of the *Bacillus subtilis* stress response transcription factor, σ B. *J Bacteriol* 189:6168–6175.
 82. Ingmer H, Brøndsted L. 2009. Proteases in bacterial pathogenesis. *Res Microbiol* 160:704–710.
 83. Frees D, Brøndsted L, Ingmer H. 2013. Bacterial proteases and virulence. *Subcell Biochem* 66:161–192.
 84. Kress W, Maglica Ž, Weber-Ban E. 2009. Clp chaperone-proteases: structure and function. *Res Microbiol* 160:618–628.
 85. Piggot PJ, Hilbert DW. 2004. Sporulation of *Bacillus subtilis*. *Curr Opin Microbiol* 7:579–586.
 86. Decker AR, Ramamurthi KS. 2017. Cell Death Pathway That Monitors Spore Morphogenesis. *Trends Microbiol* 2017/04/10. 25:637–647.
 87. Mckenney PT, Driks A, Eichenberger P. 2013. The *Bacillus subtilis* endospore: Assembly and functions of the multilayered coat. *Nat Rev Microbiol* 11:33–44.
 88. Ebmeier SE, Tan IS, Clapham KR, Ramamurthi KS. 2012. Small proteins link coat and cortex assembly during sporulation in *Bacillus subtilis*. *Mol Microbiol* 84:682–696.
 89. Tan IS, Weiss CA, Popham DL, Ramamurthi KS. 2015. A Quality-Control Mechanism Removes Unfit Cells from a Population of Sporulating Bacteria. *Dev Cell* 2015/09/17. 34:682–693.
 90. Dwyer DJ, Camacho DM, Kohanski MA, Callura JM, Collins JJ. 2012. Antibiotic-Induced Bacterial Cell Death Exhibits Physiological and Biochemical Hallmarks of Apoptosis. *Mol Cell* 2012/05/24. 46:561–572.
 91. Manteca A, Fernandez M, Sanchez J. 2006. Cytological and biochemical evidence for an early cell dismantling event in surface cultures of *Streptomyces antibioticus*. *Res Microbiol* 157:143–152.
 92. Manteca A, Mäder U, Connolly BA, Sanchez J. 2006. A proteomic analysis of *Streptomyces coelicolor* programmed cell death. *Proteomics* 6:6008–6022.
 93. Tsujimoto Y. 1997. Apoptosis and necrosis: Intracellular ATP level as a determinant for cell death modes. *Cell Death Differ* 4:429–434.
 94. Ishizawa J, Zarabi SF, Davis RE, Halgas O, Nii T, Jitkova Y, Zhao R, St-Germain J, Heese LE, Egan G, Ruvolo VR, Barghout SH, Nishida Y, Hurren R, Ma W, Gronda M, Link T, Wong K, Mabanglo M, Kojima K, Borthakur G, MacLean N, Ma MCJ, Leber AB, Minden MD, Houry W, Kantarjian H, Stogniew M, Raught B, Pai EF, Schimmer AD, Andreeff M. 2019. Mitochondrial ClpP-Mediated Proteolysis Induces Selective Cancer Cell Lethality. *Cancer Cell* 35:721-737.e9.
 95. Otto M. 2008. Staphylococcal biofilms. In: Romeo, T. (ed.) *Bacterial biofilms (current topics in microbiology and immunology)*. Springer-Verlag 207–228.
 96. Dufour D, Leung V, Lévesque CM. 2010. Bacterial biofilm: structure, function, and antimicrobial resistance. *Endod Top* 22:2–16.

97. Tolker-Nielsen T. 2015. Biofilm Development, p. 51–66. *In* Microbial Biofilms. ASM Press, Washington, DC, USA.
98. Moormeier DE, Bayles KW. 2017. Staphylococcus aureus biofilm: a complex developmental organism. *Mol Microbiol* 104:365–376.
99. Mann EE, Rice KC, Boles BR, Endres JL, Ranjit D, Chandramohan L, Tsang LH, Smeltzer MS, Horswill AR, Bayles KW. 2009. Modulation of eDNA release and degradation affects Staphylococcus aureus biofilm maturation. *PLoS One* 4.
100. Kiedrowski MR, Kavanaugh JS, Malone CL, Mootz JM, Voyich JM, Smeltzer MS, Bayles KW, Horswill AR. 2011. Nuclease modulates biofilm formation in community-associated methicillin-resistant staphylococcus aureus. *PLoS One* 6.
101. Moormeier DE, Endres JL, Mann EE, Sadykov MR, Horswill AR, Rice KC, Fey PD, Bayles KW. 2013. Use of microfluidic technology to analyze gene expression during Staphylococcus aureus biofilm formation reveals distinct physiological niches. *Appl Environ Microbiol* 79:3413–3424.
102. Whitchurch CB, Tolker-Nielsen T, Ragas PC, Mattick JS. 2002. Extracellular DNA required for bacterial biofilm formation. *Science* (80-) 295:1487.
103. Moormeier DE, Bose JL, Horswill AR, Bayles KW. 2014. Temporal and stochastic control of staphylococcus aureus biofilm development. *MBio* 5:1–12.
104. Perry JA, Cvitkovitch DG, Lévesque CM. 2009. Cell death in Streptococcus mutans biofilms: A link between CSP and extracellular DNA. *FEMS Microbiol Lett* 299:261–266.
105. Thomas VC, Sadykov MR, Chaudhari SS, Jones J, Endres JL, Widhelm TJ, Ahn J-SS, Jawa RS, Zimmerman MC, Bayles KW. 2014. A Central Role for Carbon-Overflow Pathways in the Modulation of Bacterial Cell Death. *PLoS Pathog* 10:e1004205–e1004205.
106. Popp PF, Mascher T. 2019. Coordinated Cell Death in Isogenic Bacterial Populations: Sacrificing Some for the Benefit of Many? *J Mol Biol* 431:4656–4669.
107. Kolodkin-Gal I, Verdinger R, Shlosberg-Fedida A, Engelberg-Kulka H. 2009. A differential effect of E. coli toxin-antitoxin systems on cell death in liquid media and biofilm formation. *PLoS One* 4:1–8.
108. Ma D, Mandell JB, Donegan NP, Cheung AL, Ma W, Rothenberger S, Shanks RMQ, Richardson AR, Urish KL. 2019. The Toxin-Antitoxin MazEF Drives Biofilm Formation, Antibiotic Tolerance, and Chronic Infection. *MBio* 10:e01658-19.
109. Rimer J, Cohen IR, Friedman N. Prospects & Overviews Do all creatures possess an acquired immune system of some sort?
110. Bernheim A, Sorek R. 2020. The pan-immune system of bacteria: antiviral defence as a community resource. *Nat Rev Microbiol* 18:113–119.
111. Rostøl JT, Marraffini L. 2019. (Ph)ighting Phages: How Bacteria Resist Their Parasites. *Cell Host Microbe* 25:184–194.
112. Seed KD. 2015. Battling Phages: How Bacteria Defend against Viral Attack. *PLoS Pathog* 11:1–5.
113. Lopatina A, Tal N, Sorek R. 2020. Abortive Infection: Bacterial Suicide as an Antiviral Immune Strategy. *Annu Rev Virol* 7:371–384.
114. Fineran PC, Blower TR, Foulds IJ, Humphreys DP, Lilley KS, Salmond GPC.

2009. The phage abortive infection system, ToxIN, functions as a protein-RNA toxin-antitoxin pair. *Proc Natl Acad Sci U S A* 106:894–899.
115. Durmaz E, Klaenhammer TR. 2007. Abortive Phage Resistance Mechanism *AbiZ* Speeds the Lysis Clock To Cause Premature Lysis of Phage-Infected *Lactococcus lactis*. *J Bacteriol* 189:1417–1425.
116. Lau RK, Ye Q, Birkholz EA, Berg KR, Patel L, Mathews IT, Watrous JD, Ego K, Whiteley AT, Lowey B, Mekalanos JJ, Kranzusch PJ, Jain M, Pogliano J, Corbett KD. 2020. Structure and Mechanism of a Cyclic Trinucleotide-Activated Bacterial Endonuclease Mediating Bacteriophage Immunity. *Mol Cell* 77:723-733.e6.
117. Hazan R, Engelberg-Kulka H. 2004. *Escherichia coli* *mazEF*-mediated cell death as a defense mechanism that inhibits the spread of phage P1. *Mol Genet Genomics* 272:227–234.
118. Makarova KS, Anantharaman V, Aravind L, Koonin E V. 2012. Live virus-free or die: coupling of antiviral immunity and programmed suicide or dormancy in prokaryotes. *Biol Direct* 7:1–10.
119. Tam K, Torres VJ. 2019. *Staphylococcus aureus* Secreted Toxins and Extracellular Enzymes. *Microbiol Spectr* 7.
120. Ray A, Kinch LN, De Souza Santos M, Grishin N V., Orth K, Salomon D. 2016. Proteomics analysis reveals previously uncharacterized virulence factors in *Vibrio proteolyticus*. *MBio* 7.
121. Govind R, Dupuy B. 2012. Secretion of *Clostridium difficile* toxins A and B requires the holin-like protein *tcdE*. *PLoS Pathog* 8:1–14.
122. Rai P, He F, Kwang J, Engelward BP, Chow VTK. 2016. Pneumococcal Pneumolysin Induces DNA Damage and Cell Cycle Arrest. *Sci Rep* 6:1–12.
123. Paton JC, Andrew PW, Boulnois GJ, Mitchell TJ. 1993. Molecular Analysis of The Pathogenicity of *Streptococcus pneumoniae*: The Role of Pneumococcal Proteins. *Annu Rev Microbiol* 47:89–115.
124. Walker JA, Allen RL, Falmagne P, Johnson MK, Boulnois GJ. 1987. Molecular cloning, characterization, and complete nucleotide sequence of the gene for pneumolysin, the sulfhydryl-activated toxin of *Streptococcus pneumoniae*. *Infect Immun* 55:1184–1189.
125. Martner A, Dahlgren C, Paton JC, Wold AE. 2008. Pneumolysin released during *Streptococcus pneumoniae* autolysis is a potent activator of intracellular oxygen radical production in neutrophils. *Infect Immun* 76:4079–4087.
126. Mellroth P, Daniels R, Eberhardt A, Rönnlund D, Blom H, Widengren J, Normark S, Henriques-Normark B. 2012. *LytA*, major autolysin of *Streptococcus pneumoniae*, requires access to nascent peptidoglycan. *J Biol Chem* 287:11018–11029.
127. Regev-Yochay G, Trzcinski K, Thompson CM, Lipsitch M, Malley R. 2007. *SpxB* is a suicide gene of *Streptococcus pneumoniae* and confers a selective advantage in an in vivo competitive colonization model. *J Bacteriol* 189:6532–6539.
128. Kai Soo Tan, Boon Yu Wee, Keang Peng Song. 2001. Evidence for holin function of *tcdE* gene in the pathogenicity of *Clostridium difficile*. *J Med Microbiol* 50:613–619.
129. Voth DE, Ballard JD. 2005. *Clostridium difficile* toxins: Mechanism of action and role in disease. *Clin Microbiol Rev* 18:247–263.

130. McFarland KA, Dolben EL, LeRoux M, Kambara TK, Ramsey KM, Kirkpatrick RL, Mougous JD, Hogan DA, Dove SL. 2015. A self-lysis pathway that enhances the virulence of a pathogenic bacterium. *Proc Natl Acad Sci U S A* 112:8433–8438.
131. Rosenthal AZ, Qi Y, Hormoz S, Park J, Li SHJ, Elowitz MB. 2018. Metabolic interactions between dynamic bacterial subpopulations. *Elife* 7:1–3.
132. Zhang Z, Claessen D, Rozen DE. 2016. Understanding microbial divisions of labor. *Front Microbiol* 7:1–8.
133. Tanouchi Y, Pai A, Buchler NE, You L. 2012. Programming stress-induced altruistic death in engineered bacteria. *Mol Syst Biol* 8:1–11.
134. Gross M, Marianovsky I, Glaser G. 2006. MazG - A regulator of programmed cell death in *Escherichia coli*. *Mol Microbiol* 59:590–601.
135. Bigger J. 1944. TREATMENT OF STAPHYLOCOCCAL INFECTIONS WITH PENICILLIN BY INTERMITTENT STERILISATION. *Lancet* 244:497–500.
136. Sat B, Hazan R, Fisher T, Khaner H, Glaser G, Engelberg-Kulka H. 2001. Programmed cell death in *Escherichia coli*: Some antibiotics can trigger mazEF lethality. *J Bacteriol* 183:2041–2045.
137. Tanouchi Y, Lee AJ, Meredith H, You L. 2013. Programmed cell death in bacteria and implications for antibiotic therapy. *Trends Microbiol* 21:265–270.
138. Rimer J, Cohen IR, Friedman N. Prospects & Overviews Do all creatures possess an acquired immune system of some sort?
139. Emamalipour M, Seidi K, Zununi Vahed S, Jahanban-Esfahlan A, Jaymand M, Majdi H, Amoozgar Z, Chitkushev LT, Javaheri T, Jahanban-Esfahlan R, Zare P. 2020. Horizontal Gene Transfer: From Evolutionary Flexibility to Disease Progression. *Front Cell Dev Biol* 8.
140. Thomas CM, Nielsen KM. 2005. Mechanisms of, and barriers to, horizontal gene transfer between bacteria. *Nat Rev Microbiol*. Nature Publishing Group.
141. Nagasawa R, Yamamoto T, Utada AS, Nomura N, Obana N. 2020. Competence-Stimulating-Peptide-Dependent Localized Cell Death and Extracellular DNA Production in *Streptococcus mutans* Biofilms. *Appl Environ Microbiol* 86:1–17.
142. Prudhomme M, Berge M, Martin B, Polard P. 2016. Pneumococcal Competence Coordination Relies on a Cell-Contact Sensing Mechanism. *PLoS Genet* 12:1–24.
143. Lin J, Park P, Li H, Oh MW, Dobrucki IT, Dobrucki W, Lau GW. 2020. *Streptococcus pneumoniae* Elaborates Persistent and Prolonged Competent State during Pneumonia-Derived Sepsis. *Infect Immun* 88:1–16.
144. Domenech A, Brochado AR, Sender V, Hentrich K, Henriques-Normark B, Typas A, Veening JW. 2020. Proton Motive Force Disruptors Block Bacterial Competence and Horizontal Gene Transfer. *Cell Host Microbe* 27:544–555.e3.
145. Ghigo JM. 2001. Natural conjugative plasmids induce bacterial biofilm development. *Nature* 412:442–445.
146. Cvitkovitch DG, Li Y-H, Ellen RP. 2003. Quorum sensing and biofilm formation in *Streptococcal* infections. *J Clin Invest* 112:1626–1632.
147. Hannan S, Ready D, Jasni AS, Rogers M, Pratten J, Roberts AP. 2010. Transfer of antibiotic resistance by transformation with eDNA within oral biofilms. *FEMS Immunol Med Microbiol* 59:345–349.
148. González-Pastor JE, Hobbs EC, Losick R. 2003. Cannibalism by sporulating

- bacteria. *Science* (80-) 301:510–513.
149. Hosoya S, Lu Z, Ozaki Y, Takeuchi M, Sato T. 2007. Cytological analysis of the mother cell death process during sporulation in *Bacillus subtilis*. *J Bacteriol* 189:2561–2565.
 150. López D, Kolter R. 2010. Extracellular signals that define distinct and coexisting cell fates in *Bacillus subtilis*. *FEMS Microbiol Rev* 34:134–149.
 151. Hutchison EA, Miller DA, Angert ER. 2014. Sporulation in Bacteria: Beyond the Standard Model. *Microbiol Spectr* 2:1–15.
 152. Turner NA, Sharma-Kuinkel BK, Maskarinec SA, Eichenberger EM, Shah PP, Carugati M, Holland TL, Fowler VG. 2019. Methicillin-resistant *Staphylococcus aureus*: an overview of basic and clinical research. *Nat Rev Microbiol* 17:203–218.
 153. David MZ, Daum RS. 2010. Community-associated methicillin-resistant *Staphylococcus aureus*: Epidemiology and clinical consequences of an emerging epidemic. *Clin Microbiol Rev* 23:616–687.
 154. Tong SYC, Davis JS, Eichenberger E, Holland TL, Fowler VG. 2015. *Staphylococcus aureus* infections: Epidemiology, pathophysiology, clinical manifestations, and management. *Clin Microbiol Rev* 28:603–661.
 155. Bhalla A, Aron DC, Donskey CJ. 2007. *Staphylococcus aureus* intestinal colonization is associated with increased frequency of *S. aureus* on skin of hospitalized patients. *BMC Infect Dis* 7:105.
 156. Peters PJ, Brooks JT, McAllister SK, Limbago B, Ken Lowery H, Fosheim G, Guest JL, Gorwitz RJ, Bethea M, Hageman J, Mindley R, McDougal LK, Rimland D. 2013. Methicillin-resistant *staphylococcus aureus* colonization of the groin and risk for clinical infection among HIV-infected adults. *Emerg Infect Dis* 19:623–629.
 157. Witte W, Strommenger B, Stanek C, Cuny C. 2007. Methicillin-resistant *Staphylococcus aureus* ST398 in humans and animals, central Europe. *Emerg Infect Dis* 13:255–258.
 158. Lyell A. 1989. Alexander Ogston, micrococci, and Joseph Lister. *J Am Acad Dermatol* 20:302–310.
 159. Balasubramanian D, Harper L, Shopsis B, Torres VJ. 2017. *Staphylococcus aureus* pathogenesis in diverse host environments. *Pathog Dis* 75:1–13.
 160. Otto M. 2010. Basis of Virulence in Community-Associated Methicillin-Resistant *Staphylococcus aureus* . *Annu Rev Microbiol* 64:143–162.
 161. Richardson AR. 2019. Virulence and Metabolism. *Microbiol Spectr* 7:3–11.
 162. Bronner S, Monteil H, Prévost G. 2004. Regulation of virulence determinants in *Staphylococcus aureus*: Complexity and applications. *FEMS Microbiol Rev* 28:183–200.
 163. Pragman AA, Schlievert PM. 2004. Virulence regulation in *Staphylococcus aureus*: The need for in vivo analysis of virulence factor regulation. *FEMS Immunol Med Microbiol* 42:147–154.
 164. Wardenburg JB, Bae T, Otto M, DeLeo FR, Schneewind O. 2007. Poring over pores: α -hemolysin and Panton-Valentine leukocidin in *Staphylococcus aureus* pneumonia. *Nat Med* 13:1405–1406.
 165. Lister JL, Horswill AR. 2014. *Staphylococcus aureus* biofilms: Recent developments in biofilm dispersal. *Front Cell Infect Microbiol* 4:178.

166. Park JH, Lee JH, Cho MH, Herzberg M, Lee J. 2012. Acceleration of protease effect on *Staphylococcus aureus* biofilm dispersal. *FEMS Microbiol Lett* 335:31–38.
167. Lehman MK, Nuxoll AS, Yamada KJ, Kielian T, Carson SD, Feya PD. 2019. Protease-mediated growth of *staphylococcus aureus* on host proteins is opp3 dependent. *MBio* 10.
168. Gustafsson E, Oscarsson J. 2008. Maximal transcription of *aur* (aureolysin) and *sspA* (serine protease) in *Staphylococcus aureus* requires staphylococcal accessory regulator R (*sarR*) activity. *FEMS Microbiol Lett* 284:158–164.
169. Nickerson NN, Prasad L, Jacob L, Delbaere LT, McGavin MJ. 2007. Activation of the SspA serine protease zymogen of *Staphylococcus aureus* proceeds through unique variations of a trypsinogen-like mechanism and is dependent on both autocatalytic and metalloprotease-specific processing. *J Biol Chem* 282:34129–34138.
170. Gimza BD, Larias MI, Budny BG, Shaw LN. 2019. Mapping the Global Network of Extracellular Protease Regulation in *Staphylococcus aureus*. *mSphere* 4.
171. Cassat JE, Skaar EP. 2012. Metal ion acquisition in *Staphylococcus aureus*: Overcoming nutritional immunity. *Semin Immunopathol*.
172. Grim KP, San Francisco B, Radin JN, Brazel EB, Kelliher JL, Párraga Solórzano PK, Kim PC, McDevitt CA, Kehl-Fie TE. 2017. The metallophore staphylopin enables *staphylococcus aureus* to compete with the host for zinc and overcome nutritional immunity. *MBio* 8:1–16.
173. Garcia YM, Barwinska-Sendra A, Tarrant E, Skaar EP, Waldron KJ, Kehl-Fie TE. 2017. A Superoxide Dismutase Capable of Functioning with Iron or Manganese Promotes the Resistance of *Staphylococcus aureus* to Calprotectin and Nutritional Immunity. *PLoS Pathog* 13.
174. Villanueva M, García B, Valle J, Rapún B, Ruiz De Los Mozos I, Solano C, Martí M, Penadés JR, Toledo-Arana A, Lasa I. 2018. Sensory deprivation in *Staphylococcus aureus*. *Nat Commun* 9:1–12.
175. Jenul C, Horswill AR. 2018. Regulation of *Staphylococcus aureus* Virulence. *Microbiol Spectr* 6:1–21.
176. Somerville GA, Proctor RA. 2009. At the Crossroads of Bacterial Metabolism and Virulence Factor Synthesis in *Staphylococci*. *Microbiol Mol Biol Rev* 73:233–248.
177. Liu GY. 2009. Molecular pathogenesis of *Staphylococcus aureus* infection. *Pediatr Res* 65:71–77.
178. Kobayashi SD, Malachowa N, Deleo FR. 2015. Pathogenesis of *Staphylococcus aureus* abscesses. *Am J Pathol* 185:1518–1527.
179. Lewis K. 2005. Persister cells and the riddle of biofilm survival. *Biokhimiya* 70:327–336.
180. Stewart PS. 1996. Theoretical Aspects of Antibiotic Diffusion into Microbial Biofilms. *ANTIMICROBIAL AGENTS AND CHEMOTHERAPY*.
181. Zheng Z, Stewart PS. 2002. Penetration of Rifampin through *Staphylococcus epidermidis* Biofilms. Downloaded from. *Antimicrob Agents Chemother* 46:900–903.
182. Jefferson KK, Goldmann DA, Pier GB. 2005. Use of Confocal Microscopy To Analyze the Rate of Vancomycin Penetration through *Staphylococcus aureus*

- Biofilms. *Antimicrob Agents Chemother* 49:2467–2473.
183. Lora-Tamayo J, Murillo O, Iribarren JA, Soriano A, Sánchez-Somolinos M, Baraia-Etxaburu JM, Rico A, Palomino J, Rodríguez-Pardo D, Horcajada JP, Benito N, Bahamonde A, Granados A, del Toro MD, Cobo J, Riera M, Ramos A, Jover-Sáenz A, Ariza J, Euba G, Cabo X, Pedrero S, Goenaga MÁ, Elola M, Moreno E, García-Ramiro S, Martínez-Pastor JC, Tornero E, García-Lechuz JM, Marín M, Villanueva M, López I, Cisterna R, Santamaría JM, Gómez M-J, Puente A, Cano P, Pigrau C, Sordé R, Flores X, Sorlí L, González-Míguez P, Puig L, Franco M, Jordán M, Coll P, Amador-Mellado J, Fuster-Foz C, García-Paño L, Nieto I, Muniaín MÁ, Suárez A-I, Maseguer MA, Garagorri E, Pintado V, Marinescu C, Ramírez A, Muñoz E, Álvarez T, García R, Barcenilla F, Prat L, Pérez F. 2013. A Large Multicenter Study of Methicillin–Susceptible and Methicillin–Resistant *Staphylococcus aureus* Prosthetic Joint Infections Managed With Implant Retention. *Clin Infect Dis* 56:182–194.
 184. Conlon BP. 2014. *Staphylococcus aureus* chronic and relapsing infections: Evidence of a role for persister cells: An investigation of persister cells, their formation and their role in *S. aureus* disease. *BioEssays* 36:991–996.
 185. Otto M. 2008. Staphylococcal biofilms, p. 207–228. *In* *Current Topics in Microbiology and Immunology*. Springer, Berlin, Heidelberg.
 186. Rice KC, Nelson JB, Patton TG, Yang SJ, Bayles KW. 2005. Acetic acid induces expression of the *Staphylococcus aureus* cidABC and lrgAB murein hydrolase regulator operons. *J Bacteriol* 187:813–821.
 187. Patti JM, Allen BL, McGavin MJ, Hook M. 1994. MSCRAMM-Mediated Adherence of Microorganisms to Host Tissues. *Annu Rev Microbiol* 48:585–617.
 188. Graf AC, Leonard A, Schäuble M, Rieckmann LM, Hoyer J, Maass S, Lalk M, Becher D, Pané-Farré J, Riedel K. 2019. Virulence factors produced by *staphylococcus aureus* biofilms have a moonlighting function contributing to biofilm integrity. *Mol Cell Proteomics* 18:1036–1053.
 189. Arciola CR, Campoccia D, Ravaioli S, Montanaro L. 2015. Polysaccharide intercellular adhesin in biofilm: structural and regulatory aspects. *Front Cell Infect Microbiol* 5:7.
 190. Cramton SE, Gerke C, Schnell NF, Nichols WW, Götz F. 1999. The intercellular adhesion (ica) locus is present in *Staphylococcus aureus* and is required for biofilm formation. *Infect Immun* 67:5427–5433.
 191. Dengler V, Foulston L, DeFrancesco AS, Losick R. 2015. An electrostatic net model for the role of extracellular DNA in biofilm formation by *Staphylococcus aureus*. *J Bacteriol* 197:3779–3787.
 192. Delmain EA, Moormeier DE, Endres JL, Hodges RE, Sadykov MR, Horswill AR, Bayles KW. 2020. Stochastic expression of sae-dependent virulence genes during *staphylococcus aureus* biofilm development is dependent on saes. *MBio* 11.
 193. Wang B, Muir TW. 2016. Regulation of Virulence in *Staphylococcus aureus*: Molecular Mechanisms and Remaining Puzzles. *Cell Chem Biol* 23:214–224.
 194. Le KY, Dastgheyb S, Ho T V, Otto M, Mclean RJC, Lee C. 2014. Molecular determinants of staphylococcal biofilm dispersal and structuring.
 195. Fuchs S, Pané-Farré J, Kohler C, Hecker M, Engelmann S. 2007. Anaerobic gene expression in *Staphylococcus aureus*. *J Bacteriol* 189:4275–4289.

196. Ferreira MT, Manso AS, Gaspar P, Pinho MG, Neves AR. 2013. Effect of Oxygen on Glucose Metabolism: Utilization of Lactate in *Staphylococcus Aureus* as Revealed by In Vivo NMR Studies. *PLoS One* 8:e58277.
197. Kinkel TL, Roux CM, Dunman PM, Fang FC. 2013. The *Staphylococcus aureus* SrrAB two-component system promotes resistance to nitrosative stress and hypoxia. *MBio* 4.
198. Mashruwala AA, van de Guchte A, Boyd JM. 2017. Impaired respiration elicits SrrAB-dependent programmed cell lysis and biofilm formation in *Staphylococcus aureus*. *Elife* 6:1–29.
199. Monod J. 1949. The Growth of Bacterial Cultures. *Annu Rev Microbiol* 3:371–394.
200. Bertranda RL. 2019. Lag phase is a dynamic, organized, adaptive, and evolvable period that prepares bacteria for cell division. *J Bacteriol* 201:1–21.
201. Nyström T. 2004. Stationary-Phase Physiology. *Annu Rev Microbiol* 58:161–181.
202. Finkel SE. 2006. Long-term survival during stationary phase: Evolution and the GASP phenotype. *Nat Rev Microbiol* 4:113–120.
203. Finkel SE, Zinser E, Gupta S, Kolter R. 1998. Life and Death in Stationary Phase, p. 3–16. *In* *Molecular Microbiology*. Springer Berlin Heidelberg.
204. Watson SP, Antonio M, Foster SJ. 1998. Isolation and characterization of *Staphylococcus aureus* starvation-induced, stationary-phase mutants defective in survival or recovery. *Microbiology* 144:3159–3169.
205. Patton TG, Rice KC, Foster MK, Bayles KW. 2005. The *Staphylococcus aureus* cidC gene encodes a pyruvate oxidase that affects acetate metabolism and cell death in stationary phase. *Mol Microbiol* 56:1664–1674.
206. Chatterjee I, Neumayer D, Herrmann M. 2010. Senescence of staphylococci: using functional genomics to unravel the roles of ClpC ATPase during late stationary phase. *Int J Med Microbiol* 300:130–136.
207. Kohler C, Wolff S, Albrecht D, Fuchs S, Becher D, Büttner K, Engelmann S, Hecker M. 2005. Proteome analyses of *Staphylococcus aureus* in growing and non-growing cells: A physiological approach. *Int J Med Microbiol* 295:547–565.
208. Weiss A, Broach WH, Shaw LN. 2016. Characterizing the transcriptional adaptation of *Staphylococcus aureus* to stationary phase growth. *Pathog Dis* 74:1–5.
209. Chatterjee I, Becker P, Grundmeier M, Bischoff M, Somerville GA, Peters G, Sinha B, Harraghy N, Proctor RA, Herrmann M. 2005. *Staphylococcus aureus* ClpC is required for stress resistance, aconitase activity, growth recovery, and death. *J Bacteriol* 187:4488–4496.
210. Liebeke M, Dörries K, Zühlke D, Bernhardt J, Fuchs S, Pané-Farré J, Engelmann S, Völker U, Bode R, Dandekar T, Lindequist U, Hecker M, Lalk M. 2011. A metabolomics and proteomics study of the adaptation of *Staphylococcus aureus* to glucose starvation. *Mol Biosyst* 7:1241–1253.
211. Windham IH, Chaudhari SS, Bose JL, Thomas VC, Bayles KW. 2016. SrrAB modulates *Staphylococcus aureus* cell death through regulation of cidABC transcription. *J Bacteriol* 198:1114–1122.
212. Chaudhari SS, Thomas VC, Sadykov MR, Bose JL, Ahn DJ, Zimmerman MC, Bayles KW. 2016. The LysR-type transcriptional regulator, CidR, regulates

- stationary phase cell death in *Staphylococcus aureus*. *Mol Microbiol* 2016/07/04. 101:942–953.
213. Valenti D, Vacca RA, Guaragnella N, Passarella S, Marra E, Giannattasio S. 2008. A transient proteasome activation is needed for acetic acid-induced programmed cell death to occur in *Saccharomyces cerevisiae*. *FEMS Yeast Res* 8:400–404.
 214. Marques C, Oliveira CSF, Alves S, Chaves SR, Coutinho OP, Côrte-Real M, Preto A. 2013. Acetate-induced apoptosis in colorectal carcinoma cells involves lysosomal membrane permeabilization and cathepsin D release. *Cell Death Dis* 4:1–11.
 215. Kreiswirth BN, Löfdahl S, Betley MJ, O'reilly M, Schlievert PM, Bergdoll MS, Novick RP. 1983. The toxic shock syndrome exotoxin structural gene is not detectably transmitted by a prophage. *Nature*.
 216. Fey PD, Endres JL, Yajjala VK, Widhelm TJ, Boissy RJ, Bose JL, Bayles KW. 2013. A genetic resource for rapid and comprehensive phenotype screening of nonessential *Staphylococcus aureus* genes. *MBio* 4:1–8.
 217. Stahlhut SG, Alqarzaee AA, Jensen C, Fisker NS, Pereira AR, Pinho MG, Thomas VC, Frees D. 2017. The ClpXP protease is dispensable for degradation of unfolded proteins in *Staphylococcus aureus*. *Sci Rep* 7.
 218. Zalis EA, Nuxoll AS, Manuse S, Clair G, Radlinski LC, Conlon BP, Adkins J, Lewis K. 2019. Stochastic variation in expression of the tricarboxylic acid cycle produces persister cells. *MBio* 10:1–10.
 219. Engman J, von Wachenfeldt C, Wachenfeldt C Von. 2015. Regulated protein aggregation: A mechanism to control the activity of the ClpXP adaptor protein YjbH. *Mol Microbiol* 95:51–63.
 220. Levine RL, Garland D, Oliver CN, Amici A, Climent I, Lenz AG, Ahn BW, Shaltiel S, Stadtman ER. 1990. Determination of Carbonyl Content in Oxidatively Modified Proteins. *Methods Enzymol* 186:464–478.
 221. Schmittgen TD, Livak KJ. 2008. Analyzing real-time PCR data by the comparative CT method. *Nat Protoc* 3:1101–1108.
 222. Wiser MJ, Lenski RE. 2015. A Comparison of Methods to Measure Fitness in *Escherichia coli*. *PLoS One* 10:e0126210–e0126210.
 223. McCord JM. 1999. Analysis of Superoxide Dismutase Activity. *Curr Protoc Toxicol* 00.
 224. Nakano MM, Hajarizadeh F, Zhu Y, Zuber P. 2001. Loss-of-function mutations in yjbD result in ClpX- and ClpP-independent competence development of *Bacillus subtilis*. *Mol Microbiol* 42:383–394.
 225. Setsukinai K, Urano Y, Kakinuma K, Majima HJ, Nagano T. 2003. Development of novel fluorescence probes that can reliably detect reactive oxygen species and distinguish specific species. *J Biol Chem* 278:3170–3175.
 226. Smith JJ, McFeters GA. 1996. Effects of substrates and phosphate on INT (2-(4-iodophenyl)-3-(4-nitrophenyl)-5-phenyl tetrazolium chloride) and CTC (5-cyano-2,3-ditolyl tetrazolium chloride) reduction in *Escherichia coli*. *J Appl Bacteriol* 80:209–215.
 227. Carroll RK, Weiss A, Broach WH, Wiemels RE, Mogen AB, Rice KC, Shaw LN. 2016. Genome-wide annotation, identification, and global transcriptomic analysis of regulatory or small RNA gene expression in *Staphylococcus aureus*. *MBio* 7.

228. Edgar RC. 2010. Search and clustering orders of magnitude faster than BLAST. *Bioinformatics* 26:2460–2461.
229. Bushnell B. 2014. BBMap: a fast, accurate, splice-aware aligner. Lawrence Berkeley National Lab.(LBNL), Berkeley, CA (United States).
230. Quast C, Pruesse E, Yilmaz P, Gerken J, Schweer T, Yarza P, Peplies J, Glöckner FO. 2013. The SILVA ribosomal RNA gene database project: Improved data processing and web-based tools. *Nucleic Acids Res* 41:D590–D596.
231. Li H. 2017. Minimap2: pairwise alignment for nucleotide sequences. *arXiv* 34:3094–3100.
232. Core R Team. 2019. A Language and Environment for Statistical Computing. R Found Stat Comput 2:<https://www.R-project.org>.
233. Love MI, Anders S, Huber W. 2014. Differential analysis of count data - the DESeq2 package. *Genome Biol* 15:550.
234. Oksanen J, Kindt R, Legendre P, O'Hara B, Simpson GL, Solymos PM, Stevens MHH, & Wagner H. 2008. The vegan package. *Community Ecol Packag* 10:190.
235. Albertsen M, Karst SM, Ziegler AS, Kirkegaard RH, Nielsen PH. 2015. Back to basics - The influence of DNA extraction and primer choice on phylogenetic analysis of activated sludge communities. *PLoS One* 10:e0132783.
236. Jacquet R, LaBauve AE, Akoolo L, Patel S, Alqarzaee AA, Fok Lung TW, Poorey K, Stinear TP, Thomas VC, Meagher RJ, Parker D, Wong Fok Lung T, Poorey K, Stinear TP, Thomas VC, Meagher RJ, Parker D. 2019. Dual gene expression analysis identifies factors associated with *Staphylococcus aureus* virulence in diabetic mice. *Infect Immun* 87:1–18.
237. Novick R. 1967. Properties of a cryptic high-frequency transducing phage in *Staphylococcus aureus*. *Virology* 33:155–166.
238. Chen J, Yoong P, Ram G, Torres VJ, Novick RP. 2014. Single-copy vectors for integration at the SaPII attachment site for *Staphylococcus aureus*. *Plasmid* 2014/09/02. 76:1–7.
239. Pamp SJ, Frees D, Engelmann S, Hecker M, Ingmer H, Pamp J, Frees D, Engelmann S, Hecker M, Ingmer H, Moritz E, Universita A. 2006. Spx is a global effector impacting stress tolerance and biofilm formation in *Staphylococcus aureus*. *J Bacteriol* 188:4861–4870.
240. Krute CN, Krausz KL, Markiewicz MA, Joyner JA, Pokhrel S, Hall PR, Bose JL. 2016. Generation of a stable plasmid for in vitro and in vivo studies of *Staphylococcus* species. *Appl Environ Microbiol* 82:6859–6869.
241. Lewis K. 2006. Persister cells, dormancy and infectious disease. *Nat Rev Microbiol* 5:48–56.
242. Kolter R, Siegele DA, Tormo A. 1993. The Stationary Phase of The Bacterial Life Cycle. *Annu Rev Microbiol* 47:855–874.
243. Rohmer L, Hocquet D, Miller SI. 2011. Are pathogenic bacteria just looking for food? Metabolism and microbial pathogenesis. *Trends Microbiol* 2011/05/18. 19:341–348.
244. Zhang YJ, Rubin EJ. 2013. Feast or famine: the host-pathogen battle over amino acids. *Cell Microbiol* 15:1079–1087.
245. Jaishankar J, Srivastava P. 2017. Molecular basis of stationary phase survival and applications. *Front Microbiol* 8:1–12.

246. Baker TA, Sauer RT. 2012. ClpXP, an ATP-powered unfolding and protein-degradation machine. *Biochim Biophys Acta - Mol Cell Res* 1823:15–28.
247. Frees D, Savijoki K, Varmanen P, Ingmer H. 2007. Clp ATPases and ClpP proteolytic complexes regulate vital biological processes in low GC, Gram-positive bacteria. *Mol Microbiol* 63:1285–1295.
248. Rode TM, Møretrø T, Langsrud S, Langsrud Ø, Vogt G, Holck A. 2010. Responses of *Staphylococcus aureus* exposed to HCl and organic acid stress. *Can J Microbiol* 56:777–792.
249. Maisonneuve E, Fraysse L, Moinier D, Dukan S. 2008. Existence of abnormal protein aggregates in healthy *Escherichia coli* cells. *J Bacteriol* 190:887–893.
250. Nyström T. 2005. Role of oxidative carbonylation in protein quality control and senescence. *EMBO J* 2005/03/03. 24:1311–1317.
251. Sadykov MR, Thomas VC, Marshall DD, Wenstrom CJ, Moormeier DE, Widhelm TJ, Nuxoll AS, Powers R, Bayles KW. 2013. Inactivation of the Pta-AckA pathway causes cell death in *Staphylococcus aureus*. *J Bacteriol* 195:3035–3044.
252. Maisonneuve E, Ezraty B, Dukan S. 2008. Protein aggregates: An aging factor involved in cell death. *J Bacteriol* 2008/07/11. 190:6070–6075.
253. Jelsbak L, Ingmer H, Valihrach L, Cohn MT, Christiansen MHG, Kallipolitis BH, Frees D. 2010. The chaperone ClpX stimulates expression of *Staphylococcus aureus* protein A by Rot dependent and independent pathways. *PLoS One* 5:e12752–e12752.
254. Feng J, Michalik S, Varming AN, Andersen JH, Albrecht D, Jelsbak L, Krieger S, Ohlsen K, Hecker M, Gerth U, Ingmer H, Frees D. 2013. Trapping and Proteomic Identification of Cellular Substrates of the ClpP Protease in *Staphylococcus aureus*. *J Proteome Res* 12:547–558.
255. Thomas V, Chaudhari S, Jones J, Zimmerman M, Bayles K. 2015. Electron Paramagnetic Resonance (EPR) Spectroscopy to Detect Reactive Oxygen Species in *Staphylococcus aureus*. *Bio-Protocol* 5:1–5.
256. Hibbing ME, Fuqua C, Parsek MR, Peterson SB. 2010. Bacterial competition: surviving and thriving in the microbial jungle. *Nat Rev Microbiol* 8:15–25.
257. Bauer MA, Kainz K, Carmona-Gutierrez D, Madeo F. 2018. Microbial wars: competition in ecological niches and within the microbiome. *Microb Cell* 5:215–219.
258. Ghoul M, Mitri S. 2016. The Ecology and Evolution of Microbial Competition. *Trends Microbiol* 24:833–845.
259. Cornforth DM, Foster KR. 2013. Competition sensing: the social side of bacterial stress responses. *Nat Rev Microbiol* 11:285–293.
260. Clements MO, Watson SP, Foster SJ. 1999. Characterization of the Major Superoxide Dismutase of *Staphylococcus aureus* and Its Role in Starvation Survival, Stress Resistance, and Pathogenicity. *J Bacteriol* 181:3898–3903.
261. Imlay JA. 2013. The molecular mechanisms and physiological consequences of oxidative stress: Lessons from a model bacterium. *Nat Rev Microbiol*.
262. Keyer K, Imlay JA. 1996. Superoxide accelerates DNA damage by elevating free-iron levels. *Proc Natl Acad Sci U S A* 93:13635–13640.
263. van den Esker MH, Kovács ÁT, Kuipers OP. 2017. From Cell Death to Metabolism: Holin-Antiholin Homologues with New Functions. *MBio* 8:6–10.

264. LaBreck CJ, May S, Viola MG, Conti J, Camberg JL. 2017. The Protein Chaperone ClpX Targets Native and Non-native Aggregated Substrates for Remodeling, Disassembly, and Degradation with ClpP. *Front Mol Biosci* 4:26.
265. Fischer F, Weil A, Hamann A, Osiewacz HD. 2013. Human CLPP reverts the longevity phenotype of a fungal ClpP deletion strain. *Nat Commun* 4:1397.
266. Chatterjee I, Maisonneuve E, Ezraty B, Herrmann M, Dukan S. 2011. *Staphylococcus aureus* ClpC is involved in protection of carbon-metabolizing enzymes from carbonylation during stationary growth phase. *Int J Med Microbiol* 301:341–346.
267. Chatterjee I, Schmitt S, Batzilla CF, Engelmann S, Keller A, Ring MW, Kautenburger R, Ziebuhr W, Hecker M, Preissner KT, Bischoff M, Proctor RA, Beck HP, Lenhof H-PP, Somerville GA, Herrmann M. 2009. *Staphylococcus aureus* ClpC ATPase is a late growth phase effector of metabolism and persistence. *Proteomics* 9:1152–1176.
268. Gunaratnam G, Tuchscher L, Elhawy MI, Bertram R, Eisenbeis J, Spengler C, Tschernig T, Löffler B, Somerville GA, Jacobs K, Herrmann M, Bischoff M. 2019. ClpC affects the intracellular survival capacity of *Staphylococcus aureus* in non-professional phagocytic cells. *Sci Rep* 9:1–12.
269. Davis BD. 1987. Mechanism of bactericidal action of aminoglycosides. *Microbiol Rev* 51:341–350.
270. Kannan K, Kanabar P, Schryer D, Florin T, Oh E, Bahroos N, Tenson T, Weissman JS, Mankin AS. 2014. The general mode of translation inhibition by macrolide antibiotics. *Proc Natl Acad Sci U S A* 2014/10/27. 111:15958–15963.
271. Unger L, Kisch A. 1958. Observations on Bacteriostatic and Bactericidal Action of Erythromycin. *Exp Biol Med* 98:176–178.
272. Heifets LB, Lindholm-Levy PJ, Comstock RD. 1992. Bacteriostatic and bactericidal activities of gentamicin alone and in combination with clarithromycin against *Mycobacterium avium*. *Antimicrob Agents Chemother* 36:1695–1698.
273. Ling J, Cho C, Guo L-TT, Aerni HR, Rinehart J, Söll D. 2012. Protein Aggregation Caused by Aminoglycoside Action Is Prevented by a Hydrogen Peroxide Scavenger. *Mol Cell* 2012/10/30. 48:713–722.
274. Geeraerd AH, Valdramidis VP, Van Impe JF. 2005. GInaFiT, a freeware tool to assess non-log-linear microbial survivor curves. *Int J Food Microbiol* 102:95–105.
275. Palazzolo-Ballance AM, Reniere ML, Braughton KR, Sturdevant DE, Otto M, Kreiswirth BN, Skaar EP, DeLeo FR. 2008. Neutrophil Microbicides Induce a Pathogen Survival Response in Community-Associated Methicillin-Resistant *Staphylococcus aureus*. *J Immunol* 180:500–509.
276. Beavers WN, Skaar EP. 2016. Neutrophil-generated oxidative stress and protein damage in *Staphylococcus aureus*. *Pathog Dis* 74:1–15.
277. Repine JE, Fox RB, Berger EM. 1981. Hydrogen peroxide kills *Staphylococcus aureus* by reacting with staphylococcal iron to form hydroxyl radical. *J Biol Chem* 256:7094–7096.
278. Richardson AR, Dunman PM, Fang FC. 2006. The nitrosative stress response of *Staphylococcus aureus* is required for resistance to innate immunity. *Mol Microbiol* 61:927–939.
279. Gaupp R, Ledala N, Somerville GA. 2012. Staphylococcal response to oxidative

- stress. *Front Cell Infect Microbiol* 2:33.
280. Arce Miranda JE, Sotomayor CE, Albesa I, Paraje MG. 2011. Oxidative and nitrosative stress in *Staphylococcus aureus* biofilm. *FEMS Microbiol Lett* 315:23–29.
 281. Hochgräfe F, Wolf C, Fuchs S, Liebeke M, Lalk M, Engelmann S, Hecker M. 2008. Nitric oxide stress induces different responses but mediates comparable protein thiol protection in *Bacillus subtilis* and *Staphylococcus aureus*. *J Bacteriol* 190:4997–5008.
 282. Valderas MW, Hart ME. 2001. Identification and characterization of a second superoxide dismutase gene (*sodM*) from *Staphylococcus aureus*. *J Bacteriol* 183:3399–3407.
 283. Mandell GL. 1975. Catalase, superoxide dismutase, and virulence of *Staphylococcus aureus*. In vitro and in vivo studies with emphasis on staphylococcal leukocyte interaction. *J Clin Invest* 55:561–566.
 284. Cosgrove K, Coutts G, Jonsson IM, Tarkowski A, Kokai-Kun JF, Mond JJ, Foster SJ. 2007. Catalase (*KatA*) and alkyl hydroperoxide reductase (*AhpC*) have compensatory roles in peroxide stress resistance and are required for survival, persistence, and nasal colonization in *Staphylococcus aureus*. *J Bacteriol* 189:1025–1035.
 285. Antelmann H. 2014. Oxidative Stress Responses and Redox Signalling Mechanisms in *Bacillus subtilis* and *Staphylococcus aureus* *Molecular Medical Microbiology: Second Edition*. Elsevier Ltd.
 286. Antelmann H, Helmann JD. 2010. Thiol-Based Redox Switches and Gene Regulation. *Antioxid Redox Signal* 14:1049–1063.
 287. Dubbs JM, Mongkolsuk S. 2012. Peroxide-Sensing Transcriptional Regulators in Bacteria. *J Bacteriol* 194:5495–5503.
 288. Gaballa A, Antelmann H, Hamilton CJ, Helmann JD. 2013. Regulation of *Bacillus subtilis* bacillithiol biosynthesis operons by *Spx*. *Microbiol (United Kingdom)* 159:2025–2035.
 289. Lin AA, Walthers D, Zuber P. 2013. Residue substitutions near the redox center of *Bacillus subtilis* *Spx* affect RNA polymerase interaction, redox control, and *Spx*-DNA contact at a conserved cis-acting element. *J Bacteriol* 195:3967–3978.
 290. Reyes DY, Zuber P. 2008. Activation of transcription initiation by *Spx*: Formation of transcription complex and identification of a Cis-acting element required for transcriptional activation. *Mol Microbiol* 69:765–779.
 291. Rochat T, Nicolas P, Delumeau O, Rabatinová A, Korelusová J, Leduc A, Bessi res P, Dervyn E, Kr sn y L, Noirot P, Bessie P, Dervyn E, Kra L, Korelusova J, Noirot P. 2012. Genome-wide identification of genes directly regulated by the pleiotropic transcription factor *Spx* in *Bacillus subtilis*. *Nucleic Acids Res* 40:9571–9583.
 292. Nakano S, Erwin KN, Ralle M, Zuber P. 2005. Redox-sensitive transcriptional control by a thiol/disulphide switch in the global regulator, *Spx*. *Mol Microbiol* 55:498–510.
 293. Nakano S, K ster-Sch ck E, Grossman AD, Zuber P. 2003. *Spx*-dependent global transcriptional control is induced by thiol-specific oxidative stress in *Bacillus subtilis*. *Proc Natl Acad Sci U S A* 100:13603–13608.

294. Graham JW, Lei MG, Lee CY. 2013. Trapping and identification of cellular substrates of the *Staphylococcus aureus* ClpC chaperone. *J Bacteriol* 195:4506–4516.
295. Rojas-Tapias DF, Helmann JD, Regulons S, Rojas-Tapias DF, Helmann JD. 2019. Identification of novel Spx regulatory pathways in *Bacillus subtilis* uncovers a close relationship between the CtsR and Spx regulons. *J Bacteriol* 201:1–14.
296. Engman J, Rogstam A, Frees D, Ingmer H, Von Wachenfeldt C, Wachenfeldt C Von. 2012. The yjbH adaptor protein enhances proteolysis of the transcriptional regulator spx in *Staphylococcus aureus*. *J Bacteriol* 194:1186–1194.
297. Kommineni S, Garg SK, Chan CM, Zuber P. 2011. YjbH-enhanced proteolysis of Spx by ClpXP in *Bacillus subtilis* is inhibited by the small protein YirB (YuzO). *J Bacteriol* 193:2133–2140.
298. Villanueva M, Jousselin A, Baek KT, Prados J, Andrey DO, Renzoni A, Ingmer H, Frees D, Kelley WL. 2016. Rifampin resistance rpoB alleles or multicopy thioredoxin/thioredoxin reductase suppresses the lethality of disruption of the global stress regulator spx in *Staphylococcus aureus*. *J Bacteriol* 198:2719–2731.
299. Antelmann H. 2015. Thiol-based redox switches in prokaryotes.
300. Leelakriangsak M, Thi N, Huyen T, Töwe S, Duy N Van, Becher D, Hecker M, Antelmann H, Zuber P, Huyen NTT, Töwe S, Van Duy N, Becher D, Hecker M, Antelmann H, Zuber P. 2008. Regulation of quinone detoxification by the thiol stress sensing DUF24/MarR-like repressor, YodB in *Bacillus subtilis*. *Mol Microbiol* 67:1108–1124.
301. Liu G, Zhou J, Fu QS, Wang J. 2009. The *Escherichia coli* azoreductase AzoR is involved in resistance to thiol-specific stress caused by electrophilic quinones. *J Bacteriol* 191:6394–6400.
302. Larsson JT, Rogstam A, Von Wachenfeldt C, Wachenfeldt C Von. 2007. YjbH is a novel negative effector of the disulphide stress regulator, Spx, in *Bacillus subtilis*. *Mol Microbiol* 66:669–684.
303. Elsholz AKW, Hempel K, Pöther DC, Becher D, Hecker M, Gerth U. 2011. CtsR inactivation during thiol-specific stress in low GC, Gram+ bacteria. *Mol Microbiol* 79:772–785.
304. Ole Leichert LI, Scharf C, Hecker M. 2003. Global characterization of disulfide stress in *Bacillus subtilis*. *J Bacteriol* 185:1967–1975.
305. Ge SX, Jung D, Jung D, Yao R. 2020. ShinyGO: A graphical gene-set enrichment tool for animals and plants. *Bioinformatics* 36:2628–2629.
306. Zhang Y, Zuber P. 2007. Requirement of the zinc-binding domain of ClpX for Spx proteolysis in *Bacillus subtilis* and effects of disulfide stress on ClpXP activity. *J Bacteriol* 189:7669–7680.
307. Battesti A, Gottesman S. 2013. Roles of adaptor proteins in regulation of bacterial proteolysis. *Curr Opin Microbiol* 16:140–147.
308. Chan CM, Garg S, Lin AA, Zuber P. 2012. *Geobacillus thermodenitrificans* YjbH recognizes the C-terminal end of *Bacillus subtilis* Spx to accelerate Spx proteolysis by ClpXP. *Microbiology* 158:1268–1278.
309. Flynn JM, Levchenko I, Seidel M, Wickner SH, Sauer RT, Baker TA. 2001. Overlapping recognition determinants within the ssrA degradation tag allow modulation of proteolysis. *Proc Natl Acad Sci U S A* 98:10584–10589.

310. Sharma S V., Arbach M, Roberts AA, Macdonald CJ, Groom M, Hamilton CJ. 2013. Biophysical Features of Bacillithiol, the Glutathione Surrogate of *Bacillus subtilis* and other Firmicutes. *ChemBioChem* 14:2160–2168.
311. Chandrangu P, Loi V Van, Antelmann H, Helmann JD. 2018. The Role of Bacillithiol in Gram-Positive Firmicutes. *Antioxidants Redox Signal* 28:445–462.
312. Rojas-Tapias DF, Helmann JD. 2019. Roles and regulation of Spx family transcription factors in *Bacillus subtilis* and related species, p. 279–323. *In* *Advances in Microbial Physiology*. Academic Press.
313. Nakano S, Zheng G, Nakano MM, Zuber P. 2002. Multiple pathways of Spx (YjbD) proteolysis in *Bacillus subtilis*. *J Bacteriol* 184:3664–3670.
314. Schäfer H, Heinz A, Sudzinová P, Voß M, Hantke I, Krásný L, Turgay K. 2019. Spx, the central regulator of the heat and oxidative stress response in *B. subtilis*, can repress transcription of translation-related genes. *Mol Microbiol* 111:514–533.
315. Panasenko OO, Bezrukov F, Komarynets O, Renzoni A. 2020. YjbH Solubility Controls Spx in *Staphylococcus aureus*: Implication for MazEF Toxin-Antitoxin System Regulation. *Front Microbiol* 11:1–13.
316. Peng H, Zhang Y, Trinidad JC, Giedroc DP. 2018. Thioredoxin profiling of multiple thioredoxin-like proteins in *staphylococcus aureus*. *Front Microbiol* 9:1–13.
317. Kumar JK, Tabor S, Richardson CC. 2004. Proteomic analysis of thioredoxin-targeted proteins in *Escherichia coli*. *Proc Natl Acad Sci* 101:3759–3764.
318. Arts IS, Vertommen D, Baldin F, Laloux G, Collet JF. 2016. Comprehensively characterizing the thioredoxin interactome in vivo highlights the central role played by this ubiquitous oxidoreductase in redox control. *Mol Cell Proteomics* 15:2125–2140.
319. Wong CF, Shin J, Subramanian Manimekalai MS, Saw WG, Yin Z, Bhushan S, Kumar A, Ragunathan P, Grüber G. 2017. AhpC of the mycobacterial antioxidant defense system and its interaction with its reducing partner Thioredoxin-C. *Sci Rep* 7:1–15.
320. Cha, Mee-Kyung, Yoo-Jeen Bae, Kyu-Jeong Kim, Byung-Joon Park and I-HK. 2015. Characterization of two alkyl hydroperoxide reductase C homologs alkyl hydroperoxide reductase C_H1 and alkyl hydroperoxide reductase C_H2 in *Bacillus subtilis*. *World J Biol Chem* 6:249.
321. Jönsson TJ, Ellis HR, Poole LB. 2007. Cysteine reactivity and thiol-disulfide interchange pathways in AhpF and AhpC of the bacterial alkyl hydroperoxide reductase system. *Biochemistry* 46:5709–5721.
322. Imlay JA. 2003. Pathways of Oxidative Damage. *Annu Rev Microbiol. Annual Reviews* 4139 El Camino Way, P.O. Box 10139, Palo Alto, CA 94303-0139, USA .
323. Mirzaei H, Regnier F. 2008. Protein:protein aggregation induced by protein oxidation. *J Chromatogr B Anal Technol Biomed Life Sci* 873:8–14.
324. Bednarska NG, Schymkowitz J, Rousseau F, Van Eldere J. 2013. Protein aggregation in bacteria: The thin boundary between functionality and toxicity. *Microbiol (United Kingdom)* 159:1795–1806.
325. Zamaraeva M V., Sabirov RZ, Maeno E, Ando-Akatsuka Y, Bessonova S V., Okada Y. 2005. Cells die with increased cytosolic ATP during apoptosis: A

- bioluminescence study with intracellular luciferase. *Cell Death Differ* 12:1390–1397.
326. Hersch GL, Burton RE, Bolon DN, Baker TA, Sauer RT. 2005. Asymmetric interactions of ATP with the AAA+ ClpX6 unfoldase: Allosteric control of a protein machine. *Cell* 121:1017–1027.
327. Neher SB, Villén J, Oakes EC, Bakalarski CE, Sauer RT, Gygi SP, Baker TA. 2006. Proteomic Profiling of ClpXP Substrates after DNA Damage Reveals Extensive Instability within SOS Regulon. *Mol Cell* 22:193–204.